UiT The Arctic University of Norway

Faculty of Science and Technology

A Quantitative Analysis of Seasonal and Regional Forcing on the Terminus of Store Glacier, Greenland, from High Resolution Photogrammetry

Hayden Pearson

Master's thesis in Geology GEO-3900 January 2022

Table of Contents

List of Tables

List of Equations

List of Figures

Abstract

The overarching aim of this study was to determine and quantify the primary controls on calving and flow dynamical processes across the marine terminus of Store Glacier and by inference the behavior of Greenland's tidewater outlet glaciers to climate change. Implicitly underlying this primary aim are two key research questions that emerge from review of published literature: First, why has the terminus of Store Glacier not undergone a large-scale retreat similar to Greenland's other primary marine outlet glaciers? Second, what controls that stability and how may Store Glacier respond to future atmospheric and oceanic forcing?

Data for this study consists of several thousand overlapping, geotagged images of the terminus of Store Glacier, at a ground sampling distance of ~0.4 m collected in the spring and summer of 2014. This is coupled with hourly weather data collected from the terminus of Store Glacier and weather stations run by the Geological Survey of Denmark and Greenland. Analysis shows the terminus of Store Glacier is largely controlled by the processes occurring at the ice-ocean interface as well as at the bed. The proglacial mélange exerts the greatest influence on seasonal terminus dynamics, drastically reducing the glacial velocity along the northern portion of the terminus to a rate four times lower than the period without the mélange. The mélange is influenced by prolonged periods of temperature warming as well as regional forcings like calving and winds. The close correlation between lateral strain rates of the proglacial mélange and glacier terminus show that the melange is very well coupled to the terminus.

The longitudinal and lateral strain across the terminus of Store Glacier remain stable through the study period. While there was a 0.9% increase in longitudinal strain during mélange breakup, glacial strain rate variation during the loss of the mélange proves the terminus of Store Glacier is not only dominated by calving processes at the terminus, but specifically those at the bed of the glacier. The greatest regional forcings come from the southern portion of the glacial terminus.

Using the orthoimages from the dataset it was additionally possible to predetermine the size of larger calving events by linking crevasse propagation across the terminus. This allowed for the prediction of the general shape and size of calving events up to a week before the actual event. The ability to predict the calving of marine terminating glaciers has the potential to provide immense insight into how these glaciers will react to future climate scenarios.

Foreword

I would like to offer profound thanks to UiT and Prof. Alun Hubbard[1] for allowing me a truly once in a lifetime opportunity and for providing me access to an immaculate data series in which to conduct this research. For better or worse this has fueled a passion for the Arctic and the beautiful ice which has dominated the landscape. Alun's passion and drive as well as attitude towards research created the perfect environment to allow me to create and give evidence for my own conclusions from the data without dictating what the results should be. I believe this allowed genuine thought and originality to the ideas presented. Profound thanks also goes to Henry Patton[1] for the countless hours he has spent across a myriad of timezones to provide not only advice and editing but full time help with the computer software. Having almost no coding background at the beginning, Henry was able to offer a crash course in all the programming and modeling aspects of this project. Without him the quality of data outputs would not have been what they are. The bulk of data from this thesis comes from the PhD work of Dr. Johnny Ryan[2] who collected a pristine series of orthoimages and is credited with determining the initial parameters in ImGRAFT from which this thesis built on. Thanks goes to Jason Box[3] for providing the meteorological data collected from weather stations in the Uummannaq District of Greenland. A special thank you goes out to Dr. Janet Annelli[4], Nicolette Annelli[5], Emma Murzic and Griffin Hill for their time and contributions to the editing process. Without the unwavering support and encouragement from family and friends throughout the whole process this thesis would not have been possible.

Til slutt vil jeg rette en hjertelig takk til alle de andre MSc-studentene i Røde brakke. Takk for at du fikk meg til å føle meg velkommen, inkludert og at du tok deg tid til kontinuerlig å svare på spørsmål. Selv om oppgaven er en stor prestasjon, vennskapet ditt er det beste resultatet av denne oppgaven.

[1] UiT Norges arktiske universitet Tromsø, Norway

[2] Brown University Providence, Rhode Island, USA

[3] Geological Survey of Denmark and Greenland Copenhagen, Denmark

[4] Los Alamos National Laboratory Los Alamos, NM, USA

[5] Seacoast Science Center Rye, NH, USA

1 Introduction

Anthropogenic climate change has accelerated global glacial retreat since the 1990's as well as vast decreases in Arctic sea ice area. The Greenland Ice Sheet (GrIS) is the second largest continuous body of ice in the world and between 2002 and 2007, dynamic ice imbalance due to iceberg calving was the major source of ice loss from the ice sheet as a whole (IMBIE Team 2020). Dynamic losses from fast flowing tidewater glaciers have contributed 9.1 mm of 13.7 +/- 1.1 mm of sea level rise that has come from GrIS losses (Mouginot et al. 2019), yet little is known about the driving forces within and under these glaciers (Meier et al 1987; Doyle et al. 2018). Store Glacier, the focus of this thesis, is a tidewater glacier terminating into Iserasak fjord located in Uummannaq District of western Greenland and has an expansive seasonal mélange that is typically in place from February to the latter part of May or early June. Compared to other large marine terminating glaciers in Greenland, the terminus of Store Glacier has remained stable over roughly the last century. Aerial photography since 1948 reveals a relatively stable glacial terminus (Weidick et al. 1995). Seasonal fluctuations show a +/-200 m change in the position of the terminus (Howat et al. 2010; Young et al. 2019) with increased advance and retreat observed in the spring between April and June. The overarching aim of this thesis is to determine and quantify the primary controls on calving and flow dynamical processes across the marine terminus of Store Glacier. To achieve this, high spatiotemporal resolution (0.5m) photogrammetry is used to quantify the strain and velocity across the terminus of Store Glacier and its buttressing mélange during the late-spring transition into ice-free conditions within the fjord. This knowledge will advance the understanding of why Store Glacier has not undergone a large-scale retreat like that of other primary Greenland Ice Sheet outlet glaciers as well as the calving dynamics that control the stability of Store Glacier and how it could respond to future climate forcing. Furthermore this thesis will provide a valuable empirical dataset for constraining calving models, which are currently limited by poorly resolved temporal and mechanical understanding.

1.1 Climate Change and Global Impacts

It is indisputable that human influences have warmed the ocean, atmosphere and land. In 2021 the IPCC published the 6th Assessment from Working Group I on Climate Change. In it they outline the current state of the climate. This includes implications of the current climate scenarios as well as century to millenia projected impacts if current climate extremes are allowed to continue unchecked. Each of the last four decades has been successively warmer than the one that preceded it. Global surface temperatures in the first two decades of the 21st century were 0.99˚C warmer than that of the temperatures during 1850 - 1900 (**Fig 1**). The period between 2011 and 2020 saw a temperature that was 1.09˚C warmer than the period between 1850 - 1900. The warming over the past century has been faster than that occurring at the end of the last deglacial period roughly 11,000 years ago. Greenhouse gas concentrations since 1750 are undeniably caused by human activities reaching annual averages of 410 ppm for carbon dioxide, 1866 ppb for methane, and 332 ppb for nitrous oxide in 2019. This was the highest atmospheric CO2 concentration in the last 2 million years, while the CH4 and N2O concentrations were the highest levels in the last 800,000 years. Increases of CO2 and CH4 since 1750 far exceed the natural multi-millennial changes between glacial and interglacial periods in the past 800,000 years. While land and ocean sinks have taken up a near constant proportion of released CO2, about 56%, and this is expected to increase with emissions, they will become less effective. The proportion of CO2 taken up by natural sinks will decrease with increasing emissions by the second half of the 21st century (IPCC 2021).

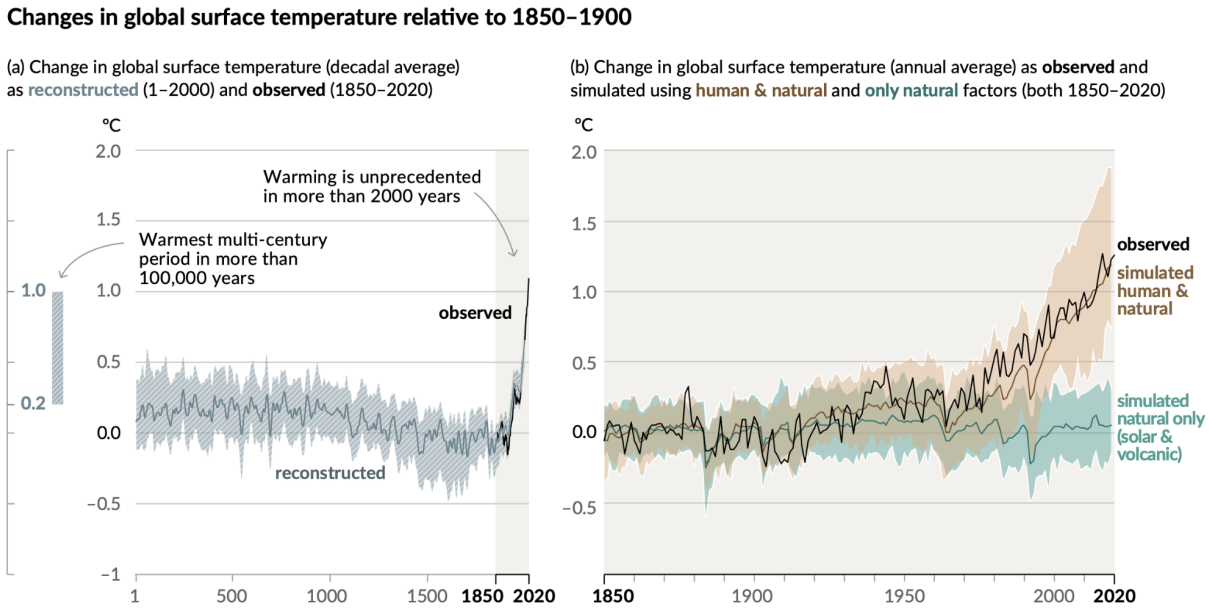

Figure 1: History of global temperature change and causes of recent warming.

Panel (a) Changes in global surface temperature reconstructed from paleoclimate archives (solid grey line, years 1–2000) **and from direct observations** (solid black line, 1850–2020), both relative to 1850–1900 and decadally averaged

Panel (b) Changes in global surface temperature over the past 170 years (black line) relative to 1850–1900 and annually averaged, compared to Coupled Model Intercomparison Project Phase 6 (CMIP6) climate model simulations (see Box SPM.1) of the temperature response to both human and natural drivers (brown) and to only natural drivers (solar and volcanic activity, green). Solid coloured lines show the multi-model average, and coloured shades show the *very likely* range of simulations. (See Figure SPM.2 for the assessed contributions to warming). Figure from IPCC, 2021.

Anthropogenic climate change is the main driver of global glacial retreat since the 1990's as well as vast decreases in Arctic sea ice area. The Arctic has seen a ~40% (**Fig. 2**) decrease in sea ice area in September and ~10% in March. The period between 2011 and 2020 saw the lowest levels of Arctic sea ice since 1850. Late summer sea ice was the lowest it had been in at least 100 years and global glacial retreat since the 1950's is believed to be unprecedented for the past 200 years. This coincides with the trend of decreased Northern Hemisphere spring snow cover since the 1950's and the observed melting of the Greenland Ice Sheet over the past two decades. The global upper ocean (0-700m) has warmed significantly since the 1970's along with increased ocean surface acidification from CO2 absorption. Global mean sea level has increased by 0.20 m between 1901 and 2018. The average increase in sea level between 1901 and 1971 was 1.3 mm/a, increasing to 1.9 mm/a between 1971 and 2006 and again to 3.7 mm/a between 2006 and 2018. The rise in global sea level since 1900 has been faster than any preceding century in the past 3000 years. Changes in the land biosphere have also altered since 1970. There has been a progressive shift of climate zones toward the poles. This is consistent with global warming and changes to the Earth's climate. Global surface temperatures have increased faster since 1970 than in any other 50 year period over the last

2000 years, with the period between 2011 and 2020 exceeding those of even the most recent multi century warm period occurring roughly 6500 years ago (IPCC 2021).

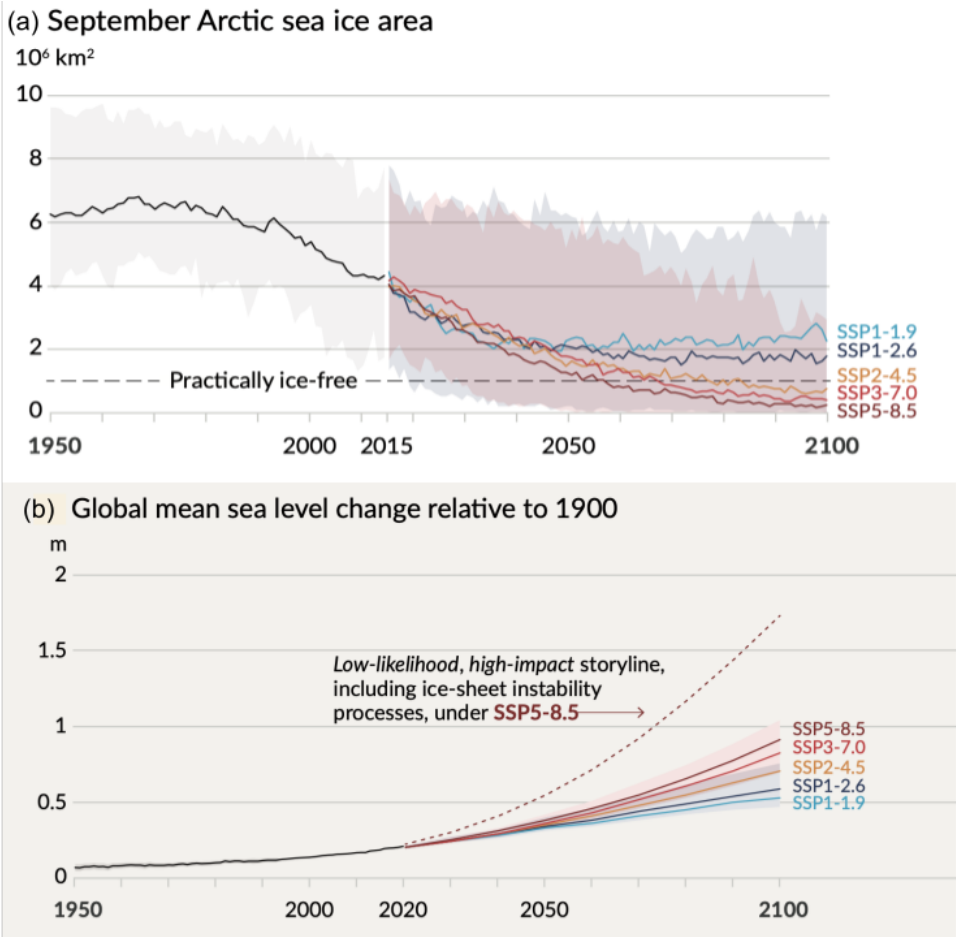

Figure 2: September Arctic sea ice area and global mean sea level change since 1900

A. September Arctic sea ice area in 106 km2 based on CMIP6 model simulations. *Very likely* ranges are shown for SSP1-2.6 and SSP3-7.0. The Arctic is projected to be practically ice-free near mid-century under intermediate and high GHG emissions scenarios.

B. Global mean sea level change in metres, relative to 1900. The historical changes are observed (from tide gauges before 1992 and altimeters **SPM** afterwards), and the future changes are assessed consistently with observational constraints based on emulation of CMIP, ice-sheet, and glacier models. Figure from IPCC 2021

Due to past and future greenhouse gas emissions many changes in the ice sheets, oceans, and global sea level will be irreversible for centuries to millennia (DeConto et al. 2021). Curbing emissions can only slow the warming trend so much and with each degree of additional warming the changes in extreme climate events becomes larger. Glaciers and ice sheets globally are committed to melting for decades to come and are irreversible on centennial time scales. This means that regional mean relative sea level will continue to rise throughout the 21st century except for areas with substantial geologic land uplift. Relative to the time period between 1995 and 2014, mean sea level rise is predicted to be between 0.28 m and 0.55 m by 2100 under the lowest greenhouse gas emission scenarios (IPCC 2021). Under the highest

greenhouse gas emission outcomes, which the globe is currently on track to meet, by 2100 the mean sea level has the potential to increase by over a meter. Due to uncertainty in ice sheet processes, a sea level rise of 2 m by 2100 and 5 m by 2150 cannot be ruled out. Over the next 2000 years sea level could rise as much as 22 m with 5˚C (**Fig. 3**) of warming due to continuing deep ocean warming and ice sheet melt (IPCC 2021). The uncertainty surrounding the implications of Greenland Ice Sheet discharge on the amount of sea level increase in the coming centuries highlights the need for continued research surrounding the dynamic glacier and ice sheet processes. This will have untold implications for ~40% of the world's population as they live within 100 km of the coast.

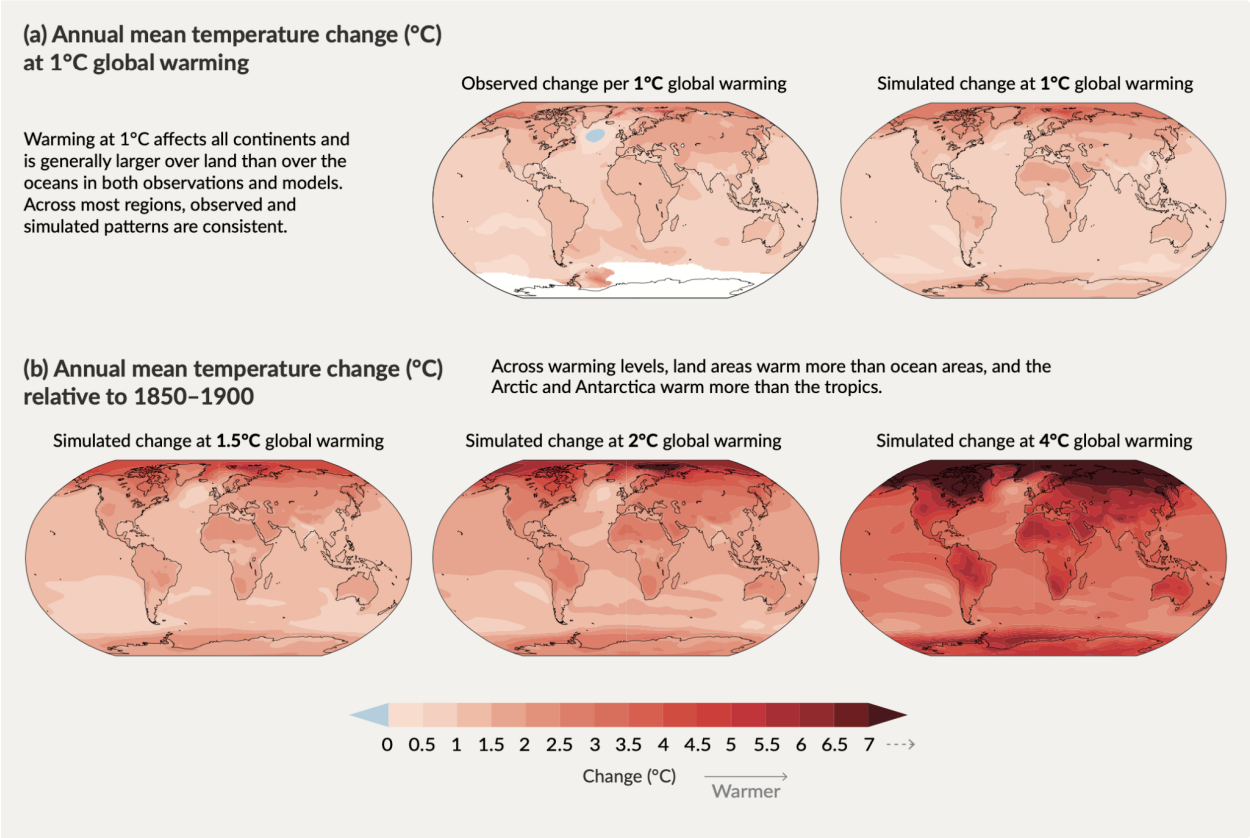

Figure 3: Changes in annual mean surface temperature.

Panel (a) Comparison of observed and simulated annual mean surface temperature change. The left map shows the observed changes in annual mean surface temperature in the period 1850–2020 per °C of global warming (°C). The right map is based on model simulations and shows change in annual multi-model mean simulated temperatures at a global warming level of 1°C (20-year mean global surface temperature change relative to 1850–1900).

Panel (b) Simulated annual mean temperature change (°C) at global warming levels of 1.5°C, 2°C and 4°C (20-year mean global surface temperature change relative to 1850–1900). Simulated changes correspond to Coupled Model Intercomparison Project Phase 6 (CMIP6) multi-model mean change (median change for soil moisture) at the corresponding global warming level, that is, the same method as for the right map in panel (a). Figure from IPCC 2021.

1.3 The Greenland Ice Sheet

The Greenland Ice Sheet (GrIS) is the second largest continuous body of ice in the world, after the Antarctic Ice Sheet, with a total sea level potential of 7.42 ± 0.05 m (Morlighem et al. 2017). GrIS is ~12% of the ice volume of Antarctica but covers a total area of 1.71 x 10^6 km^2 which is roughly 80% of the Greenland land mass (IMBIE Team 2020). At its thickest GrIS is over 3 km, with a majority thickness of ~2 km. There has been a continuous presence of ice sheets covering Greenland for the past 18 million years . This is determined through the presence of ice rafted debris and sediments recovered from deep sea coring in areas from northeast Greenland, the Fram Strait and south of Greenland (Thiede et al. 2010). GrIS was formed during the middle of the Miocene by the merging of smaller ice caps and glaciers across Greenland (Thiede et al. 2010). The formation occurred in association with the uplift of the East and West Greenland uplands; the creation of these mountains would have allowed cooling at the land surface as well as increasing the orographic precipitation of the area (Solgaard et al. 2013). The oldest ice found within the current ice sheet was formed approximately 1 m.y.a. (Yau et al. 2016). The Late Pliocene saw an intensification of glaciation in Greenland, roughly 3 m.y.a. despite the global average temperature being 2˚C to 3˚C warmer (Robinson et al. 2008), global sea level was 25m higher (Dwyer et al. 2009), and atmospheric CO2 was equal to current levels (NASA n.d.). This is thought to be the start of the major glaciations that define the Ice Age of the Pleistocene that starts ~2.6 m.y.a. This period of time allowed ~30% of the Earth to be covered in ice at its highest extent. This period also resulted in the Last Glacial Maximum (LGM) occurring in the Northern Hemisphere ~12,000 years ago (Clark et al. 2009).

Anthropogenic climate change has increased global surface temperatures to levels not seen in ~125,000 years (Plach et al. 2018; Tollefson 2021). GrIS has reacted accordingly and has been a major contributor to global sea level rise (Shepherd et al. 2012; WCRP 2018). Increases in the ice sheet surface melt and glacier flow can be directly attributed to oceanic (Holland et al. 2008; Straneo et al. 2013) and atmospheric warming (Hanna et al. 2012), however the degree of the ice sheet imbalance and course this imbalance will cause the ice sheet to go in the future remain uncertain. It is expected that the GrIS will continue to be a major contributor to sea level rise (**Fig 4**).

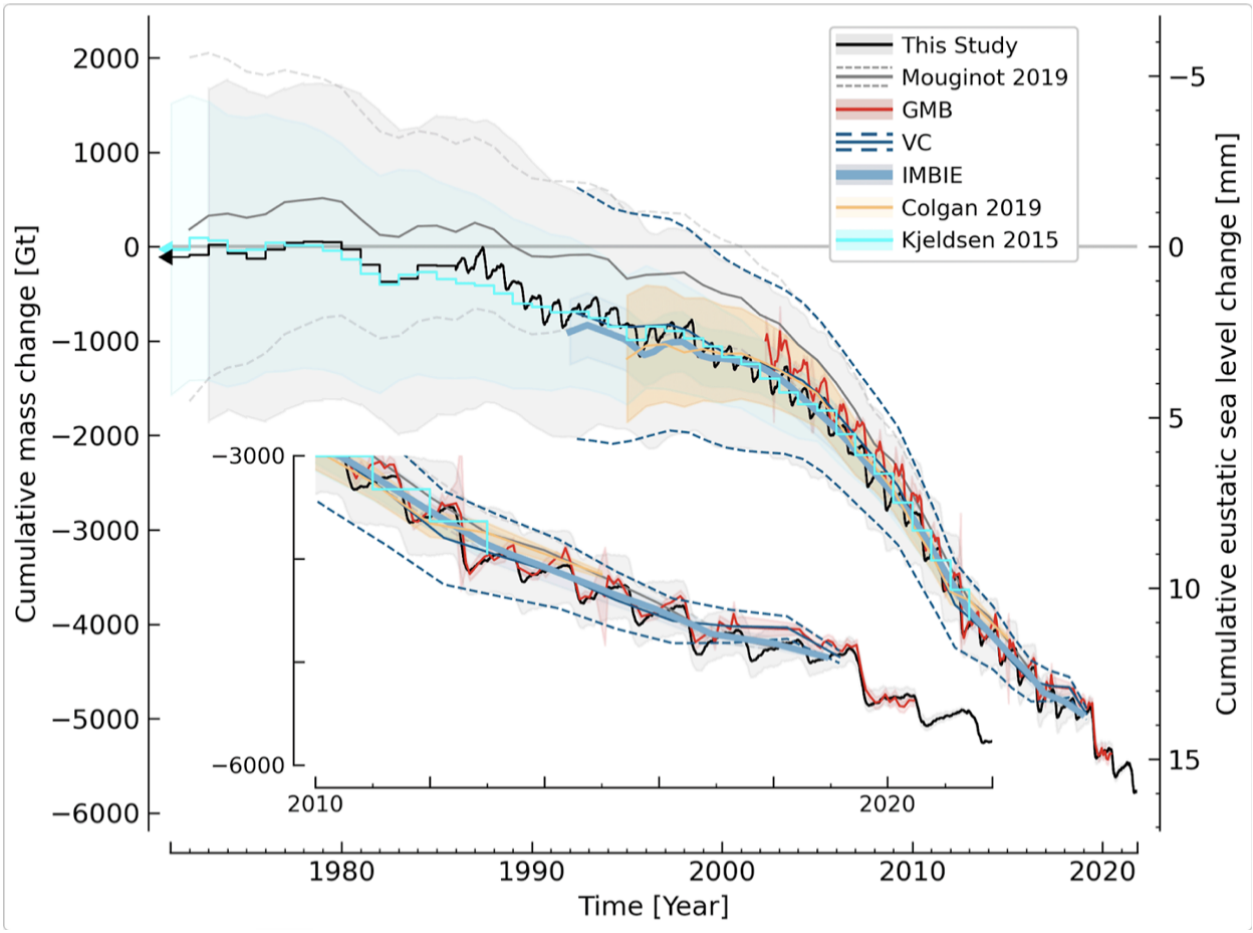

Figure 4: Sea level change as a function of mass.

Comparison between Mankoff et al 2021 and other mass balance time series. Note that various products do or do not include basal mass balance or peripheral ice masses (see Table 2). Mankoff et al. 2021 annual-resolution data prior to 1986 are the Kjeldsen et al. (2015) data adjusted as described in Sect. 5.4. Sea level rise calculated as −Gt/361.8. Inset highlights changes since 2010. Data product version 74 from 25 October 2021 used to generate this graphic. Figure from (Mankoff et al. 2021)

Ice from GrIS flows into the ocean through a series of ice streams, each having a sizable inland catchment area they connect to (Joughin et al. 2010). Fluctuations in the mass of these catchment areas, and of GrIS, occur from the variation in snow accumulation, meltwater runoff, ocean driven melting, and iceberg calving. There have been pronounced increases in air (Fettweis et al. 2017) and ocean (Straneo et al. 2013) temperatures coupled with reductions in summer cloud cover that protects the ice from surface ablation (Hofer et al. 2017). These alterations have produced increases in iceberg calving, glacial terminus retreat, submarine melting, ice flow, surface runoff, supraglacial lake formation, and drainage leading to widespread ice sheet changes, specifically the ice elevation near the ice sheet margin (**Fig. 5**). The rate of ice loss from GrIS has varied significantly between 1992 and 2018. Between 1992 and 2012 the rate of ice loss was increasing and reached a maximum in 2011 at 335 +/- 62

Gt/a (IMBIE Team 2020). This was followed by an extreme summertime melt in 2012. Since 2012 the trend has reversed with a progressive reduction of mass loss to 111 +/- 71 Gt annually by 2018. Ice loss due to increased ice discharge rose dramatically in the early 2000's when Jakobshavn Isbræ (Holland et al. 2008), along with several other glaciers in the southeastern portion of Greenland (Howat et al. 2008), increased their speed and discharge. Between 2002 and 2007, dynamic ice imbalance was the major source of ice loss from the ice sheet as a whole (IMBIE Team 2020). Since then glacial discharge has slowed (Khazendar et al. 2019) allowing the return of increased surface mass loss to become the dominant ice loss method.

The ice sheet reached a close state of balance in the 1990's but annual ice loss has increased since then, peaking in 2011 at 335 +/- 62 billion tonnes per year. Reduction in the surface mass of GrIS has driven 1,971 +/- 55 billion tonnes of ice loss mostly through meltwater runoff. This accounts for about 52% of the regional melt. The remaining 48% of the ice melt was due to increases in glacial discharge around Greenland. This is roughly 1,827 +/- 538 billion tonnes for the period between 1992 and 2018. During this time, the annual ice discharge amount rose from 41 +/- 37 billion tonnes per year in the 1990's to 87 +/- 25 billion tonnes per year. Satellite measurements show that ice loss from Greenland increased annually from 51 +/- 65 Gt in the early 1990's to 263 +/- 30 Gt between 2005 and 2010. This means that between 1992 and 2018, GrIS has lost 3,800 +/- 339 billion tonnes of ice. Regardless of the reduction in overall rate of ice loss from GrIS since 2012, the ice sheet mass balance has remained negative and added 10.6 +/- 0.9 mm to global sea level since 1992. The peak contribution was between 2007 and 2012 at 0.75 +/- 0.08 mm/a while typically annual contribution is 0.42 +/- 0.9 mm/a (IMBIE Team 2020).

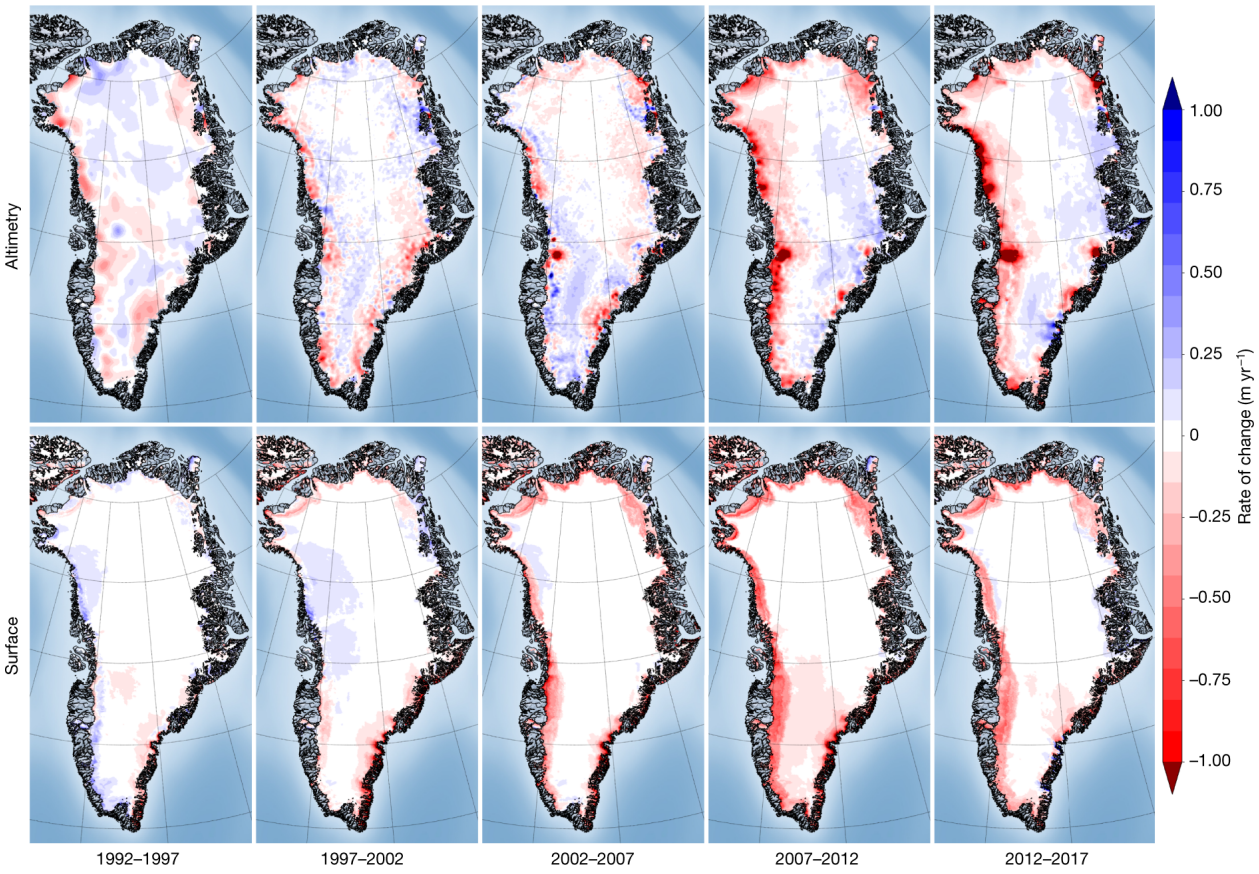

Figure 5: Greenland Ice Sheet elevation change since 1992

Greenland Ice Sheet elevation change. Rate of elevation change of the Greenland Ice Sheet determined from ERS, ENVISAT, and CryoSat-2 satellite radar altimetry (top row) and from the HIRHAM5 surface mass balance model (bottom row, ice equivalent), over successive five-year epochs (left to right; 1992-1997, 1997-2002, 2002-2007, 2007-2012, 2012-2017). Figure from (IMBIE Team 2020)

The calculated cumulative ice loss from GrIS has been close to the IPCC predicted rates of high end climate warming scenarios. The upper range climate scenarios state that by 2100 there is forecasted to be an additional 0.63m - 1.01 m of global sea level rise(IPCC 2021). Greater sea level contributions cannot be ruled out as feedback between the ice sheet dynamics and elements of the climate system could be underestimated by current climate models (Pattyn et al. 2018). Greenland ice losses have been ~36% higher (IMBIE team 2018) than that of Antarctica as consequences of the strong oceanic and atmospheric warming occurring in the Arctic. If the entirety of GrIS was to melt, it would raise global sea levels by 7.4 m (Morlighem et al. 2017). GrIS is expected to continue to be a major source of sea level rise into the future (IPCC 2014). The variability of Greenland ice loss and the impact it has on global sea level illustrates the importance of studies accounting for yearly fluctuations and glacial calving dynamics when attempting to quantify GrIS melt. The Greenland Ice Sheet has experienced an accelerated mass loss from increased glacial ice discharge as well as surface

melting over the past decades (Enderlin et al. 2014) and marine terminating glaciers are a major conduit for mass loss from the ice sheet system (Box et al. 2011; Pfeffer et al. 2008). Changes at the terminus of marine outlet glaciers create variations in the flow speedr by regulating the balance between the driving and resistive forces (Meier et al. 1987), however little is actually known about the driving forces within and under the glaciers (Meier et al.1987; Doyle et al. 2018).

1.4 Store Glacier

Store Glacier is a tidewater glacier terminating into Iserasak fjord located in Uummannaq District of western Greenland and ultimately drains in Baffin Bay (**Fig. 6**), a marginal sea within the North Atlantic (Howat et al. 2010; Walter et al. 2012; Todd et al. 2014). This is a major outlet glacier in Greenland (Walter et al. 2012) and one of eleven marine terminating in Uummannaq Bay (Howat et al. 2010). Store Glacier is furthermore the third largest outlet glacier on the western coast of Greenland following behind Jakobshavn and Rink Isbrae respectively, with a catchment area of roughly 34,000 km^2 or 1.988% of the Greenland Ice Sheet (Rigot et al 2008; (Chauché et al. 2014). The calving front of the glacier is 5.3 km wide with an aerial freeboard of up to 110 m.a.s.l. (Ahn et al. 2010; Ryan et al. 2015a) and a grounded depth in excess of 540 m roughly 1 km south of the glacial centerline. The calving front is defined by a sequence of two or three headlands and embayments that are caused by localized meltwater plume induced melting (Chauché et al. 2014). Modeling of Store Glacier shows submarine melt rates of the terminus may be upwards of 8 m/d due the large amounts of subglacial runoff being discharged (Todd et al. 2014; Xu et al. 2013). The high melt rates can be attributed to warm, ambient water in the fjord being entrained into the buoyant meltwater plumes which rise rapidly along the glacial face from 490m b.s.l.(Chauché et al. 2014; Jenkins 2011). Uummannaq fjord is the only fjord system in western Greenland that has an over-deepened trough of sufficient depth to allow the intrusion of warm oceanic saline sub-polar mode water directly to the ice sheet margin disrupting the energy and mass balance of Store Glacier (Chauché et al. 2014).

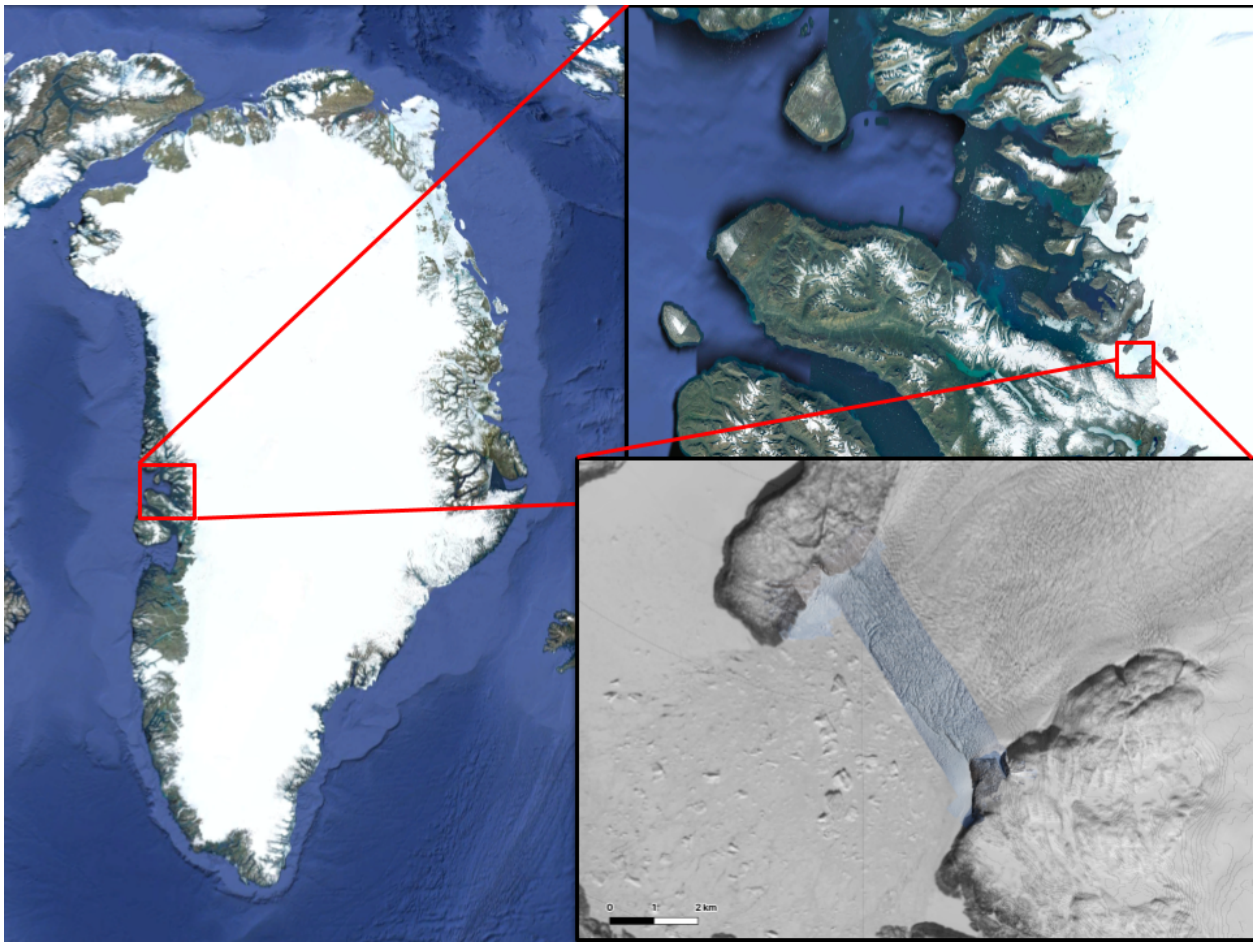

Figure 6: Location of Store Glacier, Western Greenland

Store is located in the Uummannaq District in Iserasak fjord and typically has a large ice mélange field in front of it during the winter months. The third photo in the series shows the 0.5m DEM collected in the beginning of May, 2014 overlaying the LandSat8 imagery collected during the same period of time.

The floating ice tongue of Store Glacier has thinned at a rate of roughly 1m/a since 2002 (Pritchard et al. 2009; Helm et al. 2014). However, compared to other large marine terminating glaciers in Greenland, the terminus of Store Glacier has remained stable over roughly the last century. Continued aerial photography from 1948 (**Fig. 7**) reveals a relatively stable glacial terminus (Weidick et al. 1995) resulting from a pronounced basal pinning point (Todd et al. 2014; Young et al. 2019). Seasonal fluctuations show a +/-200 m change in the position of the terminus (Howat et al. 2010; Young et al. 2019) with increased advance and retreat observed in the spring between April and June. This has been linked to the breakup of seasonal mélange which is speculated to drive increased rate of calving (Walter et al. 2012; Howat et al. 2010). The proglacial mélange typically forms in the late January or early February (Howat et al. 2010) and is proposed to exert significant backstress on the calving

terminus of Store Glacier (Todd et al. 2014; Walter et al. 2012). This effectively bookends the calving process and promotes a winter advance. Once the mélange fragments an abrupt increase in calving rate appears to drive frontal retreat to a more stable position less than a kilometer up the fjord.

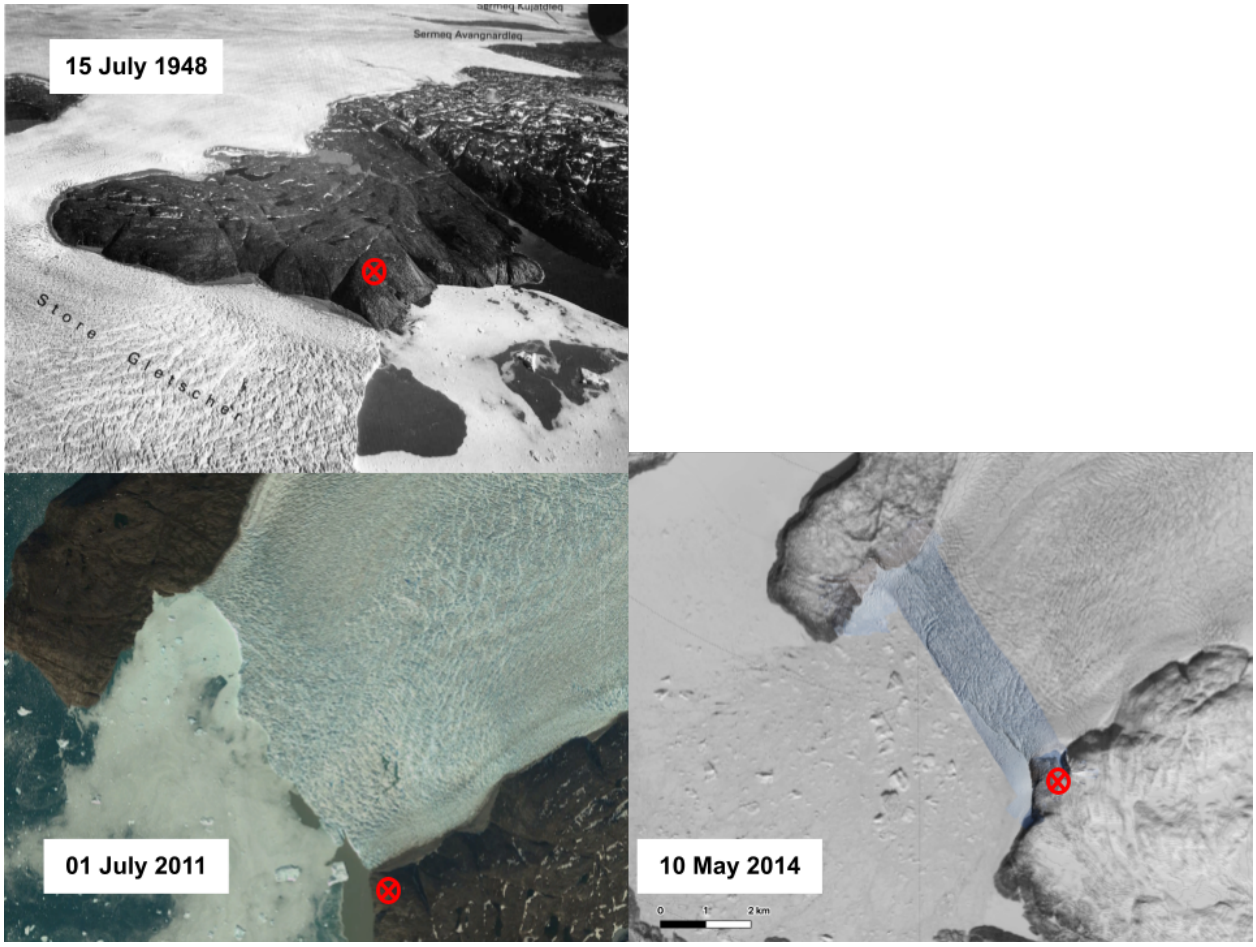

Figure 7: Aerial and satillite imager through time.

The first image was an aerial image taken in 1948 by the Danish National Survey and Cadastre (NSC) looking southeast (Weidick et al. 1995). All subsequent photos were taken by the LandSat program. In every photo series it is possible to easily view that the southern terminus of Store Glacier has changed little since 1948. In each of the LandSat images it is also possible to observe the stable position of the northern portion of the terminus and the near identical terminus profile. The red dot corresponds to the same point on the southern bedrock prominence in all three pictures.

Several in depth studies have been conducted on Store Glacier within the last 15 years in order to more accurately quantify the dynamic forces acting on the glacier. Their aim has been to make more accurate predictions of how Store Glacier will react to future climate change as well as understand why the glacier has not undergone significant retreat or thinning like other Greenland outlet glaciers. One of the earlier studies was conducted in the spring and summer of 2008 in order to examine the influence of sub-daily variations in the breakup of

the proglacial mélange , fluctuations of the tides and calving dynamics (Walter et al. 2012). This used data from seismometers, GPS, time lapse cameras, and a meteorological station set up on the ice. The resultant data displayed two modes of oceanic forcing on the horizontal speed of the glacier. These were the tidal variations and the presence or absence of the proglacial mélange . Flow speed from GPS measurements shows both semi-diurnal and diurnal peaks. The semi-diurnal peaks correspond to the local changes in tide providing evidence that would support the theory that tides can influence flow at least ~16km from the terminus where the GPS station was located (Walter et al. 2012). The glacier would be expected to additionally undergo a rapid flow response to melt lubrication in the form of basal pressurization that lasts for ~10 days. Drainage efficiency increases to the point at which basal pressurization is lost abruptly followed by a lack of correlation between horizontal glacial speed and surface melt and instead becomes characterized by sustained correlation with the semi-diurnal tidal forcing. Furthermore a terminus acceleration of ~1.5m/d over a two day period occurs after the disintegration of the abutting mélange . From this change in velocity, Walter et al. theorizes that the mélange provides ~30-60 kPa of backstress upon the terminus of the glacier, holding the terminus in place. Observations after the mélange move out show a synchronicity between flow speed, minimum ocean tidal range, and the surface air temperature. This study also showed that after the mélange has been removed glacial calving and the flow speed ~16 km upstream occur in nearly synchronous perturbations signaling an increased period of susceptibility to calving and that possibly the mélange reduces longitudinal stretching (Walter et al. 2012)(**Fig. 8**).

Using MODIS, imagery 39 marine-terminating glaciers were assessed to determine the changes that had occurred to each between 2000 and 2010, and aid in quantifying overall discharge from the Greenland Ice Sheet (Box et al. 2011). It was determined that between all the glaciers, 1368 km^2 of ice area was lost with 75% of the area change occurring above 72˚N. The count of glaciers retreating is twice that of those advancing. Additionally for glaciers with ice shelves there was no collective area gain. Store Glacier was found to be one of the most productive West Greenland calving glaciers, and that there was a 2.5 km terminus advance between 2000 and 2010. The extent of the terminus advance will be challenged in further studies. Using the yearly glacial area change from Box et al. 2011 the average area change for the 10 year period was calculated to be 0.4 km/a with an effective length increase of 0.1 km/a. The maximum annual retreat was the 2008 / 2009 melt season with a loss of 2.8

km^2 while the maximum annual advance occurred the previous season, 2007 / 2008, with an increase of 4.9 km^2 (Box et al. 2011).

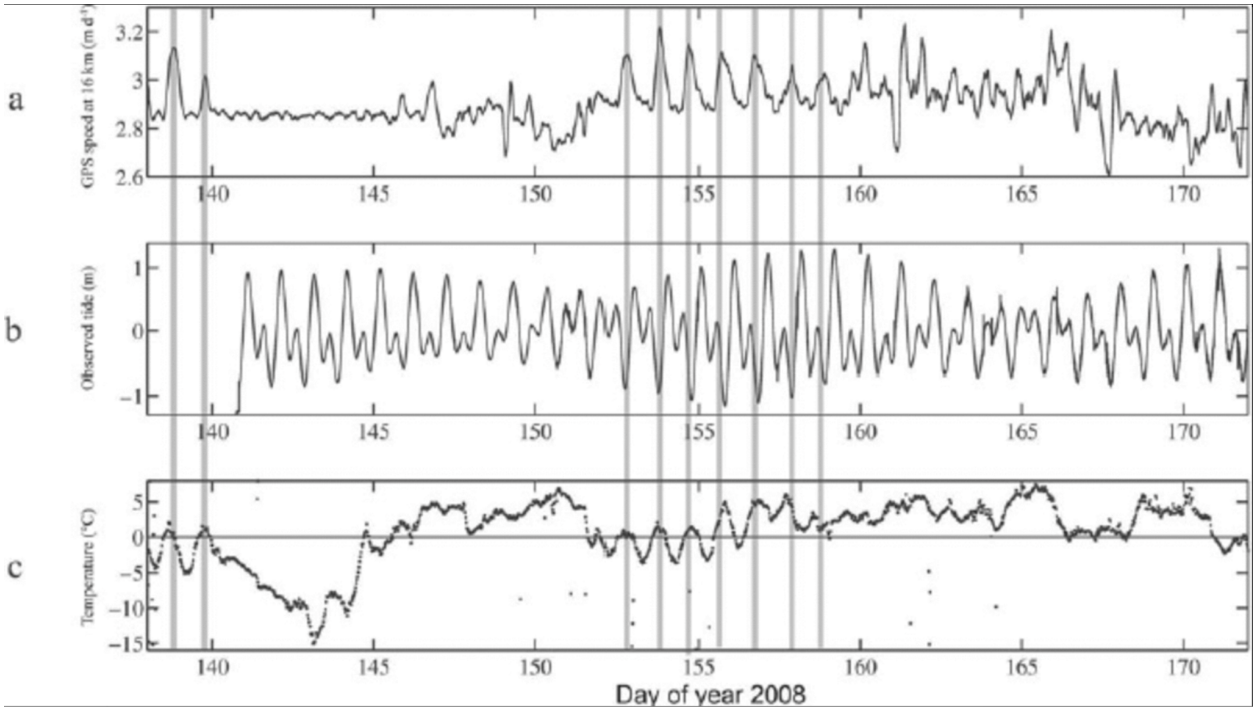

Figure 8: 2008 measurements of upstream terminus forcing.

Measurements during days 140–170 of (a) ice flow speed, from the on-ice GPS stations ~16km from the terminus, (b) measured tide in the fjord and (c) air temperature measured at an AWS co-located with the GPS station. Figure taken from (Walter et al. 2012)

Following this publication, a study modeling the melting of Store Glacier was conducted using high resolution ocean circulation modeling with the results compared to oceanographic data. The oceanographic data disclosed three major water masses in front of the terminus: relatively warm and fresh surface water; cold polar water at an intermediate depth, and warm Atlantic water below a 300m depth (**Fig. 9**). This allows for a calculated melt water flux of 93 +/- 31 m^3/s or ~3.0 +/- 1.0 m/d averaged over the whole hydrographic section. The subglacial freshwater discharge of the entire glacier is estimated to be 246 +/- 45 m^3/s which compares well with the Regional Atmospheric Climate Model value of 300 +/- 27 m^3/s for August of 2010 (Xu et al. 2013). Simulations across the terminus of the glacier show turbulent upwelling as well as spreading of a freshwater plume along the ice face coupled with robust melting on the rates of meters per day. Following the release of buoyant subglacial melt at the grounding line, the ascending flow quickly becomes turbulent and entrains ambient seawater while expanding laterally. Once it reaches a neutral buoyancy it flows horizontally away from the ice. The melt rate is greatest in the region immediately above the subglacial channel. This

is simultaneously where turbulent mixing is most effective. The melt rate decreases away from the plume core. Using modeling and a melt rate of 1 m^3/s the plume reaches a neutral buoyancy at 320 m depth where it then spreads laterally. Using a higher discharge rate (5 m^3/s) means the plume reaches neutral buoyancy at 160 m, however the inertia causes it to ascend to 100 m before sinking back to neutral buoyancy. Increasing the discharge rate also increased the calculated melt rate to 6 m/d under the same scenario, or 8 m/d under exceedingly high discharge rates (≥30 m^3/s) with fractions of the meltwater plume upwelling to the surface. The simulated melt rate for August of 2010 was 2.0 +/- 0.3 m/d which is within the uncertainty of the 3.0 +/- 1.0 m/d melt rate calculated from oceanographic data (Xu et al. 2013). It is shown that the melting is greatest at depth causing undercutting above the subglacial channels and that the average melt rate increases in conjunction with an increase in subglacial freshwater discharge and ocean thermal forcing. The melt rates are shown to increase proportionally to thermal forcing by a power of 1.2 - 1.6 and to subglacial water flux by a power of 0.5 - 0.9 showing that ocean induced melting and melting from subglacial discharge may increase in a warmer climate.

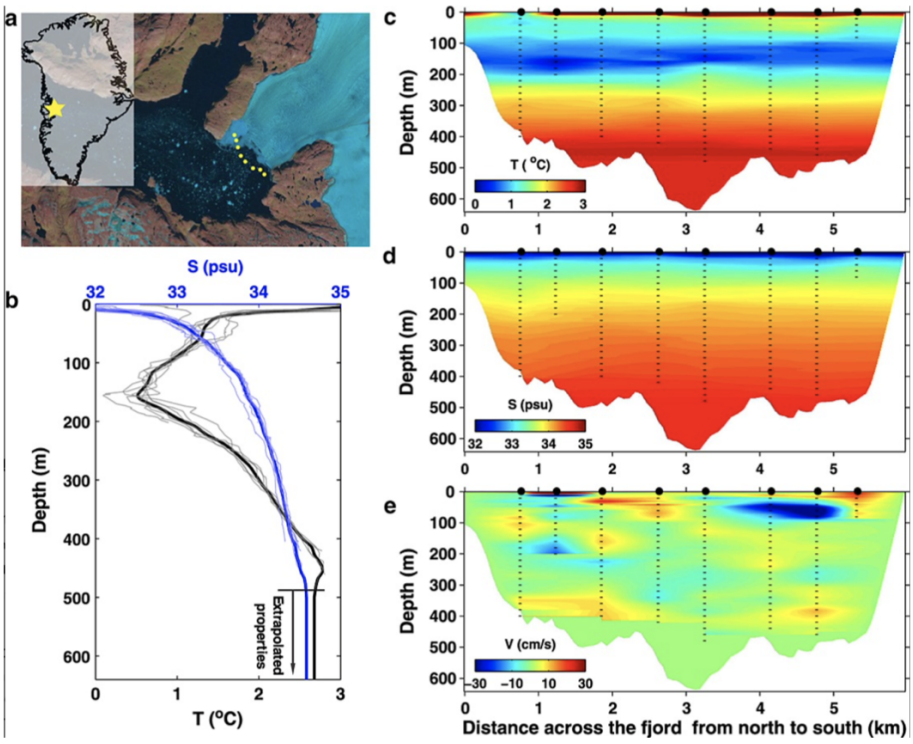

Figure 9: Water profile measurements across the terminus of Store Glacier

(a) LandSat-7 image of Store Glacier fjord with yellow dots at the location of the survey stations in August 2010, (b) T and S profiles (light lines) averaged and extrapolated to the sea floor (bold lines), (c) potential temperature (T), (d) salinity (S), and (e) water speed (V) across the hydrographic section. Positive speed indicates water moving toward the ice. Points below the seafloor are colored white. Each hydrographic station is indicated by a dot in Figures 1c–1e at 0 depth, and dash lines show the depth of the measurements. Figure taken from (Xu et al. 2013)

An additional study was published in 2016 again using the MIT General Circulation model, this time to calculate the subaqueous melting and calving rates from 1992 to 2015. This study varies slightly from Xu et al. 2013 as the effective ocean induced melt speed is the horizontally averaged maximum rate of ice melt and not the area averaged ice melt rate due to melt rate not being uniform with depth. It was determined that subaqueous melt rates are 2 - 3 times higher in the summer months as compared to winter and that since the 1990's had doubled in magnitude. This was primarily due to enhanced glacial runoff and a 1.6 +/- 0.3˚C warmer ocean temperature. In contrast to several glaciers in the study, Store Glacier remained stable due to the subaqueous melt rate being 3 - 4 times lower than the calving rate, meaning that the glacier is dominated by calving processes at the terminus (Rignot et al. 2016). The winter subglacial discharge of Store Glacier was determined to be 13 m^3/s. This is occurring when there is no runoff from the glacier. In the summer this is several magnitudes larger, with a discharge rate of 890 m^3/s, averaging 99 m^3/s for the year. This peaked in 2012 at 3.0 +/- 0.8 m/d but slowed again for the 2013 - 2014 melt season. In the 22 years that were observed, subglacial melt has increased by 2.6 $m^3/s/a$ which is a 58% increase. In that same period thermal forcing at Store Glacier increased from 2.6˚C to 4.1˚C according to the simulation carried out by the Estimating the Circulation and Climate of the Ocean, Phase II (ECCO2). As a result of the increased thermal forcing and subglacial flux at the terminus of Store Glacier, ocean induced melt speed increased from 0.8 m/d to 1.2 m/d in the winter and the summer rate increased from 1.5 m/d to 2.8 m/d. This shows that the average melt rate nearly doubled from 0.9 m/d to 1.6 m/d annually. The terminus speed from 1992 to 2014 however remained at 5.2 +/- 0.3 m/d and showed no temporal trend throughput that period. Additionally the terminus did not vary in position by more than +/- 230m since 1992, despite the increase in ocean induced melt speed the calving rate as well as ice speed have remained stable (Rignot et al. 2016). It is thought that this is due to the fact that the effective ocean induced melt speed is 2-3 times lower than the average glacier terminus speed. This means that the calving rate breaks off the frontal ice before the undercutting has a chance to really affect glacial dynamics. If the ocean induced melt and subglacial discharge increased by 50% (Rignot et al. 2016) then the melt rate could be increased enough to induce glacial retreat.

The conditions that facilitate the fast flow of Store Glacier remain poorly constrained and limited, despite the significant contribution the glacier can have on sea level rise. In order to better understand these, Doyle et al. 2018 drilled and instrumented several boreholes 30 km from the glacial terminus to monitor subglacial water pressure, temperature, electrical

conductivity, turbidity, englacial temperature and ice deformation (**Fig. 10**). The borehole data was used in conjunction with surface velocity and meteorological data to better gain insight into the mechanisms of the glacier. Upon each borehole reaching 600 m, each drained rapidly indicating that they all had direct connection to an active subglacial hydrological system. Continually high subglacial water pressures indicate a low effective pressure between 180 - 280 kPa. Small amplitude variations occurred with noticeable peaks in the surface velocity of the glacier driven by diurnal melting, rainfall, and prolonged periods of melt. Englacial deformation from borehole tilting indicated that 63 - 71% of total ice motion occurred at the bed with the remaining 29 - 37% attributed to enhanced deformation in the lowermost 50 - 100 m of the ice column. This would indicate that 88% of the motion observed at the ice surface was in fact caused by basal movement of the glacier. From the deformation results it was determined that the lowermost 100 m of glacial ice to be formed from warmer, pre-Holocene ice that is overlying 0 - 8 m of temperate basal ice (Doyle et al. 2018).

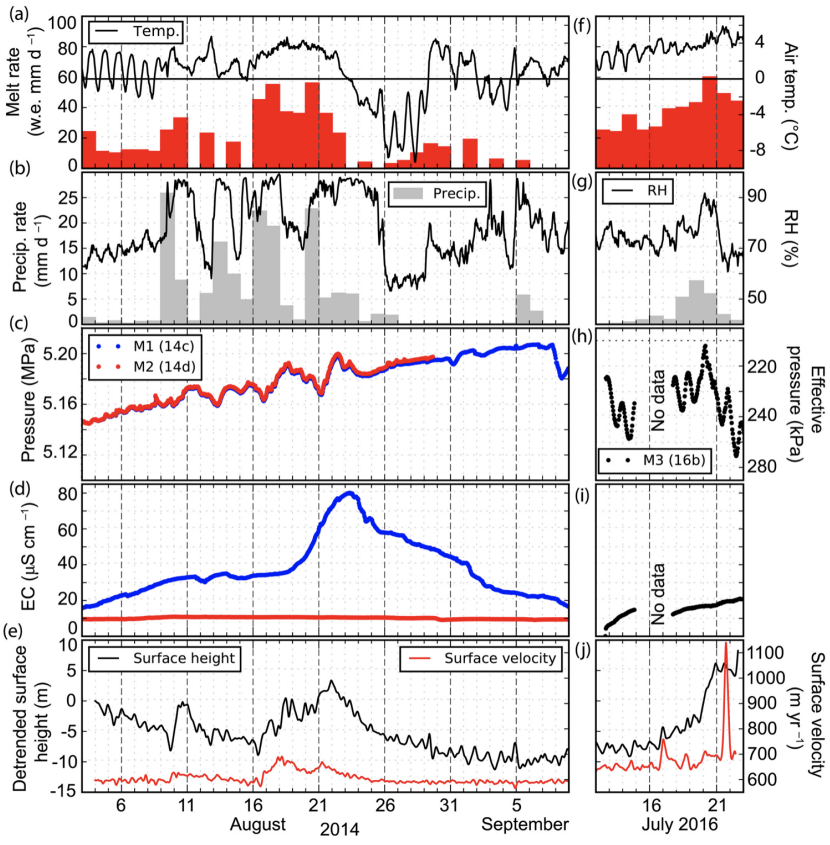

Figure 10: Time series of data collected 30 km upstream of the terminus of Store Glacier

Time series of (a) near-surface air temperature and melt rate, (b) precipitation rate and relative humidity, (c) subglacial water pressure and effective pressure, (d) EC, and (e) horizontal surface velocity and linearly detrended surface height in 2014. (f–j) Same as Figures 9a to 9e but for 2016. Figure taken from (Doyle et al. 2018).

The diverse nature of glacial calving and its complex correlation between internal glacial dynamics and climate make it challenging to incorporate in glacial and ice sheet modeling (Todd et al. 2018). Calving dynamics are poorly understood due to several reasons. Firstly calving encompasses fracture processes that span a range of spatial and temporal scales that vary based on the size and location of the glacier. They are diverse in their environmental setting and the flow is largely controlled by the processes and conditions occurring at the ice ocean interface and at the bed of the glacier. This makes both of these hard to observe let alone quantify. Crevasse depth calving criteria suggests that glacial calving will occur when surface crevasses reach sea level allowing water infiltration at which point hydrofracturing drives the crevasse through the glacial thickness. This process can occur even at cold based glaciers due to the heat exchange between the intrusion of proglacial water and glacial crevasses preventing freezing (Benn et al. 2007). Additionally calving can occur when surface and basal crevassing collectively fracture the entire ice thickness near the terminus (Nick et al. 2010).

Todd et al. 2018 used a 3D approach to realistically model the evolution of the calving front through time (**Fig. 11**) using both crevasse depth criterias as aerial photography has shown that a small number of Store Glacier's crevasses are water filled during the summer (Ryan et al. 2015a). This allowed better constraints on terminus force imbalance due to buoyancy, effect of lateral stress bridges, or environmental aspects such as undercutting of the ice by submarine melting. Store Glacier has a catchment area that extends 280 km inland to the ice divide with a maximum width of 50 km, narrowing to ~5 km at the terminus and a velocity typically peaking at 16 m/d (Todd et al. 2018). Modeling results taking into account only distributed and concentrated submarine melting show a seasonal advance and retreat of the mean terminus position by roughly 200 m. In order to accurately model the dynamics of Store Glacier and the mélange a 120 kPa pressure was applied to a thickness of 140 m for the terminus. This resulted in a 500 m advance of the terminus each spring followed by a rapid retreat when the mélange disappeared. Modeling with the mélange additionally resulted in the calving of a large tabular iceberg once the buttressing force was removed. Removal of the proglacial mélange in the model was the only parameter that was able to influence the terminus velocity showing that the modeled mélange exerts the greatest influence on the seasonal terminus dynamics (Todd et al. 2018). Without the seasonal mélange the ice velocity peaks in the early summer at 5,100 m/a before late summer deceleration brings the speed to 4,200 m/a. Following this the velocity again increases into the winter back to the

spring peak. With the ice mélange in place in February the terminus rapidly slows from 4,800 m/a to 4,150 m/a after which it gradually increases velocity until the end of May when the buttressing force is removed. At this point there is an equivalent rapid increase in ice flow at the terminus. Using the model with no calibration or tuning showed that iceberg calving dominated modeled terminus mass loss.

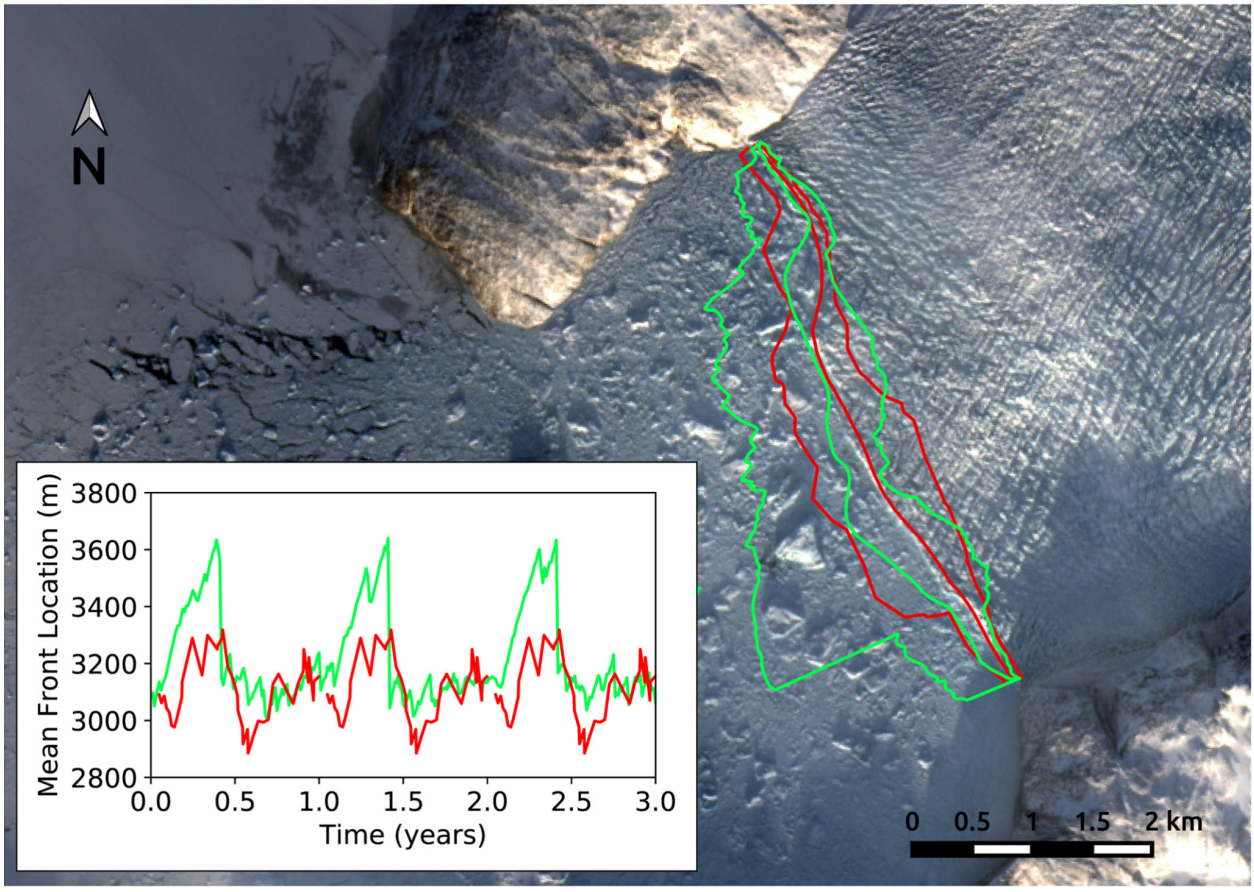

Figure 11: Modeled and observed terminus position from 2014

Modeled (green) and observed (red) maximum, mean and minimum terminus position as overlaid onto LandSat imagery. The positions are then graphed through time. Mean model positions are from the "present-day" simulation (Run 111), and observed positions from 2014 are repeated annually to allow for visual comparison. Figure taken from (Todd et al. 2018)

Of the 8.96 Gt of ice lost from the terminus annually, 74% is from calving with another 20% through distributed melting (Todd et al. 2018). The influence of the mélange reduces the calving rate from approximately 10 Gt/a to less than 1 Gt/a at the start of the mélange season. As the terminus advances the modeled calving rate gradually increases resulting in the gained mass through the mélange season rapidly decreasing once the mélange is gone. In the absence of ice mélange or submarine melting the modeled terminus calves predominantly large icebergs with no seasonal trend and a persistent floating tongue to the south (Todd et al. 2018). Results from the modeling of the proglacial mélange further suggest that the

stabilizing influence extends beyond the mélange season due to the deceleration and dynamic thickening of the terminus. Terminus thickening stabilizes the ice front against increased melting in the summer. This however does not protect against submarine melting inhibiting the formation of a permanent floating ice shelf or concentrated plume melting having a disproportionately large and destabilizing effect by breaking stress bridges and promoting iceberg calving (Todd et al. 2018).

Studies targeted over Store Glacier during the last ~15 years have revealed a range of factors at play determining its relative stability and inter-annual dynamic behavior. Semidiurnal velocity peaks ~16 km from the glacial terminus demonstrate the forcings are translated longitudinally through the ice mass (Walter et al. 2012; Todd et al. 2018) and that subaqueous melt rates increase from discharge rate of 13 m^3/s in the winter by several magnitudes during the summer to 890 m^3/d. Additionally subglacial melt has increased by 2.6 $m^3/s/a$ between 1992 and 2015. Despite this and an increase in ocean induced melt, the terminus speed remained stable at 5.2 +/- 0.3 m/d between 1992 and 2014 (Rignot et al. 2016). Borehole data 30 km from the terminus provided evidence for an active subglacial hydrological system below 600 m and borehole deformation indicated that 88% of observed surface motion is caused by basal movement (Doyle et al. 2018). Terminus velocity changes and modeling suggests that the mélange exerts ~30 - 120 kPa across the thickness of the glacier (Walter et al. 2012; Todd et al. 2018) allowing the seasonal growth of Store Glacier. This thesis examines the glacial calving dynamics of Store Glacier, and the corresponding upstream glacial response in unprecedented detail. This knowledge will advance the understanding of why Store Glacier has not undergone a large-scale retreat like that of other primary GrIS outlet glaciers as well as what controls the stability of Store Glacier and how it could respond to future climate forcing. Furthermore this thesis will provide a valuable empirical dataset for constraining calving models, which are currently limited by poorly resolved temporal and mechanical understanding.

1.5 Seasonal Proglacial Ice Mélange

The terminus of Store is abutted by an ice mélange that typically forms in the latter part of January or February (Howat et al. 2010) and reaches a peak extent in late April, disappearing between mid-May and early June (Walter et al. 2012; Howat et al. 2010)(**Figure 12**). The ice mélange is a dense conglomerate of icebergs, brash ice, and sea ice (Amundson et al. 2020)

forming when ocean currents or surface winds are unable to effectively expel icebergs from the proglacial fjord (Amundson et al. 2020; Burton et al. 2018). The icebergs trapped in the mélange matrix constitute some of the world's largest granular clasts ranging in size from 10-1000m (Burton et al. 2018) and thickness may vary by hundreds of meters depending on iceberg concentration (Walter et al. 2012). Ice mélange formation in the Uummannaq district of Western Greenland appears to form only when both the air and water temperatures in the fjord are low enough to permit growth of a thick sea ice matrix in the interstitial gaps between the icebergs (Burton et al. 2018; Walter et al. 2012; Amundson et al. 2020). Several studies in western Greenland determined that the mélange in the area acts as a poorly sorted, granular ice shelf (Xie et al. 2019; Cassotto et al. 2015; Amundson et al. 2010; Burton et al. 2018) due to the transmitted stresses on the glacier terminus as well as the influence it can have on iceberg calving and the water column of the proglacial fjord.

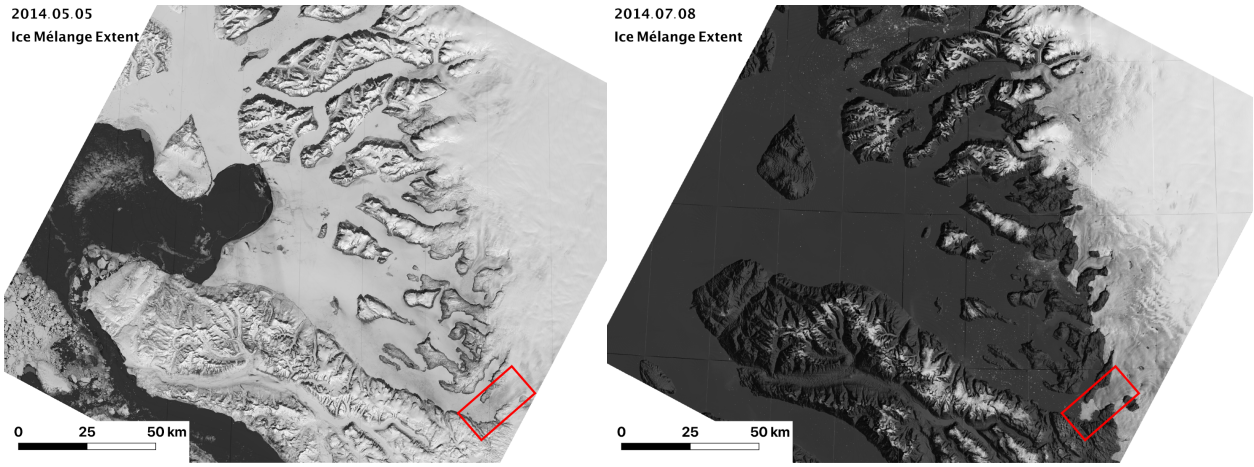

Figure 12: Proglacial mélange extent for the spring of 2014

LandSat8 imagery from 5 May 2014 and 8 July 2014 showing the extent of the mélange at the beginning of the study period to the period when it was observed to be evacuated from the fjord around Store, outlined in red. In the imagery from July the debris plume from extruded ice is visible in the proglacial fjord. The position of the terminus in both images show that it remained stable in the same position even after the breakup of the mélange .

Iceberg calving rates are often well correlated with the formation and breakup of the ice mélange , having a small increase in glacial velocity occurring after the mélange loses strength (Amundson et al. 2020; Howat et al. 2010; Amundson et al. 2010; Xie et al. 2019; Walter et al. 2012). The ice mélange is pushed down fjord during winter glacial advance roughly at glacial flow speed (Amundson et al. 2020) suggesting that the mélange is also pushing back on the calving front with a similar resistive buttressing force. This can be observed through the deformation of the ice mélange and formation of shear bands along the

fjord margins (Joughin et al. 2008; Burton et al. 2018; Amundson et al. 2020). The roughness of the fjord walls provides an anchor for the granular structure of the mélange and are responsible for the primary resistive stress impeding the mélange flow (Burton et al. 2018)(**Fig. 13**). Further resistive force is provided by the grounded icebergs that are trapped within the matrix. These act as grounding pylons within the ice, constricting the fjord and providing basal drag to the floating parts of the mélange. The resistive force exerted by the ice mélange does not need to be extensive in order to bind together the heavily fractured glacial terminus (Amundson et al. 2010) or to inhibit large icebergs from capsizing (Burton et al. 2018). The mélange 's ability to constrain calving events depends not only on the thickness and extent of the mélange or the amount of icebergs entrapped within it, but also on the fjord geometry (Amundson et al. 2020). Modeling conducted by both Burton et al. 2018 and Amundson et al. 2020 suggest that the resistive forces from the mélange may become enough to influence the terminus calving rates when the length to width ratio of the ice mélange is greater than 3 (Amundson et al. 2020; Moon et al. 2015) possibly explaining some of the variation between proglacial mélange in fjord systems of similar regions.

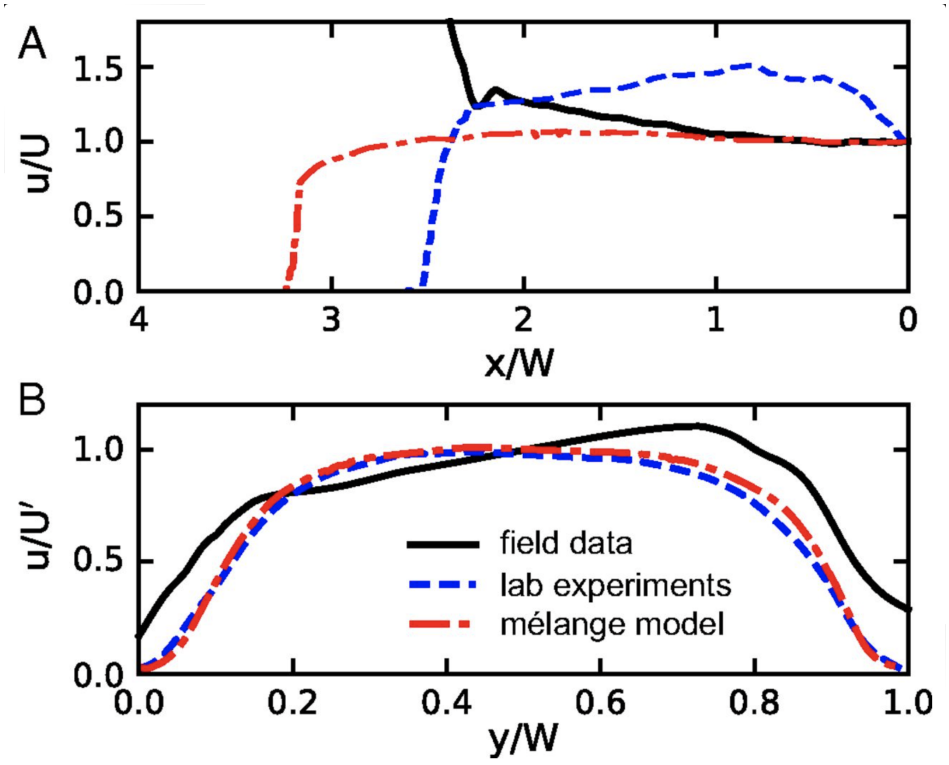

Figure 13: Longitudinal and lateral glacial velocity from data, expirements, and modeling

(*A*) Time-averaged longitudinal velocity profiles taken along the middle of the fjord (y=W/2). The velocity is normalized by the terminus velocity at x=0. (*B*) Time-averaged transverse velocity profiles across the fjord. There is no slip along the walls of the fjord at y/W=0 and y/W=1. Figure taken from (Burton et al. 2018)

The proglacial mélange has further indirect effects on glacial systems through its impedance or alteration of the fjord dynamics. Ice mélange alters the spatial distribution of buoyant forcing through the concentration of meltwater fluxes near the glacial terminus (Amundson et al. 2020) by trapping calved icebergs. These are a major source of freshwater within the fjord (Burton et al. 2018; Moon et al. 2018). Not only can this affect the buoyant forces, it also alters the salinity of the water column near the glacial terminus. The presence of mélange can influence the circulation patterns within the fjord (Walters et al. 1988). The roughness seen from above is also translated below the waterline with grounded icebergs providing barriers that would direct currents throughout the water column. The irregularity of the basal topography imparts drag on the fjord currents (Amundson et al. 2010) thereby altering the heat transport (Amundson et al. 2020; Truffer et al. 2016) to the glacial terminus. Disappearance of the proglacial mélange would not only change calving dynamics by altering the force balance but would allow the inclusion of warmer ocean currents to more easily influence the subglacial terminus melt systems.

2 Research Questions

The overarching aim is to determine and quantify the primary controls on calving and flow dynamical processes across the marine terminus of Store Glacier, Uummannaq Embayment to better understand the mechanics of Store Glacier, and by inference the behavior of Greenland's tidewater outlet glaciers and how they are responding to climate change. Implicitly underlying this primary aim are two key research questions that emerge from review of published literature: First, why has the terminus of Store Glacier not undergone a large-scale retreat similar to Greenland's other primary marine outlet glaciers? Second, what controls that stability and how may Store Glacier respond to future atmospheric and oceanic forcing?

These overarching research questions will be addressed by testing the following hypotheses based from our current understanding of the Store Glacier system:

1) How does topographic configuration impact calving dynamics and glacier stability?
2) To what extent is the terminus of Store Glacier buoyant or grounded on its bed?
3) What are the key controls on the seasonal frontal dynamics of Store Glacier?
4) What controls the frequency and magnitude of calving events at Store Glacier?
5) How do frontal calving processes impact on both local and upstream flow dynamics?

3 Data and Methods

In order to properly answer these, several different data sources have been collected and analyzed. The main dataset is from repeated unmanned aerial vehicle (UAV) surveys across the terminus of Store Glacier and was collected between May and July 2014. This consisted of several thousand overlapping, geotagged images of the terminus at a ground sampling distance of roughly 0.4 m. Processing of these images also allowed for creation of high resolution orthophotos and digital elevation models (DEMs) having a vertical accuracy of +/- 1.9 m (Ryan et al. 2015b). This will be coupled with meteorological data that was collected

via an autonomous weather station (AWS) set up at the terminus of Store Glacier in May of 2014 and Danish Meteorological Data collected from the Qaarsut weather station that became operational in November of 2000. The primary analysis will focus on the localized temperature trends. Finally using the BedMachine(version 3) data the impacts of the fjord bathymetry can be investigated.

Topographic configuration of the fjord is key to understanding the stability of Store Glacier. BedMachine data allowed for the creation of a calculated mask layer showing where the terminus ice is floating or basally pinned. This data can then be paired with the UAV-derived ice-surface elevation data and bathymetry to show section profiles across the terminus of the glacier. Determining if the terminus of Store Glacier is floating or grounded will allow the calving dynamics to be better understood and quantified. This will additionally lend support to determining the terminus stability and topographic impact on the calving dynamics. There is some speculation as to where the grounding line of the glacier is, with some hypothesizing that it is up to 2 km inland of the glacial terminus (Todd et al. 2018). A potentially extended floating terminus would allow for extensive submarine melt at the terminus as well as buoyant forcing fracturing the glacier and aiding calving. Determination of this floatation criterion can also be applied to the proglacial fjord to find grounded icebergs. Formation of large grounded bergs within the mélange matrix would further inhibit terminus movement down the fjord. Topographic configuration of the fjord is additionally key to understanding the stability of Store Glacier. Elevation and bathymetric profiles across the terminus of Store Glacier can be used to determine the presence of basal pinning aiding in investigation of terminus stability over the past 73 years. Basal pinning and bottlenecking of the terminus will allow the glacier to remain in a stable location despite having seasonal growth and retreat (Åkesson et al. 2018). Furthermore a shallow bathymetric sill will have an influence on the calving dynamics of the glacier in part by controlling the fracture dynamics of the ice. There is potential implication of a large-scale retreat of Store Glacier if it were to become unpinned by force imbalances at the terminus.

Manipulation of the UAV data, processing of the DEMs through ImGRAFT, coupled with the meteorological data will allow better understanding of the controls on the seasonal frontal

dynamics of Store Glacier. Use of the DEMs, with the orthophotos overlaid, provides a visual of how the glacier moves and experiences stresses throughout the study period both with the presence of the proglacial mélange and after the breakup occurs. Additional processing of the DEMs in ImGRAFT allows for the creation of compressional strain rates, extensional strain rates and velocity profiles across the terminus for the study period. These can be used to quantify the visual observations across the glacier in order to better understand the stress forces occurring not only around calving events but also from the proglacial mélange . Coupling all this with meteorological data can correlate anomalies within the data to glacial processes that occur during the same time period. Using the strain data allows for further investigation into the controls on the frequency and size of the calving dynamics at Store Glacier. Due to the high frequency of the UAV data collected, there is a fairly complete timeline of the glacier activity preceding large calving events. The strain rate analyses will detail movement within the ice itself to show the localized forcing around a calving event as well as how the glacier reacts after the ice is calved. Since the UAV data spans the period of the mélange expulsion from the fjord, glacial dynamics are uniquely able to be probed not only before and after the mélange is in place, but also during the period in which it weakens and breaks apart.

Knowing how the glacier reacts with or without the proglacial mélange is a significant determining factor in understanding how the frontal calving processes affect not only the glacial flow at the terminus but the impact that it can have upstream. Together, the bathymetric/subglacial, UAV and meteorological datasets provide a powerful and comprehensive toolset allowing for a quantitative and high resolution analysis of Store Glacier's calving and terminus dynamics.

3.1 Photogrammetry Data

Data for the quantitative analysis of Store Glacier came from several different sources. The bulk of the data was provided via personal communication by Prof. Alun Hubbard and Dr. Johnny Ryan and collected via UAV sorties over Store Glacier (**Fig. 14**) in the spring and summer of 2014. This consisted of several thousand overlapping, geotagged images of the terminus at a ground sampling distance of roughly 0.4m. Processing of these images also

allowed for creation of high resolution orthophotos, digital elevation models (DEMs) having a vertical accuracy of +/- 1.9 m (Ryan et al. 2015b) and the use of feature tracking as well as structure from motion to create a velocity analysis of the glacial terminus and mélange. Sampling of stationary bedrock on either side of the terminus of Store Glacier created an estimated mean vertical uncertainty of +/- 1.0m within the surface elevation models.

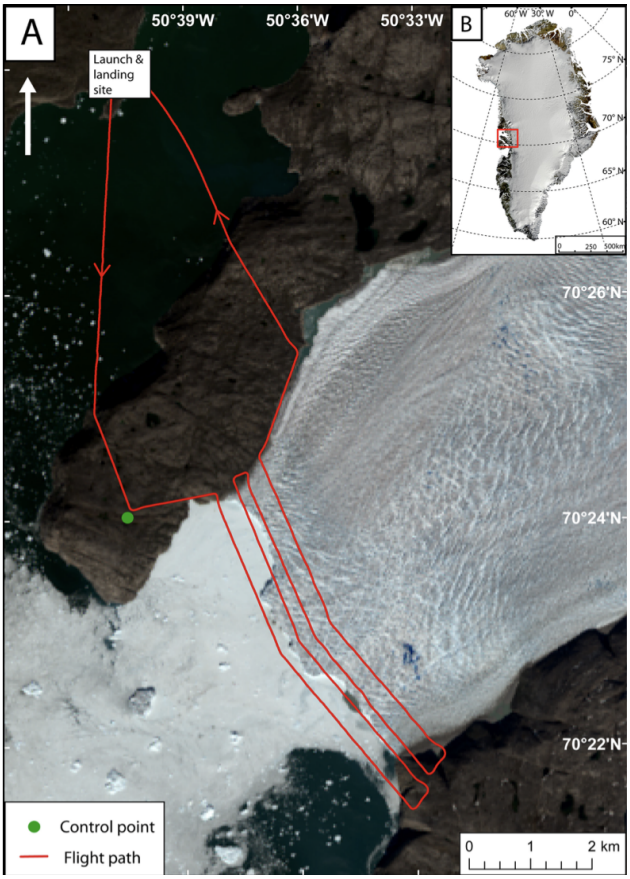

Figure 14: UAV path over Store Glacier

(a) A typical UAV sortie over Store Glacier. The back- ground map is a Landsat 8 true colour image from 12 June 2013. The red line shows the UAV flight path on the 2 July 2013. **(b)** Lo- cation of Store Glacier in the Uummannaq region, West Greenland on a MODIS mosaic image of Greenland (Ryan et al. 2015b; Kargel et al. 2012)

The drone used to capture the images was an off-the-shelf Skywalker X8 drone piloted by an autopilot controlled by Ardupilot. The use of off the shelf parts for the data collected method keeps the acquisition cost low and allows the equipment to be easily repaired and replaced or the process to be easily replicated. The Skywalker drone has a wingspan of 2.12m generating enough lift to carry the ~1kg camera payload. Due to its expanded polypropylene foam construction it is lightweight, being powered by a 10Ah lithium polymer battery connected to a 910W brushless motor and an 11x7 folding prop. This allows the drone to carry the additional payload for an hour between 55kmh and 70kmh for a maximum range of 60km.

Using an autopilot the drone was programmed to carry out a 30km to 40km survey across the terminus of Store Glacier. The Ardupilot used a Atmel 2560, 8 bit controller pre-programmed using a PC (**Fig. 15**). The drone was additionally able to be controlled using standard 2.4 Ghz RC controls if needed for take off and landing. The autopilot used real time GPS and magnetometer for navigation as well as a triple axis accelerometer and gyroscope for stabilization paired to a barometric pressure sensor to determine altitude. This allowed the drone to follow user defined waypoints for navigation, maintain a constant elevation of 300 m.a.s.l, and sustain the ~70km/h over ground speed to capture the images of the terminus. Using DEMs from the Greenland Ice Mapping Project allowed for waypoint selection to have the UAV avoid collision with the steep walls of the fjord. The Ardupilot was able to trigger the camera at user-defined times or distances at or between navigational waypoints (Ryan et al. 2015b).

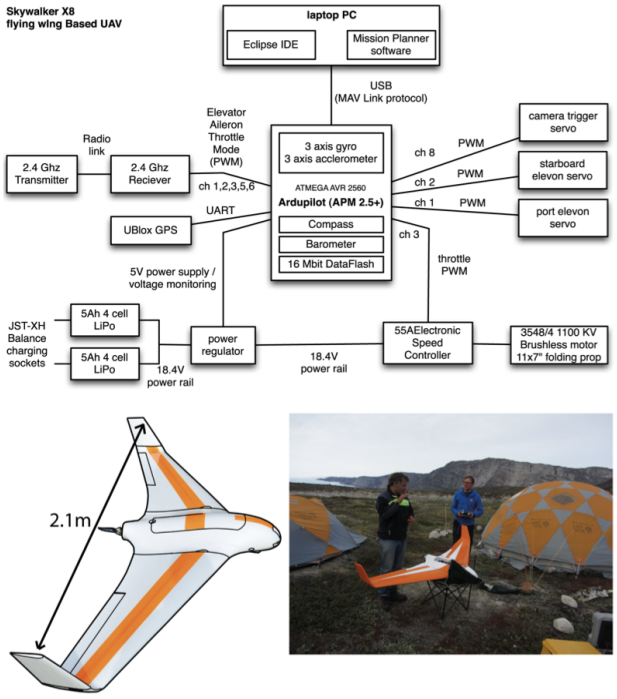

Figure 15: Flowchart of UAV control setup.

Flowchart of the control set-up and picture of the UAV at base camp (Ryan et al. 2015b)

The camera used to collect the photos was a 10.1 megapixel Panasonic Lamix DMC-LXS equipped with a 24mm wide angle zoom lens. This was set to a 5.1mm focal length (35 mm equivalent) creating a 73.7° horizontal and 53.1° vertical field of view creating a 450m x 750m over ground frame. A short exposure time or 1/1600 and focal ratio of 8 were used to prevent overexposure and blurring of the glacial terminus. The camera was mounted inside

the drone and a UV lens was placed over the camera recess opening (Ryan et al. 2015b). This simultaneously sealed and protected the lens and camera. The drone was programmed to fly 4 transects across the terminus of Store Glacier with a 250 m offset between each one creating a ~40km flight path. The offset allowed a side overlap of 70% between each pass. Using the data from the drone, photos were able to be time stamped, allowing the camera to automatically trigger upon reaching a horizontal displacement of 40m. The overlap was essential in being able to use the Agisoft PhotoScan Pro software to process the aerial photos into 3D models that can be exported as orthophotos and DEMs. Roughly 1000 photos were captured for each survey over the 12.8km^2 terminus area. More detailed collection method information can be found in Ryan et. al 2015.

3.1.1 GIS Processing

The Agisoft PhotoScan software created dense point clouds containing roughly 68 million points, allowing exportation into a Geotiff file with a pixel resolution of ~0.5m. Creation of the DEM geotiff file allowed the data to be viewed in Qgis. The geotiff files were loaded into the GIS software and the project coordinate system was set based on the information contained within the file. In this case, EPSG: 32622 (UTM zone 22N using the WGS 84 datum), allowing the correct global projection of the data. The geotiff file was then rendered into a hillshade from single-band grey. The initial altitude was retained at 45^o, the azimuth was altered from 315^o to 90^o, and the Z factor was maintained at 1. These hillshade parameters (**Table 1**) gave the best definition across the glacial terminus allowing easier differentiation between the mélange and the terminus of Store Glacier as well as being able to identify crevasses that could be of interest in large calving events. DEMs were aligned by ascending date in order to look for files that had an error within their initial georeferencing as well as viewing glacial movement through time. Files that did not align with the group would show alterations to the bedrock position on either glacial flank. DEMs that presented with an error in the georeferencing were then exported as a non-georeferenced raster in order to align it with DEMs that were in the correct reference projection. The bedrock additionally provided a stable point of reference in which to determine the extent of glacial movement. Elevation was determined using linear profiles and a geotiff as a single band pseudocolor layer with a minimum value of 0 and a maximum of 100 to correspond with ice elevation across the terminus. The elevation was displayed using an inverted Red-Yellow-Blue colorband so that

red corresponded with high elevation and a 50% opacity allowing it to be viewed overlaying the hillshade DEM (**Table 2**).

Data Layer	Render	Altitude	Azimuth	Z Factor	Opacity
DEM	Hillshade	45˚	90˚	1	100%
Bedmachine V3 0.5m	Hillshade	45˚	315˚	1	100%
Bedmachine V3	Hillshade	45˚	315˚	1	100%

Table 1: Final Qgis parameters for DEM rendering.

Final parameters for the QGis processing of the DEM data. These created the best quality results for the displaying of each data layer within the program. EPSG: 32622 was the project coordinate system while EPSG: 3413 was used for larger bathymetric datasets, allowing for each data layer to be correctly georeferenced in the correct global position.

Data Layer	Render	Color	Max/Min Value	Opacity
Elevation	Single-band Pseudocolor	Inverted RdYlBu	100 / 0	50%
Orthophoto	GeoTIFF	N/A	N/A	50%
Bedmachine 0.5m depth	Single-band pseudocolor	Turbo	0 / -800	50%
Bedmachine depth	Single-band pseudocolor	Turbo	0 / -800	50%

Table 2: Final processing parameters of draped GIS layers

Parameters for layers draped onto the DEM data allowing multiple layers to be projected and viewed over the hillshade topography.

Large calving events typically occur from a single starting point close to the flanks and present as multiple, closely aligned fissures or as a linear area of decreased elevation compared to the surrounding topography. Once the initial crevassing was determined, propagation could be monitored by observing other crevasse formation towards the mid glacier terminus of the initially identified crevasse. Secondary and tertiary crevasses established the rough outline of the calving event. This was enhanced if crevassing started perpendicular to the calving face of Store Glacier and could be traced back into other large parallel crevassing. The orthophotos were draped onto the DEM to visually determine if there was water inflow, either from the fjord or from surface melt runoff, into the crevassing areas.

Flotation processing of the terminus and mélange was done using the Bedmachine_v3 data and collected DEMs. Using the Raster Calculator tool in Qgis allowed for the creation of a mask layer to highlight areas of floating ice. The Bedmachine was the bigger dataset so the UAV data was reprojected into EPSG: 3413 (WGS 84 / NSIDC Sea Ice Polar Stereographic North) in order to properly overlay on the bathymetry dataset. Using Surfer the Bedmachine layer was clipped to the area around Store Glacier and resampled to 0.5 m resolution in order to create a smoother output layer. A bedrock mask layer was created using the polygon tool and following the bedrock margin along the north and south side of the fjord (**Fig. 16**). For the calculation of the mask layer, the buoyant factor of the ice was assumed to be c. 1/10. This was determined using the density of ice, 917 kg/m^3, and the density of seawater which is 1025 kg/m^3.

$$BF = (1025\ kg/m^3 - 917\ kg/m^3)/1025\ kg/m^3$$

$$BF = 0.1054$$

Equation 1: Bouyancy Factor Calculation

Using the assumed buoyancy factor, depth of the ice was determined by reprojected elevation by -10 to account for the ice not seen from the topographic elevation. I.e. the elevation would be one tenth of the actual thickness of the ice, therefore multiplying the elevation by -10 while

also assuming that the elevation topography of the ice matches that of the basal topography of the ice would give ice depth.

$$\frac{1}{10} Ice\ Thickness\ =\ Elevation$$

$$Ice\ Thickness\ =\ Elevation\ \times 10$$

$$Depth\ =\ -10(Elevation)$$

Equation 2: Ice thickness and depth calculation.

To determine where the ice was floating if the reprojected DEM depth was less than or equal to that of the Bedmachine bathymetry a no data value of zero was assigned. This is due to the fact that the depth of the ice could not be greater than the depth of the fjord, therefore the ice would be grounded. Additionally if the depth of the ice was also equal to the bathymetry it would be grounded so a no data value was assigned to this parameter as well. A no data value of zero was applied to the bedrock using a mask layer since this area contained no floating ice. If the ice didn't meet any of the prior criteria then it was assigned a value of 1 and the ice would be floating. The resultant layer was then overlain on the DEM in order to highlight the portions of the mélange and the terminus determined to be floating.

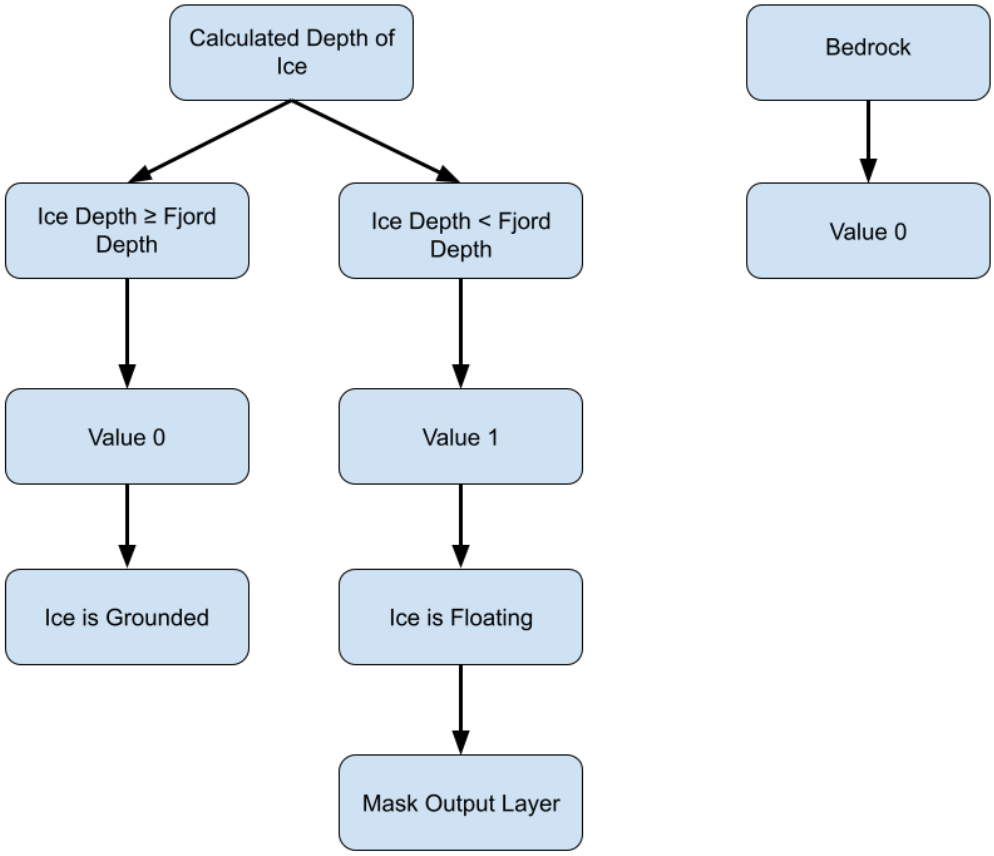

Figure 16: Processing flowchart for creation of the floating ice mask.

Processing flowchart for the creation of the floating ice mask overlay. Where the program determined the ice to be floating a value of one was assigned. Bedrock was assigned a no data value because it was not looked at during this part of the study.

Ice mélange extent was determined by using LandSat 8 imagery from 5 May 2014 and 8 July 2014. This showed the extent of the mélange at the beginning of the study period and again for the period after the mélange breakup was observed around Store Glacier from the collected DEMs. For the May imagery the data used was LandSat 8; OLI/TIRS combined; processing correction level L2SP; path 012; row 010; acquired 05 May 2014 and processed 11 September 2020; Collection 2; Tier 1; Band 4 and ATRAN. The July data used was LandSat 8; OLI/TIRS combined; processing correction level L2SP; path 012; row 010; acquired 08 July 2014 and processed 11 September 2020; Collection 2; Tier 1; Band 3 and URAD. This combination allowed for a visible light (orthophoto) overlay on a DEM.

3.1.2 ImGraft Processing

Using ImGRAFT software the data from Store Glacier can be further processed to determine the terminus velocity as well as extensive and compressive strain rates within the ice. Test runs were initially completed using the parameters established by Dr. John Ryan in his data processing. Image Georectification and Feature Tracking Toolbox (ImGRAFT) provides a flexible, adaptable, open-sourced tool able to process large volumes of imagery with a high degree of automation in order to obtain quantitative data in the form of glacial displacement (Messerli et al. 2015). This program uses MatLab and assimilates the rectification and feature tracking of the glacial images to produce velocity fields that require minimal post processing filtering. The quantitative aspect relies heavily on the ability of the images to be georectified within a coordinate system and is greatly aided by a quality, high resolution DEM and correlating imagery from the same period of time (Messerli et al. 2015). Since the DEMs within this project were produced from high quality aerial imagery, the data series aligns exactly. Ground control points (GCP) are also needed to develop a meaningful coordinate system. In this case twelve large boulders, six from each side of the glacier, were used. These were surveyed with a dual frequency GPS receiver and located within the UAV images. As the bedrock doesn't move within the defined window of data collection, it provides a stable location in each of the frames observed. GCPs can also be defined manually in instances where it is harder to discern the glacial ice from surrounding features.

ImGRAFT uses *image pairs* to track features by a process called *template match* between *Image A* and *Image B* (**Table 4**). The ice displacement in ImGRAFT is determined using a normalized cross correlation (NCC) feature tracking algorithm (Messerli et al. 2015) in order to measure template similarity. While NCC does not perform well in areas of poor visual contrast or changing snow conditions, it performs very well in areas of high visual contrast (Heid et al. 2012), such as the terminus of Store Glacier. Instead of tracking a feature through time, ImGRAFT uses a static grid following the same image coordinates allowing for better comparison between velocity fields of different time periods. *Image A* refers to the template image, while *Image B* refers to the search image. *Image pairs* can be any combination of images from the dataset (Messerli et al. 2015). For the processing of the data from Store Glacier, *Image A* was the first image in the user defined time series, while *Image B* was the next consecutive DEM. The optimal time between *image pairs* varied depending on how

much motion was expected and the quality of the consecutive DEM. For Store Glacier it was generally no greater than three days. The glacial movement is such that the software encounters more errors the greater the time gap. Additionally large, persistent features across the terminus occasionally calved out.

Lowering the *processing resolution*, defined as 'how many pixels get tracked', results in more pixel information in ImGRAFT creating a better spatial density of data. Since the orthophotos are at a 0.5 m resolution, this translates into every pixel within the DEM being 0.5m x 0.5m. The user defines the *width and height* of the template in which the software captures surface texture and patterns based on the pixels within the image. The search region is then defined within the program by user input of the *maximum displacement*. This allows the software to look for the same texture pattern within that defined range. The *max displacement* is based around the original location of the selected points within the *template*. Features that move farther than the user defined distance are ignored by the software. Since Store Glacier can move at distances of c.10m per day, increasing this distance as well as the *width and height* will allow the software to better track features across the terminus when time intervals between images increase. Georectification is the process by which 3-D real world coordinates are assigned to the corresponding pixel in the 2-D image. This is done because oblique imagery lacks the spatial information needed to extract useful quantitative distance information; the image is a 2-D representation of a 3-D landscape (Corripio 2004; Härer et al. 2013; Messerli et al. 2015). The georectification process is carried out on the offset data for all *image pair* combinations within the data series.

Actual displacement is calculated as the difference in the 3-D points between *Image A* and *Image B*. The velocities are then calculated by dividing the actual displacement from the change in geographic location by the time interval between the DEMs used in the *image pair*. *Correlation coefficient* and *signal to noise ratio* thresholds can then be used to filter the velocity fields. These are both user defined filters and altering the value must be done with some care as it is possible to remove more positive matches than mismatches within the data. A strict *correlation coefficient* threshold means that the correlation peak between points must match with a greater certainty. Similarly the *signal to noise* threshold compares the matched points in order to determine what background noise can be filtered out. Both these are determined within the NCC algorithm for the *template match*. A method to check the correctness of the processed data is to compare the velocity of the glacier along the fjord margins with that along the centerline (**Fig. 17**). Given the basal drag exerted by the bedrock

on the glacier, it can be assumed that these areas will have a lower velocity than that of the center of the glacier. If the velocity is even or inverse of this, there could be an issue with the processing inputs.

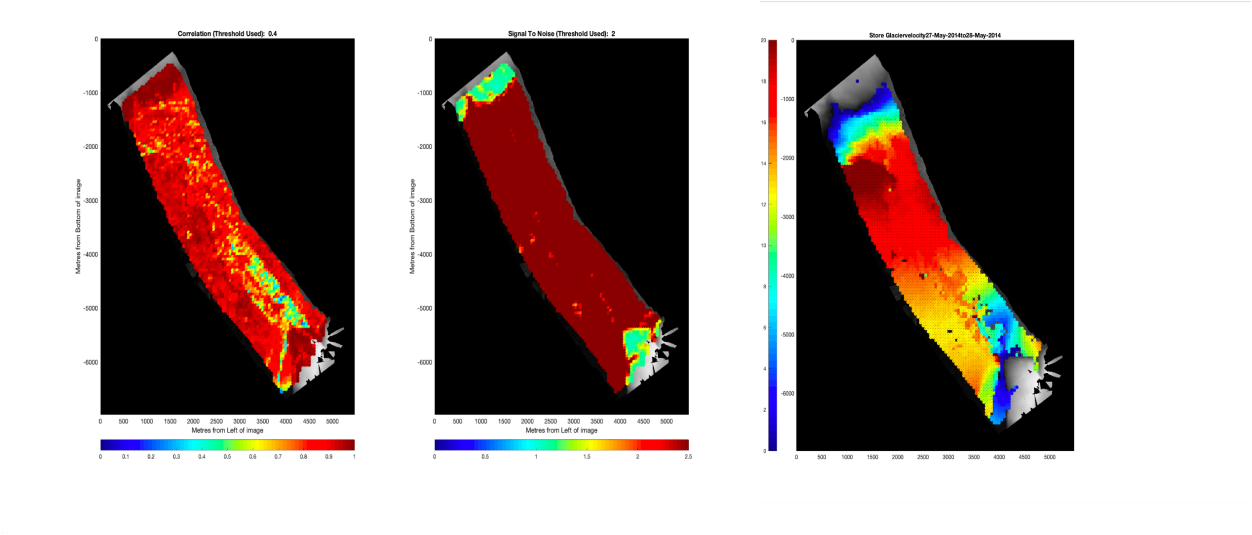

Figure 17: Inital MatLab outputs from ImGRAFT processing

Going from left to right, correlation threshold, signal to noise ratio, and glacial velocity seen as a MatLab output before being processed in QGis. Initial outputs were checked here before exporting in order to determine if the ImGRAFT script had run correctly. Having a high glacial velocity along the fjord margin, or large amounts of false data would indicate an issue in the program.

In order to determine the best ImGRAFT settings for the sorties across the terminus of Store Glacier, systematic analysis was conducted based on the original values from Ryan et al. 2015. The period between 31 May 2014 and 01 June 2014 was used as a calibration period for the software as this range produced the best velocity output with little error from the original processing. Recreating this encountered two errors within the shapefile and geotiff outputs. The first was the spot of high velocity on the northern portion of the glacier and the second consisting of two velocity arrows in the southern portion facing perpendicular to the majority of the velocity flow. The most noticeable is located on the bedrock which should have no relative velocity compared to the glacier. For analysis, each parameter was changed individually and run within ImGRAFT to display the differences the processing parameter would have on the dataset. Running the parameters through the program also highlighted any errors that arose within the final strain rate and velocity outputs. Each section displays the compressive strain rate, extensive strain rate, and velocity in that order. While the initial run selected created high quality outputs for DEMs correlated to either the next day or with a single day gap between, DEMs with a three day difference were shown as a complete

quiescence of the glacier (**Fig. 18**). While this was initially thought to be a massive cyclic dormancy period following glacial calving, it was in fact the inability of the program to track coordinates on such a large time scale due to the velocity of Store Glacier. While there were still periods of lower glacial velocity and strain rate succeeding large glacial calving, it was not on the magnitude originally noticed.

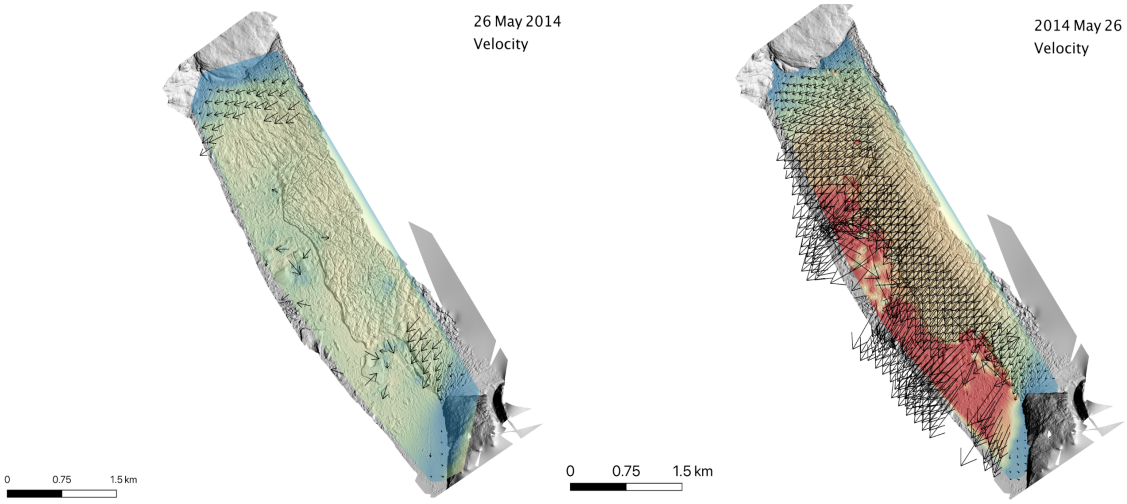

Figure 18: Initial run parameters compaired to refined parameters.

The velocity output for 26 May 2014 with the initial ImGRAFT parameters (left) and the revised parameters (right). The previous available imagery for the creation of the DEM was 23 May 2014. With the initial *maximum displacement* values used, that software was not able to accurately find a matching template due to the time and movement elapsed across the terminus. Extending the search distance led to a better glacial velocity and strain rate outputs and showed that the period of initial quiescence was in fact caused by the software misinterpreting the movement of the glacier.

After determining the best parameters for the dataset, timeframes were processed with ImGRAFT (**Fig. 19**). This consisted of comparing two consecutive DEMs to allow the software to accurately determine glacial velocity, as well as the extensive and compressive strain rate within the ice. Parameters of the software were altered prior to the final outputs in order to optimize the data contained within the DEMs. Firstly the arrow size of the velocity output shapefile was altered within the writeArrowsToShape.m file. Using line 87 through 89 of the code the head length was reduced from 0.4 to 0.3. Similarly the head width of the velocity arrows was changed from 0.5 to 0.4. This allowed the arrows to be plotted in a less cluttered manner with the GIS software. As for the strain rate outputs, the arrowheads were completely removed since the outputs would be color coded with the GIS software. Using the coding in featureTrackingStrainRates.m, line 397 through 399 allowed the head length and head width to be set to 0. The arrow length was set to 0.25 in order to declutter the final data output. The data parameters were altered using edit_FeatureTracking.m. This is where the DEM inputs were specified along with the main processing parameters. Using line 5 the

processing resolution was able to be set to 100. This created the best spatial density for the dataset without having too much data extracted from the files. Line 12 allowed the width and height to be set to 120, allowing the search template to be overlain on an area slightly greater than the processing resolution in order to better capture the surface features of the glacier. Maximum displacement was specified in line 15 and set to 80. Since Store Glacier has a higher velocity, using a higher maximum displacement allowed ImGRAFT to look for the search template pattern at a greater offset distance. Signal to noise ratio was set to 2 using line 19 in order to reduce the amount of unrelated background data, while the correlation threshold, line 23, was set to 0.4. A correlation threshold of 0.4 allows the program to be able to match similarities in the templates with a base level of 40% certainty. Due to the dynamic nature of Store Glacier and the amount at which the glacier changes through time this allows the program flexibility to match corresponding points within the ice. File A (lines 34 and 35) and file B (lines 38 and 39) being the DEM inputs for the specified range of data. The output directory was specified in line 52 allowing batches to have all the corresponding data files created within the same folder. The naming of each file was specified in line 59 and was done using the date range for the data, followed by each of the parameter values used, and the resolution of the DEM allowing Qgis to easily identify the files when selecting specific batches to view. After the script was run the initial velocity data was examined in MatLab along with the correlation threshold data and the signal to noise outputs to ensure correct processing before being loaded into Qgis. The mean horizontal velocity uncertainty was estimated to be +/- 0.55 m/d and is likely an error from interpolation of point vectors.

ImGRAFT data outputs were able to be loaded directly into QGis (**Table 3**). Color coding of the compressive and extensive strain rate allowed the vectors to be red and blue respectively. The velocity layer was color coded in an inverse Red-Yellow-Blue color ramp with 0 m/d as the minimum and 25 m/d as the maximum. This allowed any velocity of ≥ 25 m/d to show as red across the terminus. Opacity for the velocity was set to 50% allowing it to overlay the hillshade. The velocity layer was clipped using the bedrock mask since all bedrock has no velocity and therefore doesn't need to be included within the dataset.

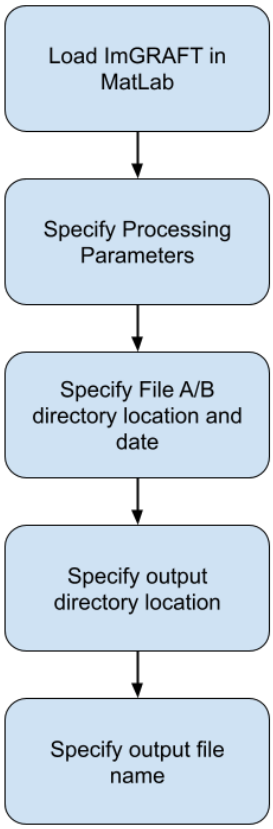

Figure 19: Processing flowchart of ImGRAFT processing

Data Layer	Render	Color	Max/Min Value	Opacity
Velocity	Clipped single-band pseudocolor	Inverted RdYlBu	25 / 0	50%
Extensive strain rate	Shapefile Line	Blue	N/A	100%
Compressive strain rate	Shapefile Line	Red	N/A	100%

Table 3: Final ImGRAFT processing parameters for GIS rendering.

Parameter	Description and Units	Value
Template match	NCC measures the similarity between the template created in the first image to the corresponding template in the second image.	N/A
Image Pair	A consecutive set of images.	N/A
Image A	The first image in an image pair, used to create the search template.	N/A
Image B	The second image in an image pair that the template search is applied to.	N/A
Processing resolution	Ratio of how many pixels get tracked across an image.	100
Width and height	The user-defined size of the search template defined in pixels.	120
Maximum displacement	The maximum offset distance in meters the program will look for a pattern from the search template.	80
Correlation coefficient	The certainty of a found point must match with the initial searched point as a percent.	0.4
Signal to noise ratio	Threshold which a found point must exceed to be separated from background noise.	2

Table 4: ImGRAFT processing parameters and imputs corresponding description and values used in DEM processing.

3.1.3 Calculation of the Glacial and Mélange Strain Rate

To calculate the strain rate of the mélange and the glacier separately a mélange mask was created for each day from 10 May 2014 to 13 June 2014 (**Fig. 20**). This was done by using the bedrock mask as a boundary layer and using the floating ice mask to manually determine the best possible outline of the glacier terminus for each day. Once the mask was created, it was used to clip the extensive and compressive strain rate layers via the vector geoprocessing tool to obtain only those that are on the ice mélange . Taking the difference of the mélange mask layer and the strain rate data allowed the glacier strain rate to be isolated. Once the strain rate was isolated for each day, the numerical data was extracted from the attributes table and inserted into excel, divided by each calendar day. The ImGRAFT processing creates two strain rate outputs as longitudinal (PSR3) and lateral (PSR1) strain rate. The strain rate results are expressed as a unitless positive or negative value that corresponds to extensional and compressional strain rate respectively. Using Excel to calculate the daily average allowed the average strain rate for both glacier and mélange PSR3 and PSR1 to be found for the period between 10 May and 13 June 2014. Additionally using Excel the daily strain rate averages for each parameter could be graphed as a function of time in order to determine how the strain rate varies with and without the mélange .

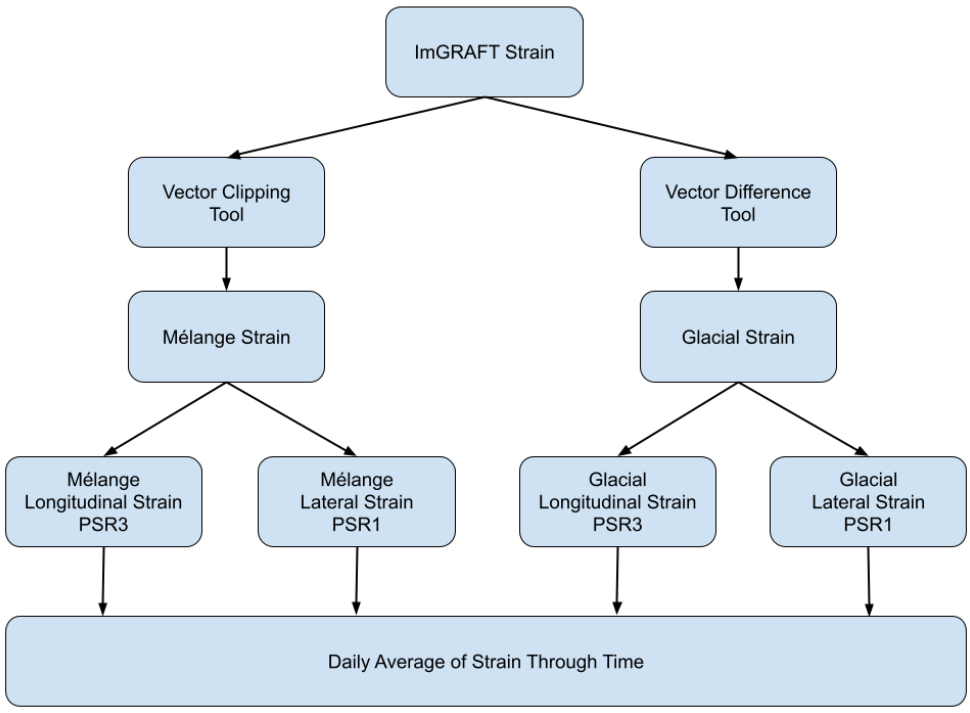

Figure 20: Processing flowchart for detemination of strain rates.

Processing flowchart for the calculation of average strain rates across the terminus of Store Glacier and the proglacial mélange. The final outputs from the GIS clipped layers were exported into Excel for the final calculation of the average strain rate rates.

3.1.4 Calculation of the Glacial and Mélange Velocity

In order to calculate the velocity of both the mélange and the glacier the ImGRAFT output file had to be first converted. Since the velocity data is displayed in a raster format, it has to be first converted to a vector layer. This was done using the Polygonize tool in order to be able to extract the velocity values out of the attributes table of the layer. Next the velocity file was clipped using the mélange mask following the same steps as the strain rate layers (**Fig. 21**). The vector clipping tool was used to obtain the mélange velocity and vector difference tool was used to obtain glacial velocity. The attributes table for each could then be exported into Excel in order to calculate the daily average velocity for the mélange and glacier. This was then plotted over the study period in order to see how the velocity changes through the timeseries. Additionally shapefile masks were made across the northern, central and southern portion of the glacier to trim the velocity further and investigate localized dynamics across the terminus and mélange . Values from each of the clipped velocities were exported into Excel in order to determine the average for each region as well as the maximum velocity and the day on which it occurred. This could then be used to calculate the localized acceleration for each of the three regions across the glacial terminus.

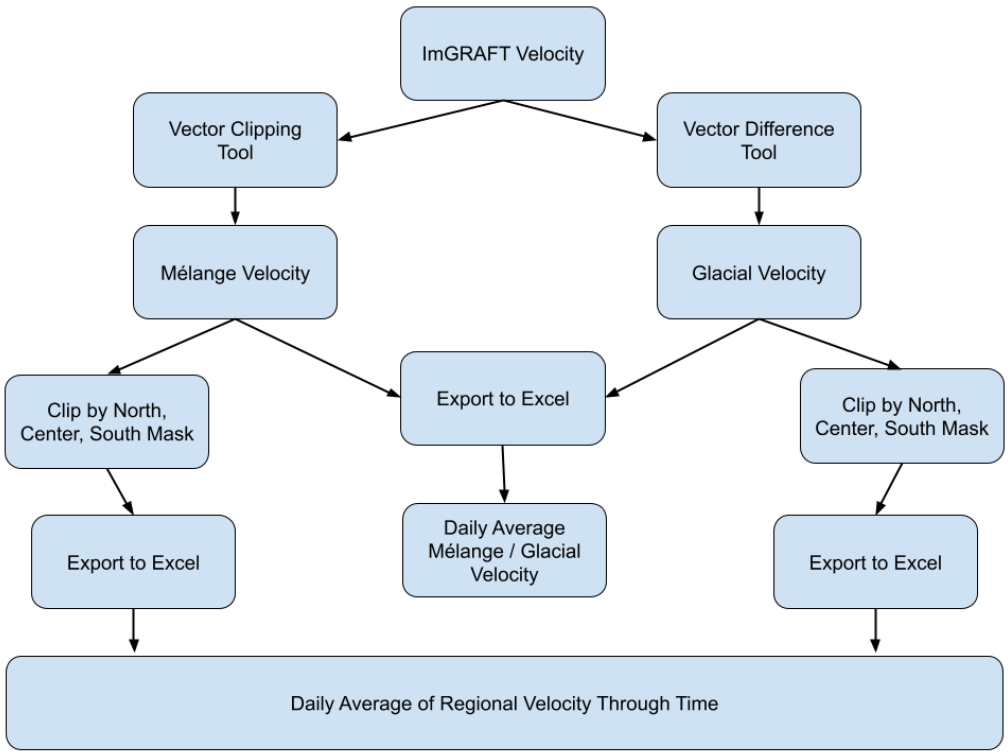

Figure 21: Processing flowchart for the claculation of velocities.

Processing flowchart for the calculation of average velocities across the terminus of Store Glacier and the proglacial mélange . The final outputs from the GIS clipped layers were exported into Excel for the final calculation of the average strain rate rates. This allowed for the creation of averaged values for the localized portions of the mélange and glacier in addition to the overall daily value.

3.2 Meteorological Data

Meteorological data came from two different weather stations (**Table 5**). The first was an automatic weather station (AWS) that was set up near the terminus of Store initially in May of 2014 by S. Doyle and T.J. Young. This station collected temperature data as well as wind velocity and precipitation data every fifteen minutes. The data provided from this station for this study started 26 July 2016 and went through 1 August 2019. While this station was set up at the study location, the window of data collection spanned outside of the timeframe that the UAV data was collected from the drone sorties. For this reason an interpolated weather dataset was made using data collected by the Danish Meteorological Institute (DMI). DMI maintains weather observations starting in 1958 for various weather stations located around Greenland as well as on the Greenland ice sheet (Cappelen 2020).

There are two DMI weather stations located near the terminus of Store Glacier (**Fig. 22**), the first being Uummannaq / Uummannaq Heliport. This station was operational from 1 January 1961 through 21 August 1989 by DMI and then from 23 January 2004 through 30 June 2006 by Mittarfeqarfiit (MIT), the predecessor to the Greenland Airport Authority (GVL). Due to the gaps in data collection and the stoppage prior to the data across the terminus of Store Glacier being collected, it was decided to use the second of the two stations. The second station is located at Qaarsut and started operation 23 November 2000. Other than a brief gap between 23 October 2005 until 01 February 2006, presumably caused during the switch from DMI to MIT operation, there is a complete dataset up through 2019 that corresponds with the UAV sorties as well as the later AWS data collected. These weather stations collected hourly weather forecasts but for purposes of data interpolation, only the date, time and corresponding temperature was collected. All temperatures from the weather stations were the dry bulb temperature and were recorded in Celcius. Meteorological data for Qaarsut was provided via personal communication with Jason Box at the Geologic Survey of Denmark and Greenland while the AWS station data was provided by Prof. Alun Hubbard.

The meteorological data provided from DMI changed formatting in 2013 (**Fig. 23**) and additionally had to be rendered into a usable configuration from the initial text file into a comma-separated values file. Creating the interpolated dataset for Store Glacier was done

using Excel calculations to compare the data collected at 4213 to the data collected at the AWS for the period of 1 January 2017 though 1 August 2019. Though the AWS data started in July of 2016, it was decided to start at the beginning of the calendar year in order to align both data sets more accurately. The average daily temperature for this period was calculated for every day in which there was correlated data between the two stations in order to create the most realistic interpolation of the data. Next the daily temperature difference between the two weather stations for the specified date range was calculated and the average of all the daily temperature differences was obtained. It was assumed that this calculated average is the typical constant difference in temperature between the terminus of Store Glacier and 4213. Applying it to the 4213 data set creates an extended record for the area around the terminus of Store Glacier.

Station Name	ID	Location	Elevation
Store Automatic Weather Station	AWS	N 70.399˚ W 50.668˚	N/A
Uummannaq/ Heliport	04212	N 70˚40’ W 52˚07’ / N 70˚41’ W 52˚07’	39 m.a.s.l. / 2 m.a.s.l.
Qaarsut	04213	N 70˚44’ W 52˚42’	88 m.a.s.l.

Table 5: Name and location of weather stations.

The three different weather stations located near the terminus of Store. This study only used the data from the AWS and 04213. The AWS dataset was collected nearer to the terminus of the glacier than the other two stations run by DMI and provided an extended period of constant data collection from which an interpolated dataset could be constructed. Station 04213 located at Qaarsut provided a better continual dataset than that of 04212 throughout the study period as well as the timeframe from which the AWS dataset was compiled. Critical gaps in operation and change in location for station 04212 made it less consistent than 04213.

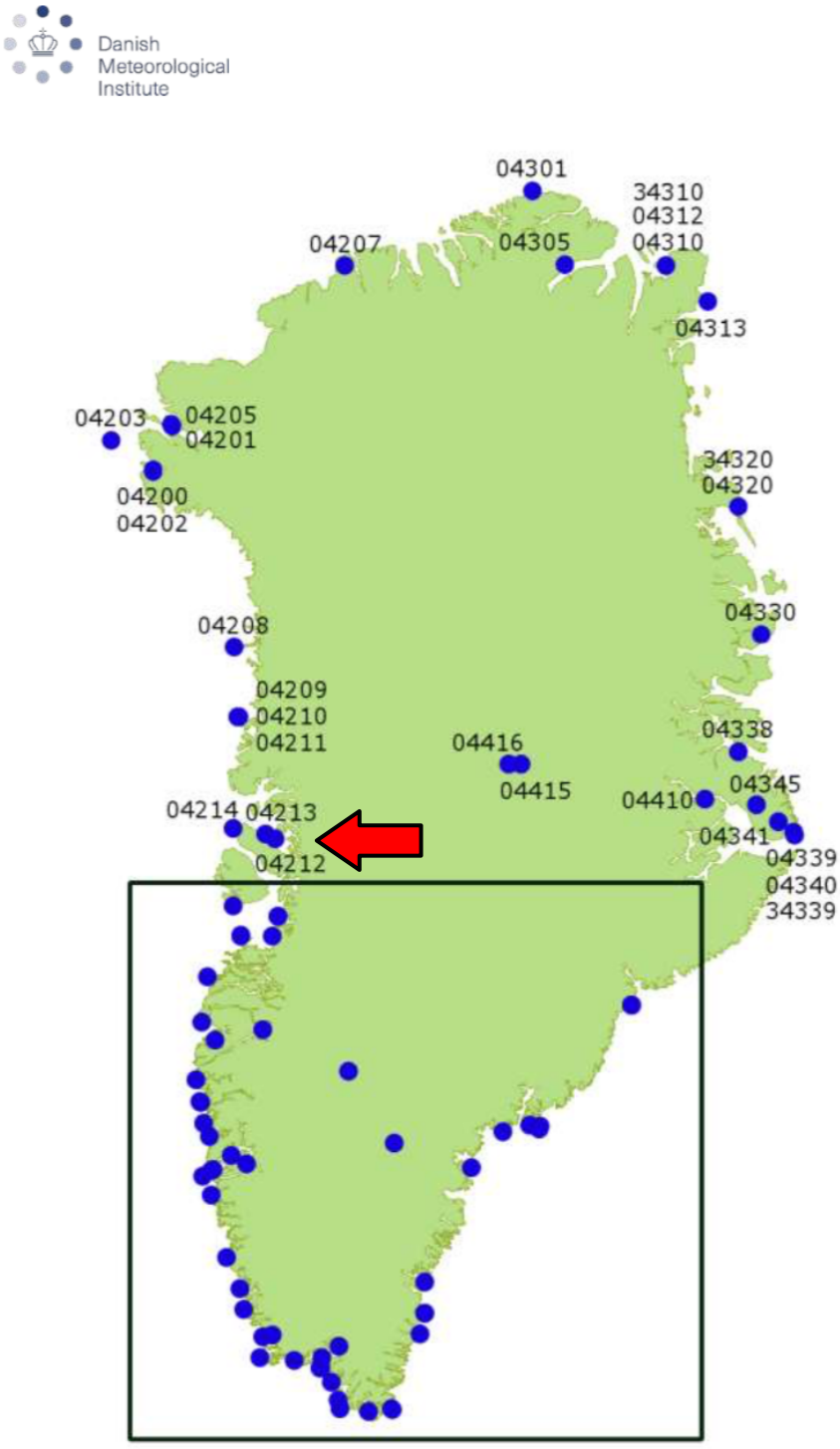

Figure 22: Danish Meterological weather station locations across Greenland

Station positions in Greenland. The official WMO station identifier for Greenland consists of 5 digits "04xxx". On the map the station identifiers "04xxx" are used. The national station identifiers describing manual precipitation stations in Greenland consist of 5 digits "34xxxx", also used on the map. These identifiers with five digits are used in the "old" data sets before 2014, where the in front "0" is omitted i.e. "4250" for Nuuk. In the "new" data sets "00" is added to all station identifiers, so they consist of 6 digits i.e. 425000 for Nuuk. Concerning the national station identifiers "50" is added to the station identifiers in the "new" data sets, so they consist of 7 digits i.e. 3423450 for Sisimiut (Cappelen 2020). The red arrow points to the two weather stations located near Store glacier. Graphics by M. Scharling.

Headers in synoptic data series-files

Parameter	Description
stat_no	4 digit station number, all in the format '4xxx'
year	Year of observation
month	Month of observation
day	Day of observation
hour	Hour of observation (UTC)
dd/365	Mean wind direction over the 10-minute period preceding the observation. In 1 or 10-degree intervals. 0 applies to calms. 990 applies to variable wind directions
ff/301	Mean wind speed (0.1 m/s) over the 10-minute period preceding the observation
n/801	Cloud cover (octas; 0/8 clear sky -> 8/8 overcast). 9 apply to obscured sky, due to fog or heavy snow, and therefore no available observation
pppp/401	Air pressure (0.1 hPa) at mean sea level
ttt/101	Dry bulb temperature (0.1°C)
txtxtx/113	Absolute maximum temperature (0.1°C). Observation period depends on the interval of SYNOP time intervals, normally 12 hours at 6 and 18 hours UTC
tntntn/123	Absolute minimum temperature (0.1°C). Observation period depends on the interval of SYNOP time intervals, normally 12 hours at 6 and 18 hours UTC
rh/201	Relative humidity (%)
rrr6*/603	6 and 12 hours accumulated precipitation (0.1 mm). -1 applies to more than 0 mm, but less than 0.1 mm. Normally 6 and 18 hours UTC cover 12 hours; 0 and 12 hours UTC cover 6 hours. In rare occasions rrr6 could also cover more than 12 hours
sss	Snow depth (cm). -1 applies to less than 0.5 cm. -2 applies to snow cover not continuous

Headers in synoptic data series-files

Parameter	Description
Station	6 digit station number, all in the format '4xxx00'
År	Year of observation
Måned	Month of observation
Dag	Day of observation
Time (utc)	Hour of observation (UTC)
101	Mean air temperature (°C; 2 metres above ground). Mean of drybulb temperatures last hour. If not available, drybulb temperature (°C); minute = 0. Time resolution 1 or 3 hours. 1 hour. V98, SAVS, GIWS. 3 hours; one station; ARGOS; Summit.
112	Absolute maximum temperature (°C; 2 metres above ground). Absolute maximum temperature last hour. V98.
113	Absolute maximum temperature (°C; 2 metres above ground). Absolute maximum temperature last 12 hours. V98, SAVS.
122	Absolute minimum temperature (°C; 2 metres above ground). Absolute minimum temperature last hour. V98.
123	Absolute minimum temperature (°C; 2 metres above ground). Absolute minimum temperature last 12 hours. V98, SAVS.
201	Mean relative humidity (%). Mean of relative humidity last hour. If not available, relative humidity; minute = 0. Time resolution 1 or 3 hours. 1 hour. V98, SAVS, GIWS. 3 hours; one station; ARGOS; Summit.
301	Mean wind speed (m/s; 10 metres above ground) observed last 10 min; minute = 0. Time resolution 1 or 3 hours. 1 hour. V98, SAVS, GIWS. 3 hours; one station; ARGOS; Summit.
305	Highest 3 sec. wind speed (m/s; 10 metres above ground) last hour. If not available, highest 3 sec. wind speed (m/s) observed last 10 min. V98, SAVS, GIWS.
365	Mean wind direction (degrees; 10 metres above ground) observed last 10 min; minute = 0. 0 applies to calms. Time resolution 1 or 3 hours. 1 hour. V98, SAVS, GIWS. 3 hours; one station; ARGOS; Summit.
371	Mean wind direction (degrees; 10 metres above ground). Mean of wind direction last hour. If not available, mean wind direction (degrees) observed last 10 min. 0 applies to calms. Time resolution 1 or 3 hours. 1 hour. V98, SAVS, GIWS. 3 hours; one station; ARGOS; Summit.
401	Air pressure (hPa) at mean sea level; minute = 0. V98, SAVS, GIWS.
504	Accumulated sunshine duration (hours) last hour. Six stations. V98; Aasiaat, Nuuk, Narsarsuaq Radiosonde, Tasiilaq, Ittoqqoortoormiit, Danmarkshavn.*
550	Mean incoming (global) radiation (W/m^2) last hour. Six stations. V98; Aasiaat, Nuuk, Narsarsuaq Radiosonde, Tasiilaq, Ittoqqoortoormiit, Danmarkshavn.
601	Accumulated precipitation (mm; about 3 metres above ground) last hour. V98. **
603	Accumulated precipitation (mm; about 3 metres above ground) last 12 hours. V98. One station; Hellman; Mitt. Kangerlussuaq.**
609	Accumulated precipitation (mm; about 3 metres above ground) last 24 hours. V98. One station; Hellman; Mitt. Kangerlussuaq.**
801	Cloud cover (%); minute = 0. Observations of obscured sky are converted to overcast if possible using additional weather information, otherwise cloud cover is missing. Six stations. V98; Aasiaat, Nuuk, Qaqortoq, Tasiilaq, Ittoqqoortoormiit, Danmarkshavn. Twelve stations; SAVS; Mitt. Upernavik, Mitt. Quarsut, Mitt. Ilulissat, Mitt. Aasiaat, Mitt. Kangerlussuaq, Mitt. Sisimiut, Mitt. Maniitsoq, Mitt. Nuuk, Mitt. Paamiut, Mitt. Narsarsuaq, Mitt. Kulusuk, Mitt. Nerlerit Inaat. ***

Figure 23: Naming nomeclature changes for Danish Met. weather stations

On the left is a description of parameters in the old data format. Resolution 1 to 24 hours. Parameter numbers connected to the "new" data format shown in the table on the right are indicated together with the corresponding parameter code in the "old" data format. Parameters given in 0.1 - values (ff, pppp, ttt, txtxtx, tntntn, rrr6) are to be divided with 10 to obtain the actual value. Remember that in order to obtain i.e. daily acc. precipitation, you cannot just add precipitation using the observations at 0, 6, 12 and 18 hours UTC. The precipitation at 0 and 12 hours UTC cover 6 hours; precipitation at 6 and 18 hours UTC cover 12 hours and therefore the precipitation at 0 and 12 hours UTC are embedded in the precipitation at 6 and 18 hours UTC. Description of parameters in the new data format on the right. Resolution from 1 to 24 hours. All parameters given with one decimal except 201, 365, 371, 550 and 801 (Cappelen 2020).

4 Results

4.1 Topographic Configuration of Store Glacier

The terminus of Store Glacier is constrained by a fjord that is 5.1 km wide, with bedrock prometories on both sides of the glacier that aids in funneling the ice. Moving 9 km upstream, the fjord width increases to 7.3 km with an additional increase to over 10 km wide 4.5 km farther up the fjord. In addition to the fjord narrowing, the bedrock alters the glacial flow by 44.15˚ to the south as it advances along the northern bedrock margin. There is an additional 32.46˚ turn after the terminus. This bedrock step system contrasts with the southern margin that only varies by 7.13˚ to the south over the same distance (**Fig. 24**). There is evidence from the DEMs spanning 7-12 June 2014 that the ice along the fjord is fast ice frozen to the bedrock.

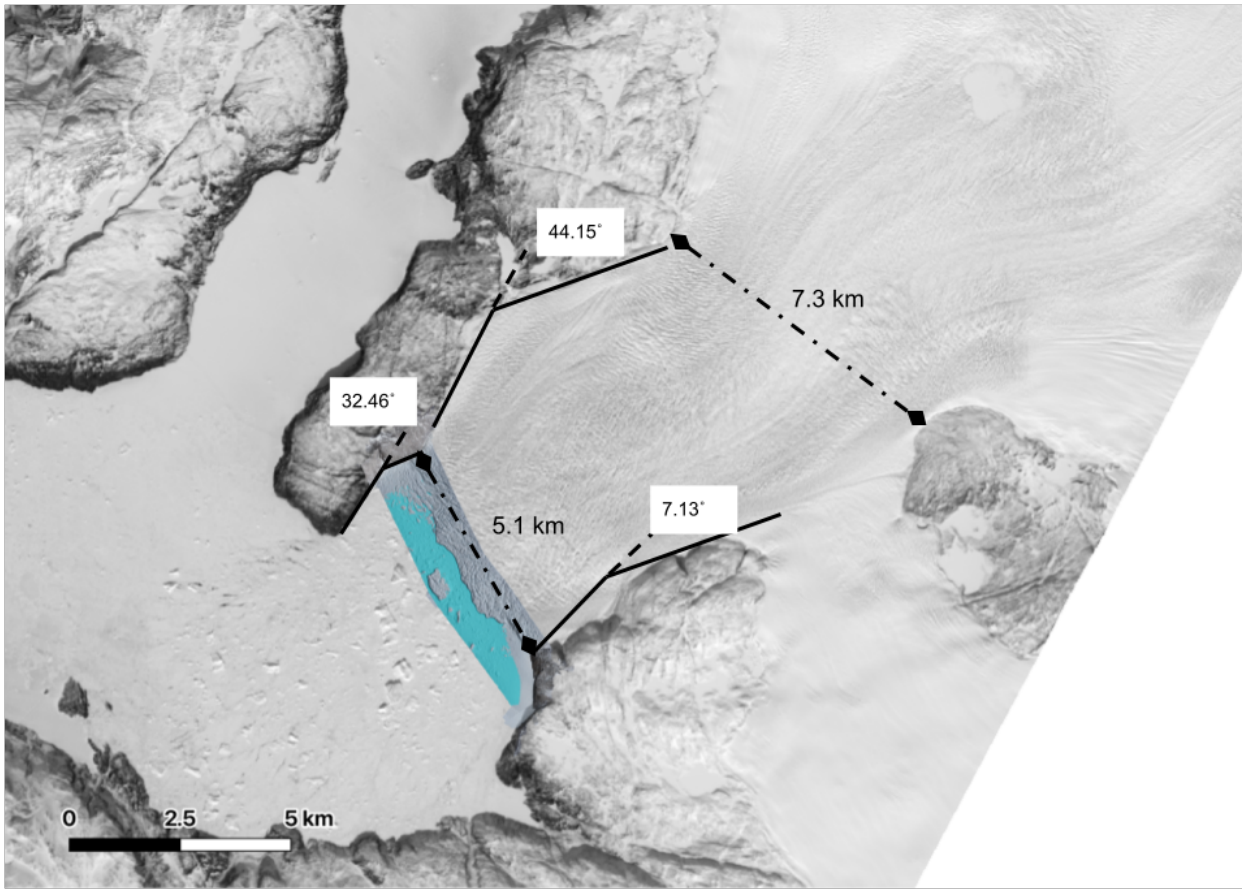

Figure 24: Fjord geometry around the terminus of Store Glacier

The fjord geometry upstream of Store Glacier highlighting the alteration in fjord width and flow angle. Due to the decrease in fjord width and the angular alteration in geometry the glacier bottlenecks as it advances.

Elevation and bathymetric profiles were taken across the terminus of Store Glacier and show the terminus is grounded throughout the data series (**Fig. 25, 26, 27**). The profile taken across the northern portion of the fjord (A - A') there is a gradual shallowing from 418 m.b.s.l. to 282 m.b.s.l. over a distance of 1.31 km. The basal topography then peaks sharply to 248 m.b.s.l. before sinking back to 366 m.b.s.l. The ice thickness above the peak is 80.1 m increasing to 113.4 m at the end of the glacial DEM. A profile taken along the centerline (B - B') of the glacier and following the same orientation shows a pronounced basal sill directly under the terminus of the glacier, rising from 672 m.b.s.l. to 232 m.b.s.l. over a distance of 3.21 km. This then drops sharply back to 535 m.b.s.l. over a much shorter distance of 1.06 km. Ice elevation over the bathymetric peak has an elevation of 125.6 m which increases to 127.98 m at the end of the terminus DEM. Looking at the southern profile (C - C') there is a drastic increase from 682 m.b.s.l. to sea level over 2.44 km with an ice elevation of 125.1 m. A cross section profile (D - D') of the fjord shows that the southern side has an abrupt shallowing that starts just north of the glacial centerline, increasing over 1800 m to sea level at a 12.2˚ slope to meet the southern bedrock flank. The rest of the fjord bathymetry presents as a subglacial U-shaped valley reaching a depth of 390 m.b.s.l. The deepest part of the immediate proglacial fjord is 781 m.b.s.l.

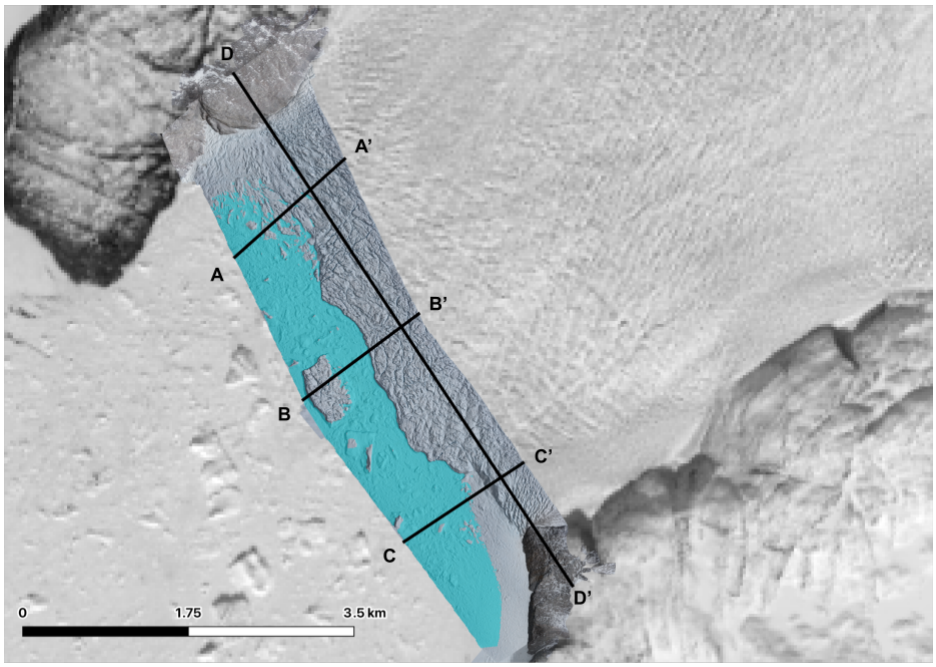

Figure 25: The profiles used for the determination of fjord depth as compared to glacial elevation across the terminus of Store Glacier.

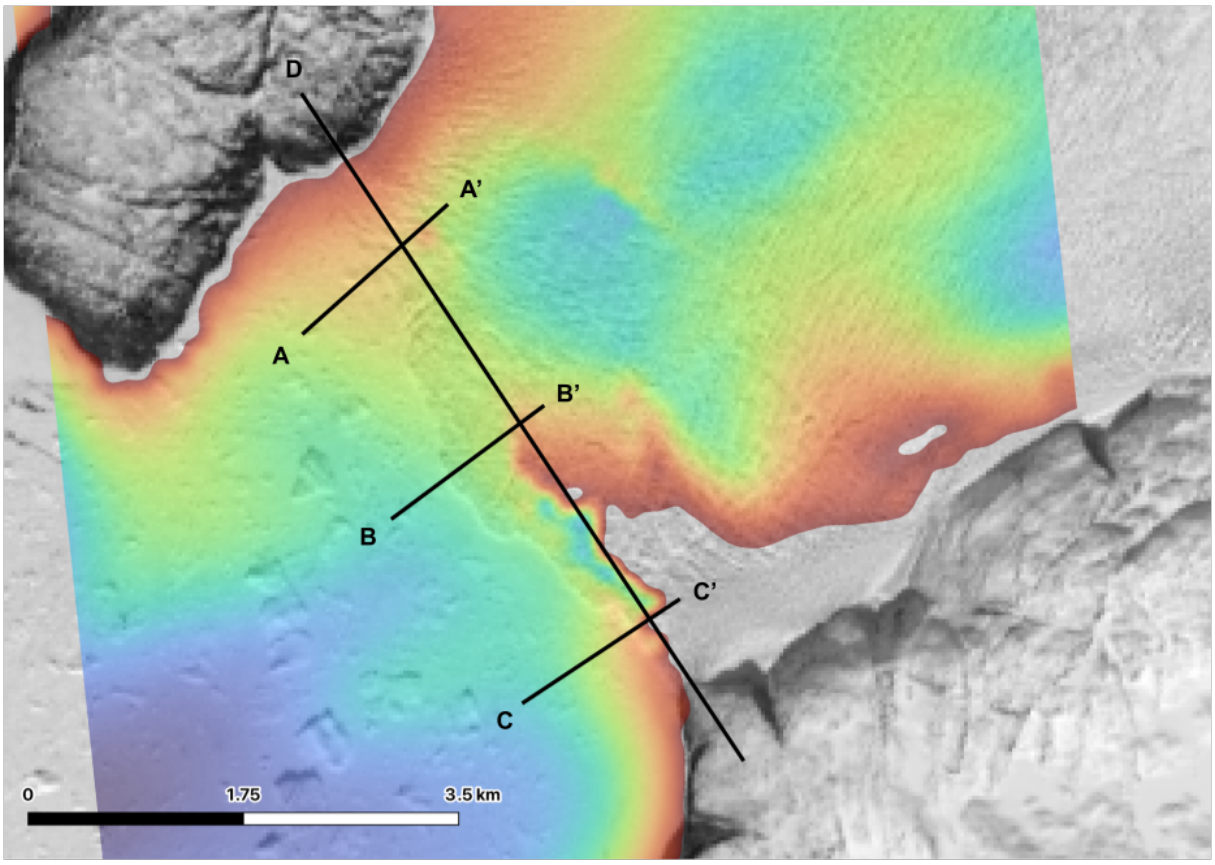

Figure 26: Fjord bathymetry resampled at 0.5m resolution from the Bedmachine_v3 data showing depth under the selected terminus profiles across the terminus of Store Glacier.

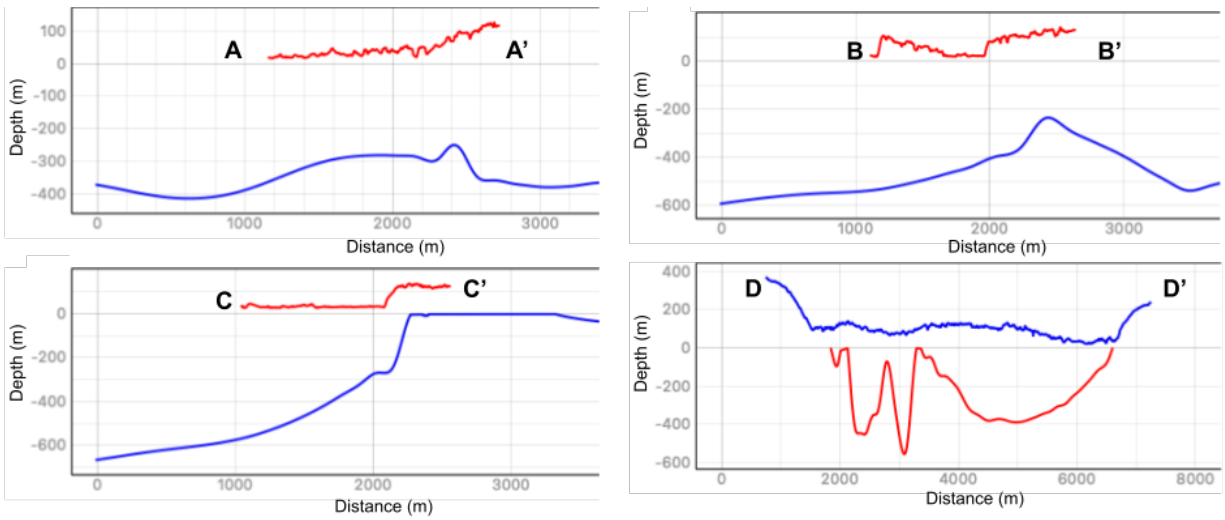

Figure 27: Cross section elevation and depth profiles across the terminus of Store Glacier

Cross section profiles corresponding to the elevation and bathymetric profiles mapped in Figure 25 and 26. There is a shallowing visible along the southern portion of the fjord however there is some discrepancy within the modeled data. The bathymetry profiles show the fjord has a pronounced basal pinning spanning its width.

4.2 Bathymetric Configuration of Store Glacier

The proglacial mélange remains in place across the terminus of Store Glacier from the start of the data series on 10 May 2014 until the period of 4 - 7 June 2014 at which point it is evacuated from the fjord. There is residual mélange deterioration within the proglacial fjord until 12 June 2014 after which there is no calculated data. This was caused simultaneously by the calving event that occurred between 4 - 7 June, the weakening caused by the temperature spike noted in the meteorological data as well as high katabatic winds coming off the glacier. We know about the calving and the winds from field observations taken during the field season in 2014. The mass influx of ice into the fjord from a calving event is enough to fracture the sea-ice bonds between icebergs thus reducing the rigidity of the mélange (Robel 2017). Prior to the mélange evacuation from the fjord, there is imagery from 5 May 2014 showing that the maximum extent at this date reached 116 km down the fjord following a direct path from the terminus of Store Glacier to the edge of the mélange .

Elevation profiles and GIS modeling determine that the mélange produces large, grounded icebergs (**Table 6**). The largest of these appears on 17 May 2015 and will be referred to from here as Iceberg A (IB-A). IB-A stays in approximately the same orientation without overturning and ~350 m from the terminus and for 6 days until 23 May 2014. The length and width of IB-A was measured to be 626 m x 439 m. The depth of the fjord in this area slopes from 469m to 532m. Using the depth plus the height above sea level it was possible to calculate the overall height of the iceberg. The calculated volume of the iceberg is 1.41×10^8 m^3 with a total mass of c. 1.3×10^{11} kg. After 23 May there is a three-day gap before the next DEM series is able to be created. On 26 May 2014 there was a partial large iceberg in roughly the same position as IB-A was on the 23rd. This iceberg is in a different orientation as well as not being fully captured by UAV photography. As such it is unable to be measured but still exhibits surface crevassing similar to that of IB-A. It is theorized that this is the same iceberg but that during the three-day gap of information that a portion of the large iceberg calved off as it shifted position down the fjord. For this reason the iceberg will be referred to as IB-A2. IB-A2 stayed in the fjord for an additional 6 days, with the last visual observation of it on 1 June 2014. There is another gap to the 3rd of June, at which time IB-A2 is no longer in the immediate vicinity of the terminus. The same calving event occurring between 16 and 17

May 2014 created additional icebergs and ice rafted debris that appeared in the proglacial fjord immediately after. To the immediate south of IB-A was a smaller grounded iceberg, IB-B. This iceberg appears to have overturned during calving due to the fairly smooth exposed ice. Due to this overturning there is also less of IB-B that is deemed to be grounded. However, IB-B is observed in roughly the same position and orientation from the initial calving on 17 May, until the iceberg moves away from the immediate terminus vicinity on 1 June 2014. IB-B didn't change shape or orientation for the 15 days that it was within the proglacial fjord. IB-B is trapezoidal in shape with the long side measuring 435 m, the short side measuring 246 m, and a width of 298 m.

Between 20 May 2014 and 22 May 2014 the southern terminus of the glacier experienced a comparatively smaller calving event to the one on the 17th that produced a grounded iceberg. In the 13 days IB-C moved away from the terminus at a near constant visual speed, with the largest jumps in iceberg position being between 23 - 26 June and 1 - 3 June. These correspond directly with the gaps in data from UAV collection. IB-C does not overturn after the initial calving event. IB-C is trapezoidal in shape measuring ~294m by 276 m by 236 m by 324 m. IB-D appears from a calving event that occurs sometime between 10 - 13 May 2014. IB-D is observed in the fjord until the calving event that created IB-C. IB-D is the rough shape of a pentagon with sides measuring 211 m by 118 m by 227 m by 135 m by 134 m.

Several small icebergs were created and observed in the immediate vicinity of the northern terminus until 11 June 2014. IB-E has a centerline length of 157 m and a centerline width of 118 m, while IB-F measures 196 m by 92 m along its respective centerlines. Both icebergs appear after the move out of the mélange and move in a southern direction before disappearing or changing enough that they were not recognizable past 10 June 2014. Since both were floating throughout the period they were visible, the volume is assumed to be less than the calculated value since the fjord depth was used to determine the height of each iceberg. 12 June sees the release of a large portion of ice along the fjord margin that was assumed to be fast ice and frozen to the bedrock. Both of these calving events produced no large, grounded icebergs.

Calving Event	Terminus Region	Iceberg	Overturns	Volume	Mass	Days Visible
16 - 17 May	Central	IB-A	No	$1.41x10^8$ m^3	1.3 x 10^{11} kg	6
16 - 17 May	Central	IB-A2	No	N/A	N/A	6
16 - 17 May	Central	IB-B	Yes	$5.28x10^7$ m^3	$4.83x10^{10}$ kg	15
20 - 22 May	Southern	IB-C	No	$4.05x10^7$ m^3	$3.72x10^{10}$ kg	13
10 - 13 May	Southern	IB-D	Yes	$1.82x10^7$ m^3	$1.67x10^{10}$ kg	7
4 - 7 June	Northern	IB-E	Yes	$>5.67x10^6$ m^3	$>5.20x10^9$ kg	3
4 - 7 June	Northern	IB-F	Yes	$>5.76x10^6$ m^3	$>5.28x10^9$ kg	3

Table 6: Tracked icebergs within the study period

Each of the observed and trackable icebergs created by glacial calving during the study period between 10 May and 13 June with their respective estimated volume, mass and how many days they were visible in the proglacial fjord before moving or deforming enough they were not able to be compared to the previous set. Volume was calculated using the visible surface geometry and assuming the icebergs mirror this below the waterline. Additionally volume calculations used the shallowest depth when grounded for calculation.

4.3 Glacial and Mélange Strain Rates

The longitudinal strain rate (PSR3) across the glacial terminus and mélange was extensional while the lateral strain rate (PSR1) was compressional as determined by the positive and negative values (**Fig. 28**). The average strain rate for the study period of 10 May 2014 through 13 June 2014 for the mélange was 1.320 u/a for PSR3 and -1.119 u/a for PSR1. The glacial strain rate during the same period was 1.199 u/a for PSR3 and -0.843 u/a for PSR1. There is a multi-day increase in mélange longitudinal strain rate leading to a drastic reduction in overall strain rate between 16-17 May and 26-27 May. For the period of 16-17 May the strain rate peaks at 1.63 u/a before decreasing by 38% to 1.01 u/a. The longitudinal strain rate during the period before 20 May is fairly stable, averaging 1.23 u/a, despite the large calving event occurring on 16 – 17 May. The period between 26-27 May sees the 23 June peak of 1.49 u/a decrease by 3.4% to 1.44 u/a on 26 May before reducing to 0.75 on 27 May, an overall reduction of 49.7% from 23 May. On 1 June 2014 there was an increase in the lateral mélange strain rate to -1.57 u/a before it decreased to -1.06 u/a then increasing again to 4 June reaching -2.17 u/a. The glacial terminus sees a slight increase in lateral strain rate during this time, peaking at -1.09 u/a on 3 June, however it remains fairly consistent throughout the study period with an average of -0.84 u/a. After 1 June 2014 there was a continuous increase in longitudinal strain rate until 12 June 2014, peaking at 2.08 u/a, after which there was no collectible data from the mélange . There are several increases in glacial longitudinal strain rate occurring on 22 May, 26 May, and 3 June of 1.64 u/a, 1.65 u/a, and 1.38 u/a respectively. These correspond with several calving events that occur along the southern portion of the terminus. After 4 June with the evacuation of the mélange , the longitudinal glacial strain rate begins a gradual increase through the end of the study window on 13 June 2014 as shown by the average longitudinal strain rate increasing from 1.15 u/a to 1.16 u/a.

The longitudinal strain rate for the glacier increased by 0.9% from 1.15 u/a prior to the mélange break-up period to 1.16 u/a in the period succeeding it. The mélange increased by 29.2% from 1.14 u/a prior to 1.61 u/a. The lateral strain rate across the glacier for this same period remained at -0.84 u/a while for the mélange it increased by 33.3% from -0.94 u/a to -1.41 u/a (**Table 7**).

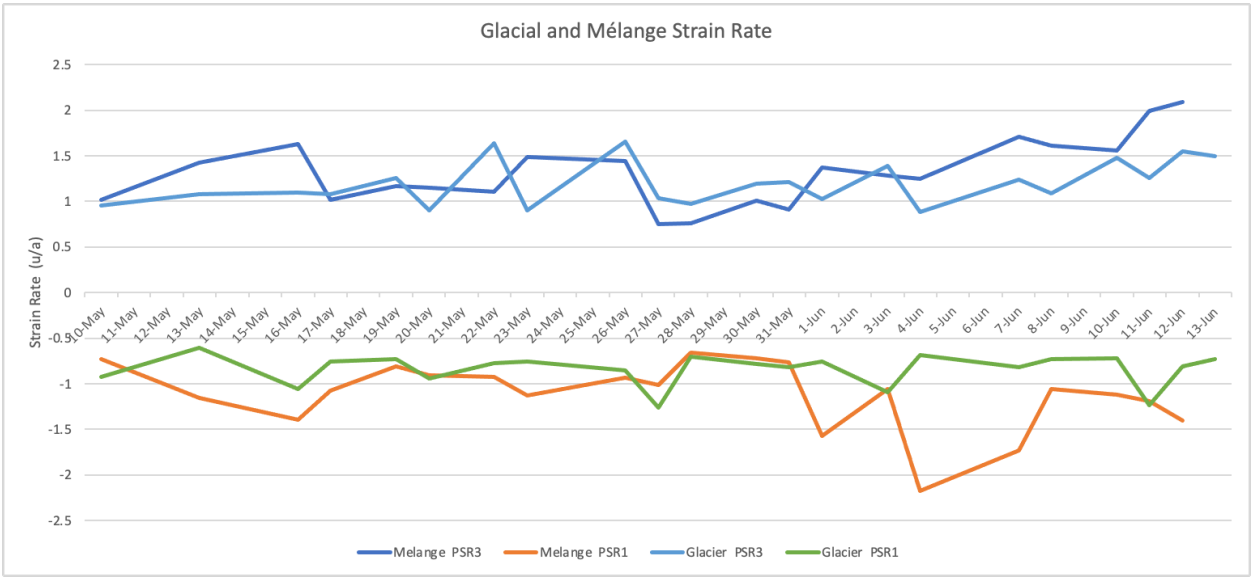

Figure 28: Average daily strain across the mélange and glacial terminus.

Glacial and mélange average daily strain rate profiles throughout the period between 10 May and 13 June 2014. PSR3 corresponds to longitudinal strain rate down the glacial centerline, while PSR1 is lateral strain rate across the width of the glacier. Decrease in lateral strain rate (negative increase) correlates with increases in ice compression while increases in longitudinal strain rate correlate to increased extension. Strain is a unitless value while strain rate is in units/annual (u/a).

Location	PSR3 Average strain rate	PSR3 (Longitudinal) Pre Breakout	PSR3 (Longitudinal) Post Breakout	PSR1 Average strain rate	PSR1 (Lateral) Pre Breakout	PSR1 (Lateral) Post Breakout
Glacier	1.19 u/a	1.15 u/a	1.16 u/a	-0.84 u/a	-0.84 u/a	-0.84 u/a
mélange	1.32 u/a	1.14 u/a	1.61 u/a	-1.12 u/a	-0.94 u/a	-1.41 u/a

Table 7: Longitudinal and lateral strain averages corresponding to mélange evacuation.

Longitudinal and lateral strain rate for both the glacial and the mélange averaged for the time period between 10 May and 31 May 2014 prior to the mélange break out. Post breakout comes from the time period defined by the start of the increase of mélange PSR3 spanning from 1 June to 13 June 2014.

4.4 Glacial and Mélange Velocity

The average velocity for the mélange during the period from 10 May to 13 June 2014 was 25.1 m/d while that of the glacier was 21.6 m/d (**Fig. 29**). There are several velocity spikes corresponding to 16 May, 22 May, 26 May, 3 June, 7 June, and 10 June. In these instances the glacial and mélange velocities are fairly similar until the event on 10 June when the mélange increases to 64.6 m/d and the terminus of Store Glacier reaches 50.8 m/d (**Fig. 30**). The greatest acceleration seen during the study period was between 8 June and 10 June 2014 for the mélange with a 21.1 m/d^2 rate of acceleration. Conversely for the glacier the largest acceleration was observed between 23 and 26 May 2014 and was 22.2 m/d^2. The greatest slowdown of the mélange occurred between 22 May and 23 May with an acceleration of -19.6 m/d^2 while for the glacier it was an acceleration of -21.7 m/d^2 between 11 and 13 June 2014.

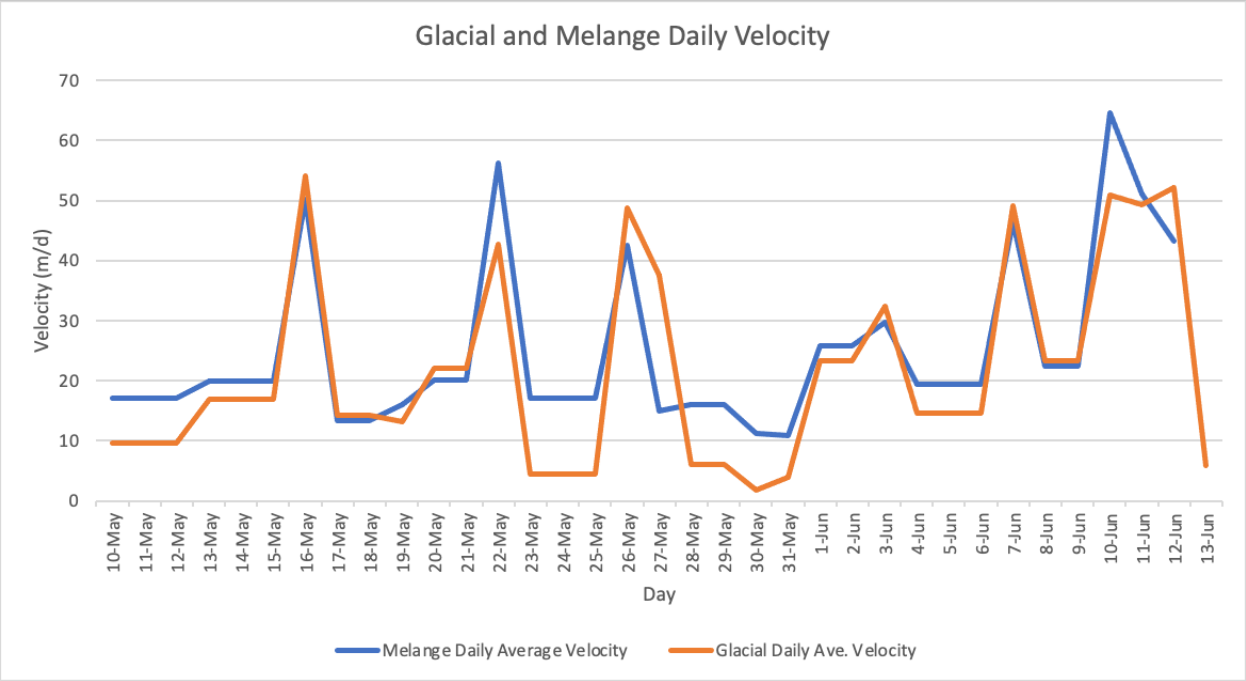

Figure 29: Average daily velocity across the glacial terminus and proglacial mélange showing correlation between glacial and mélange advance.

On 16 May the glacier velocity increased greater than the mélange to 54.1 m/d while the mélange only reached 50.2 m/d. The 22 May event had the mélange reaching 56.2 m/d while the glacier reached 42.7 m/d. The trend is then repeated for 26 May with a glacial velocity of 48.8 m/d and the mélange at 42.5 m/d. The event on 3 June 2014 sees the lowest increase of all calving events with the mélange reaching 29.7 m/d and the glacier reaching 32.5 m/d.

This is about half the velocity of all other events observed during this timeframe. Once the mélange starts breaking up after 4 June there is an increase in mélange velocity to 46.4 m/d and the glacier increased to 49.1 m/d. The speed slows on the 8th to 22.4 m/d and 23.3 m/d respectively before increasing to 64.6 m/d for the mélange and 50.8 m/d for the glacier. The mélange then slows by 33.1% to 43.2 m/d before there is no more available data on 13 June 2014. Conversely the glacier stays at an elevated velocity for 3 days, increasing to 52.1 m/d on 12 June before slowing drastically to 5.9 m/d on 13 June.

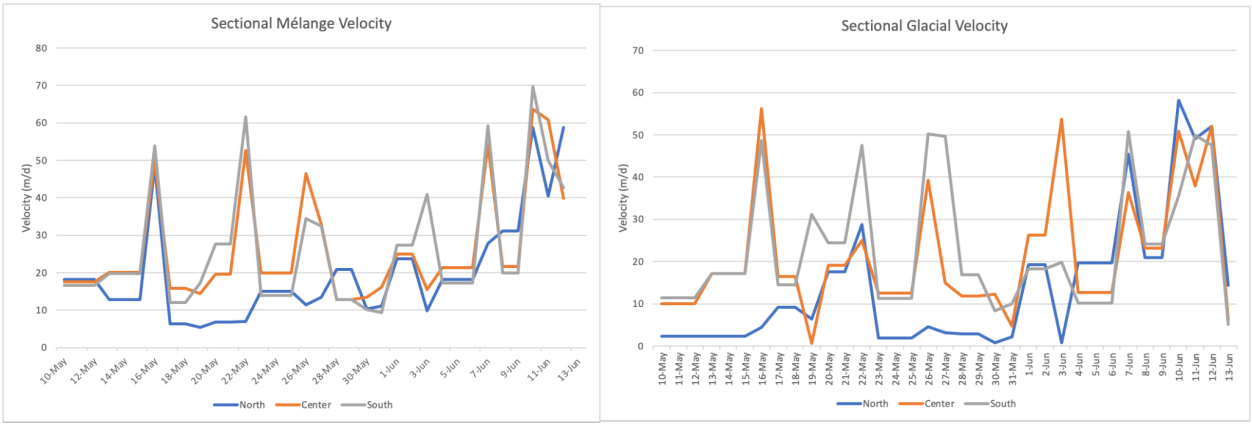

Figure 30: Regional average velocities across the terminus and mélange.

A graph showing the daily average velocity of each regional section across the terminus and mélange for the period between 10 May and 13 June 2014. After 12 June there is no velocity data for the proglacial mélange as the entirety had been evacuated from the fjord directly in front of Store Glacier. Regional velocity shows that there are different glacial dynamics across the terminus of Store that are translated into the movement of the proglacial mélange .

The sectional velocity data across the terminus and the mélange reveals that the northern section of the fjord experiences a lower average daily velocity then the central or southern portion (**Table 8**). The average velocity for the northern portion was 19.8 m/d and 13.9 m/d for the mélange and terminus respectively. This was 24% lower for the mélange and 34% lower for the glacier when compared to the central region. The average centerline mélange velocity was 26.1 m/d and the glacier was 21.8 m/d. The centerline velocities were comparable to that of the southern portion of the terminus. This region had an average mélange velocity of 26.0 m/d and an average glacial velocity of 22.9 m/d. The maximum average regional velocities for the mélange occured all on 10 June 2014 and were 58.7 m/d for the north, 63.7 m/d for the centerline and 69.6 m/d for the south. Compared to the glacier, only the maximum velocity for the north occurred on 10 June with a rate of 58.1 m/d. The maximum for the glacial centerline was 56.2 m/d and occurred on 16 May 2014, coinciding

with the large calving event that occurred between 16 - 17 May. The maximum for the southern section of the glacial terminus occurs on 7 June 2014 in concurrence with the observed mélange breakout and was 50.8 m/d. Looking at the velocity peaks in both the mélange and glacial terminus, there is a strong correlation between mélange velocity peaks and glacial velocity peaks. The peak periods further correspond to observed calving events and the peaks of the longitudinal strain rate (PSR3). Additionally the acceleration of the mélange is closely linked with that of acceleration calculated across the terminus of Store Glacier (**Fig. 31**).

Location	Average Velocity	Max Velocity
Northern mélange	19.8 m/d	58.7 m/d
Centerline mélange	26.1 m/d	63.7 m/d
Southern mélange	26.0 m/d	69.6 m/d
Northern Glacier	13.9 m/d	58.1 m/d
Centerline Glacier	21.2 m/d	56.2 m/d
Southern Glacier	22.8 m/d	50.8 m/d

Table 8: A table containing the average and maximum velocities across each of the three regions of the glacial terminus and mélange .

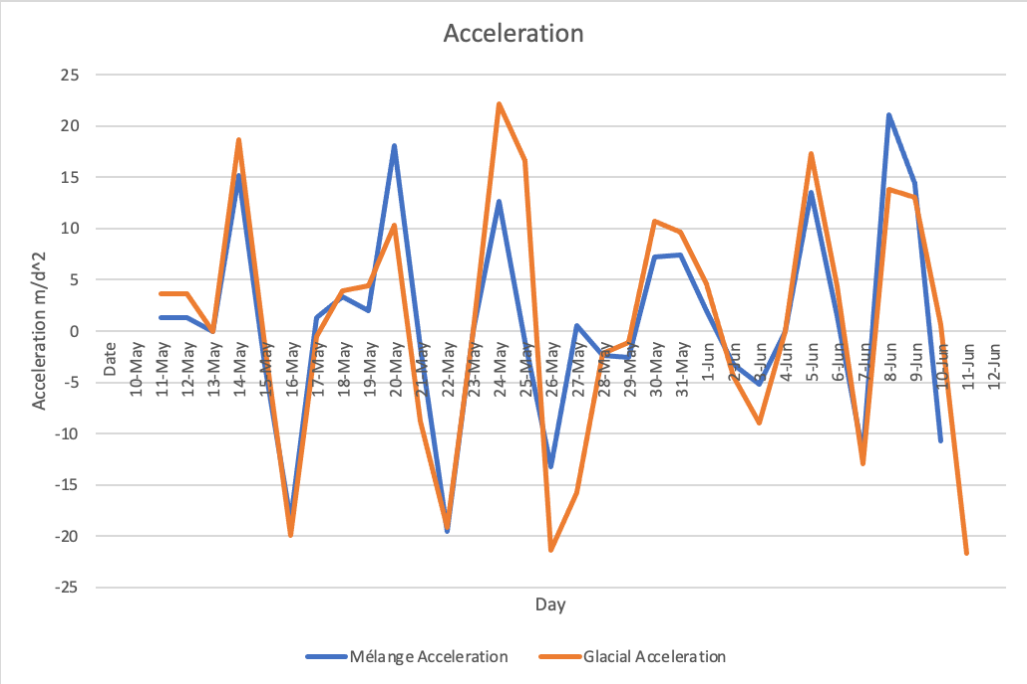

Figure 31: Average acceleration across the terminus and mélange.

A graph showing the daily average acceleration across the terminus and mélange for the period between 10 May and 13 June 2014. After 12 June there is no acceleration data for the proglacial mélange as the entirety had been evacuated from the fjord directly in front of Store Glacier. Average velocity correlation provides evidence for the general coupling of the mélange and the terminus while the mélange is in place.

4.5 Meteorological Data

AWS data shows that the average wind direction over the three-year period of available data is 185.5˚. The typically cyclic winter cooling (**Fig. 32**) in 2014 was interspersed with several temperature spikes above 0˚C on 9 Jan (+0.56˚C), 29 Jan (+0.16˚C), and 28 February (+0.96˚C)(**Fig. 33**). Despite this there is still evidence of the ability for the thick mélange to be formed at the beginning of the study period on 10 May. There is a warming trend that begins 24 March and continues through 22 July 2014 with the first major prolonged temperature swing above 0˚C occurred during the period between 31 May and 7 June 2014. Prior to this the temperature had reached a maximum of +1.95˚C on 29 May 2014.

The temperature on 31 May was -0.1˚C increasing rapidly to +6.5˚C two days later on 2 June. Between 1 and 7 June the average temperature was +4.5˚C while the week previous the average temperature was +0.2˚C. Between 31 May and 2 June the temperature rose from -0.11˚C to +6.54˚C. May 31 was the last time there would be subzero temperatures until 26

September 2014. Following this rapid increase, the temperature dropped back to +3.15˚C on June 4. June 5 and 6 see another large temperature spike to +6.11˚C and +5.32˚C respectively. June 7 the temperature dropped back to +0.88˚C (**Fig. 34**).

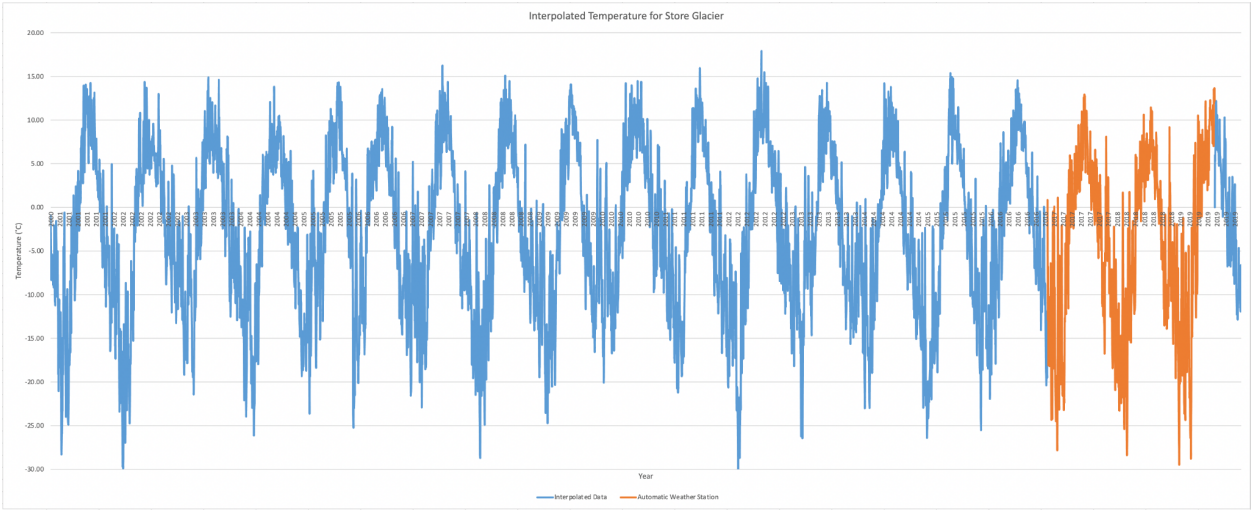

Figure 32: AWS and interpolated temperature data for Store Glacier

Temperature data from Store glacier from the fall of 2000 until the fall of 2019. The graph in blue represents the interpolated data that was calculated using the DMI weather station. The data in orange represents the data collected from the AWS and subsequent overlap period with the 4213 DMI weather data. Interpolated data was calculated by taking the average daily temperature difference between the AWS and the DMI weather station for the period between 2017 and 2019 to then extrapolate the AWS data.

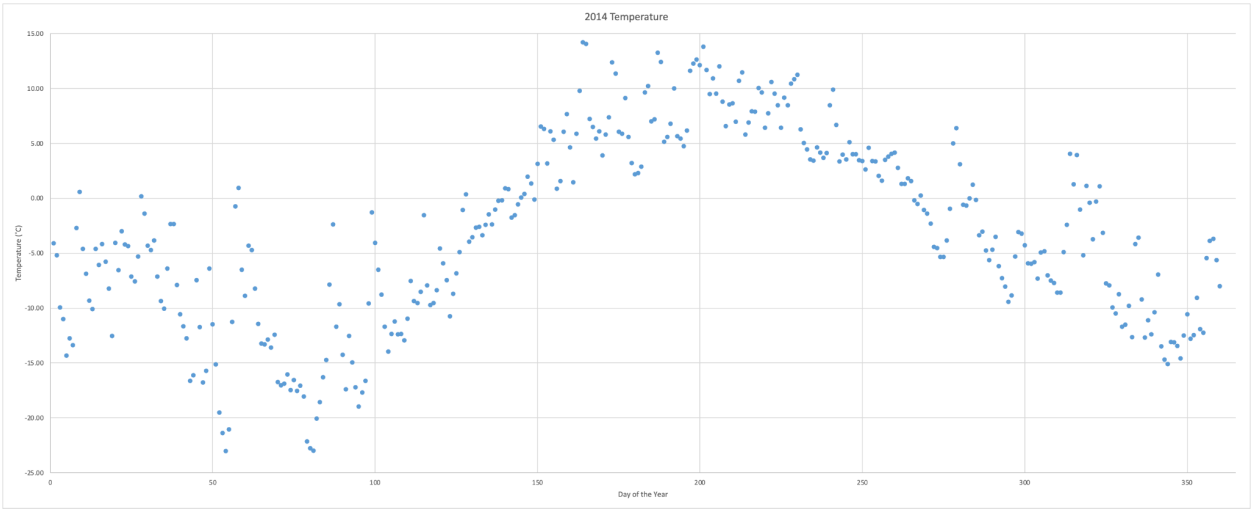

Figure 33: Interpolated AWS temperature data for 2014

Interpolated AWS temperature data from 2014. The mélange was evacuated from the fjord between 4 and 7 June 2014. This coincides with the first major temperature swing above 0˚C. The temperature on 31 May was -0.1˚C increasing rapidly to +6.5˚C two days later on 2 June. Between 1 and 7 June the average temperature was +4.5˚C while the week previous the average temperature was +0.2˚C.

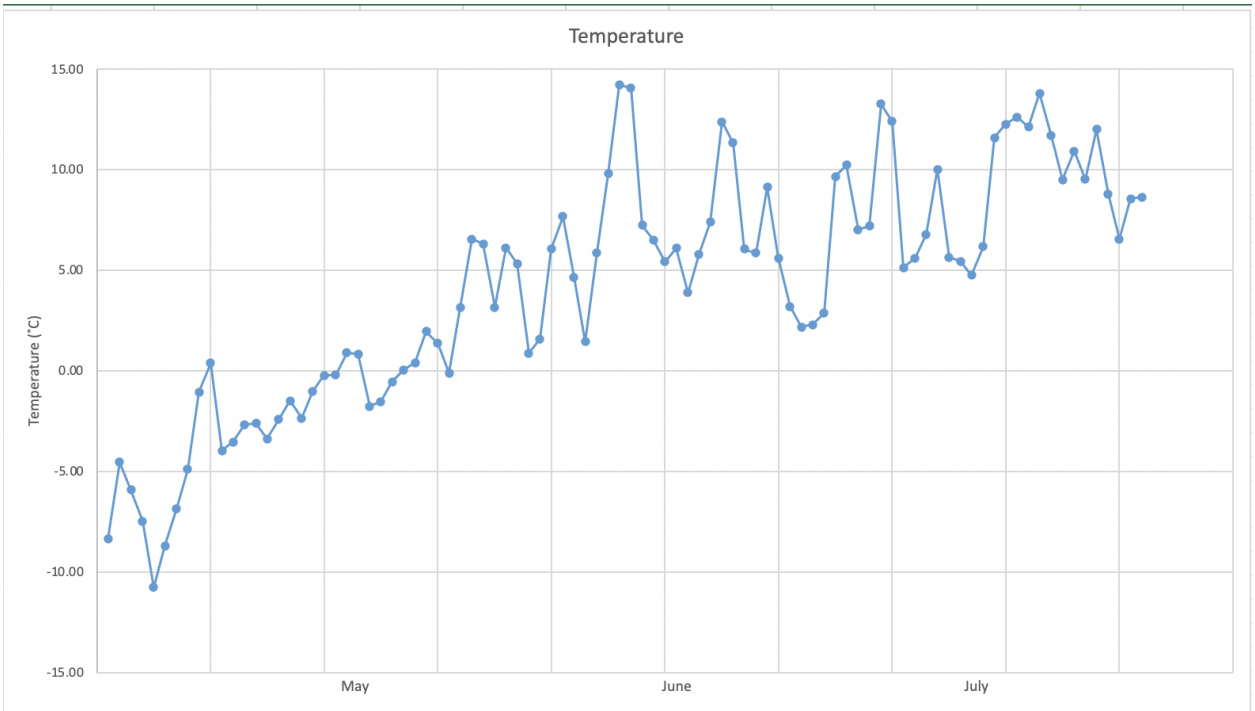

Figure 34: Highlighted temperature for the study period between May and July 2014.

A temperature graph showing the period of time corresponding to when the orthophotos were collected. There is a large temperature spike above +5˚C at the beginning of June which directly corresponds to the weakening and move out of the proglacial mélange observed in the aerial imagery. Prior to this period of time the temperature had warmed at a slower rate with the maximum temperature previously reaching approximately +2˚C.

5 Discussion

5.1 Crevasse Propagation as a Method to Predict Calving Size

Using the UAV imagery from the 2014 field season it was possible to predetermine the size of larger calving events by looking at the crevasse propagation across the terminus of Store Glacier. This was easiest in the earlier part of the season when the mélange was still buttressing the calving face, allowing the approximate size and shape of large calving events to be determined up to a week before the actual ice block breaks off. Even after 7 June 2014 when most of the mélange had been evacuated from the fjord, it was still possible to use crevasse propagation to determine calving events, though at a faster pace due to the decrease in the duration of time icebergs stayed in the proglacial fjord. From the available data four distinct, major calving events outlined by prior crevasse formation between the period of 10 May and 02 July were identified. These events ranged in both overall size as well as presence of proglacial mélange and time since formation to ice breaking off. The first two events occurred between 10 May - 17 May 2014 (**Fig. 35**) and again between 17 May - 22 May 2014 (**Fig. 36**) respectively.

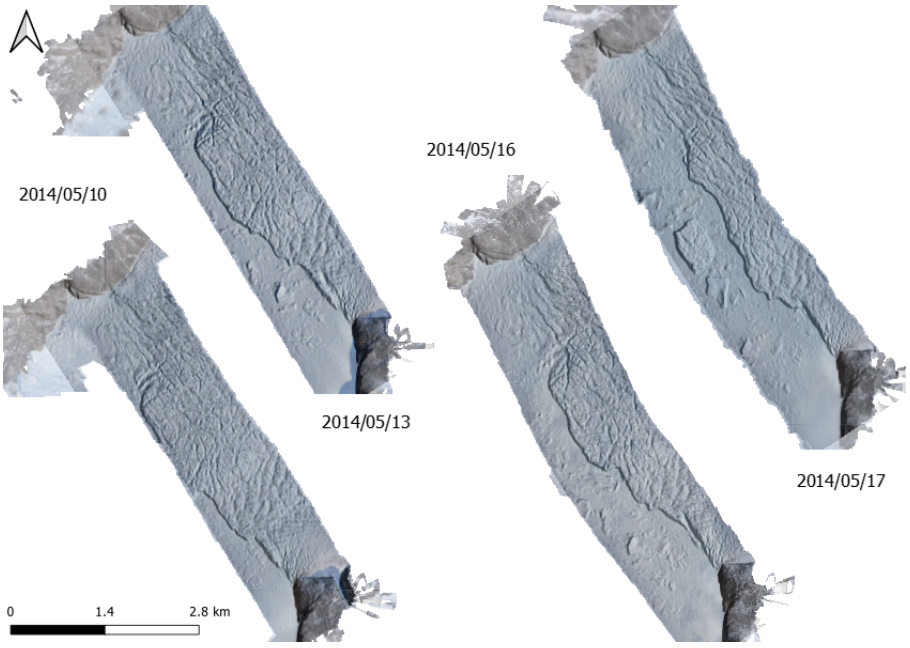

Figure 35: Crevasse propigation for the calving event between 10 May and 17 May 2014.

The first calving event occurred between 10 and 17 May with crevasse formation from the north side of the terminus of Store. This big event is occurring simultaneously with a smaller event on the southern side. Both these events occur with proglacial mélange and clearly defined crevasse propagation. Zooming in on the high resolution orthophoto shows there is no water flowing into the crevasse from the fjord or from surface meltwater streams. The northern event appears to be adding stabilization to the terminus. After it breaks off the rest of the calving face retreats back rapidly in order to regain equilibrium.

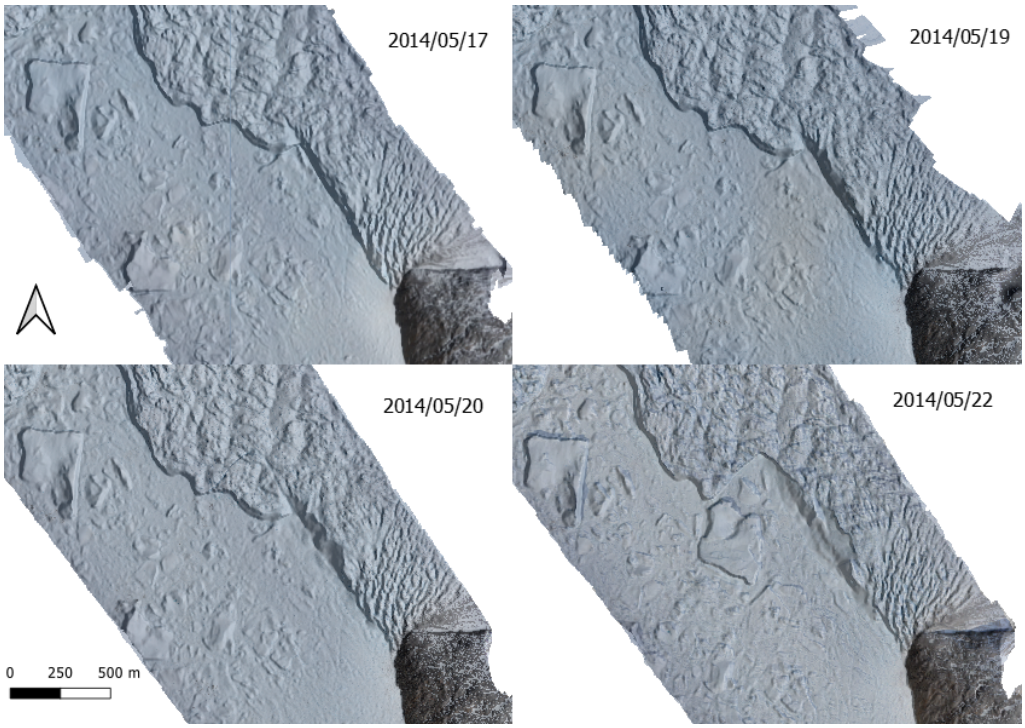

Figure 36: Crevasse propigation for the claving event occuring between 17 May and 22 May 2014

A smaller event terminating around 22 May showing the crevasse formation from both the parallel and perpendicular margin forming almost a complete right angle. Due to the presence of mélange the block appears held in place before overturning which is visible on 22 May.

These events were before the mélange evacuated the fjord as well as before the temperature increase on 31 May 2014 that signaled the breakup of the mélange. The first event was initially outlined on 10 May 2014, 7 days before the observed calving event. Furthermore this was the largest event seen in the observational time period and produced iceberg IB-A. For six days after the calving event the iceberg didn't overturn and complete capsizing was never observed. Since the depth of the fjord was known, as well as the length, width, and height of the iceberg above sea level a rough estimate of the volume and mass can be calculated (**Fig. 37 & 38**). The volume of the iceberg was c. 1.41 x 10^8 m^3 and assuming the density of ice is 917 kg m^{-3} the mass of the ice was c. 1.3 x 10^{11} kg. This was 62% larger than any of the other observed calved icebergs. While the initial event was only the north western edge of the central region, once that piece broke free it allowed for the rest of the terminus to calve producing the grounded iceberg. The breakout of this piece appeared to create a ripple effect increasing the calving along the terminus where the glacier attempted to regain equilibrium. Looking at the period leading up to the calving event, there is a 42.4% increase in lateral

compressional strain rate within the glacier (**Fig. 39**) between 13 May and 16 May coupled with an 18.6 m/d^2 acceleration of the glacier. This causes the mélange to accelerate by 15.2 m/d^2 and have a 17.6% increase in lateral compressional strain rate while simultaneously increasing the longitudinal extensional strain rate by 11.3%. Furthermore even though the crevasses cut through the terminus the ice block appears to be held in place for at least a day, presenting as a cracking event with no visible water influx. The second event follows the same pattern. In the days preceding the calving event there is a 44.7% increase in the lateral compressional strain rate (**Fig. 40**) of the glacier coupled with a 10.3 m/d^2 acceleration of the terminus. This creates an 18.1 m/d^2 acceleration across the mélange, however the lateral compressional strain rate only increases by 2.1% and the longitudinal strain rate decreases by -3.9% between 20 May and 22 May 2014. The reason for this is because the calving event occurs over a much longer period of time, with partial collapses of the southern terminus occurring prior alleviating terminus strain.

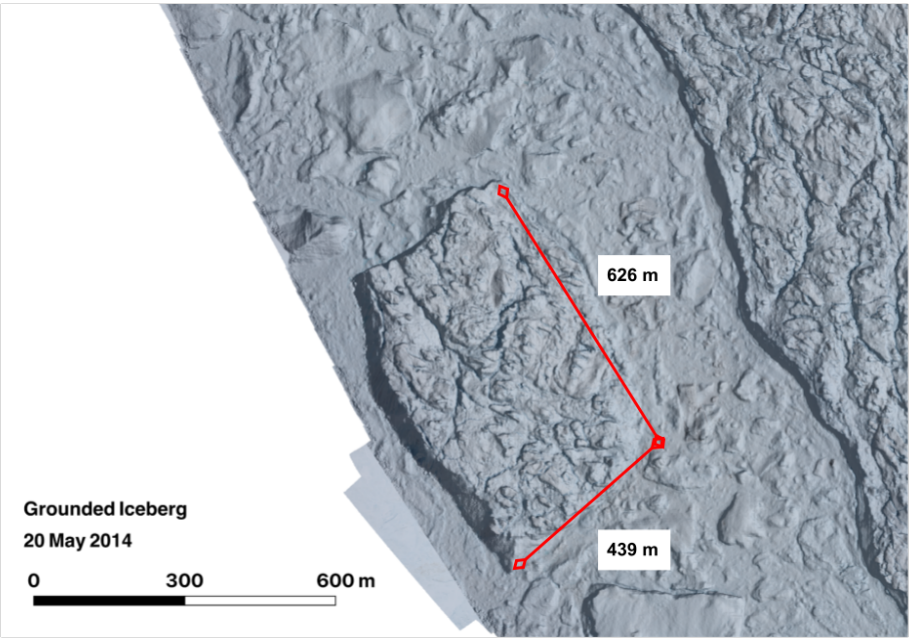

Figure 37: Topographic demensions of iceberg IB-A

Dimensions of the calved iceberg on the 20th of May 2014. The depth of the fjord in this area slopes from 469m to 532m. Since the elevation profile of the iceberg shows it is angled back towards the terminus of Store, the shallower depth was used in the calculation of the volume. Using the depth plus the height above sea level it was possible to calculate the overall height of the iceberg. The calculated volume of the iceberg is 1.41x10^8 m^3.

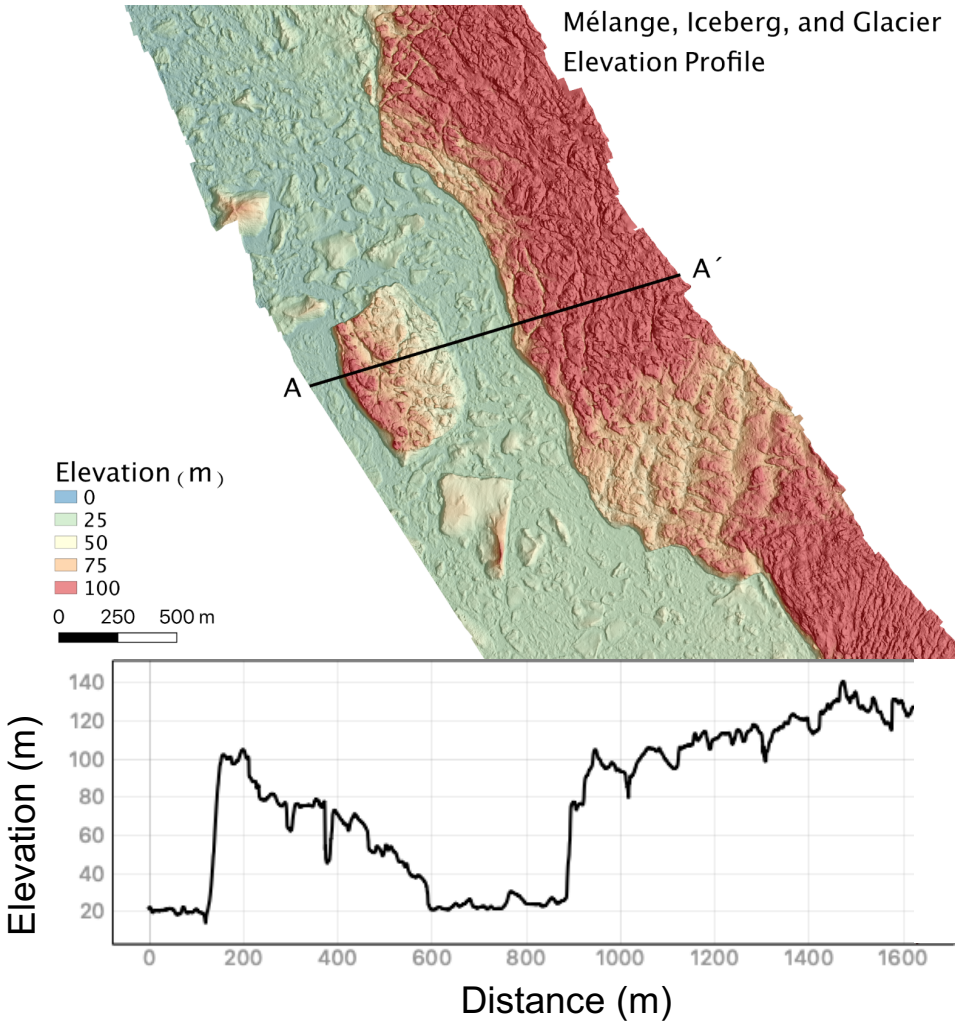

Figure 38: Depth and elevation profiles of iceberg IB-A.

Elevation profile from A to A' across the mélange , iceberg, and terminus. The calving event ending May 17 produced the large, grounded iceberg in the foreground. This iceberg measures over 100 m.a.s.l. in height, while the surrounding mélange has a minimum height of roughly 20 m.a.s.l.

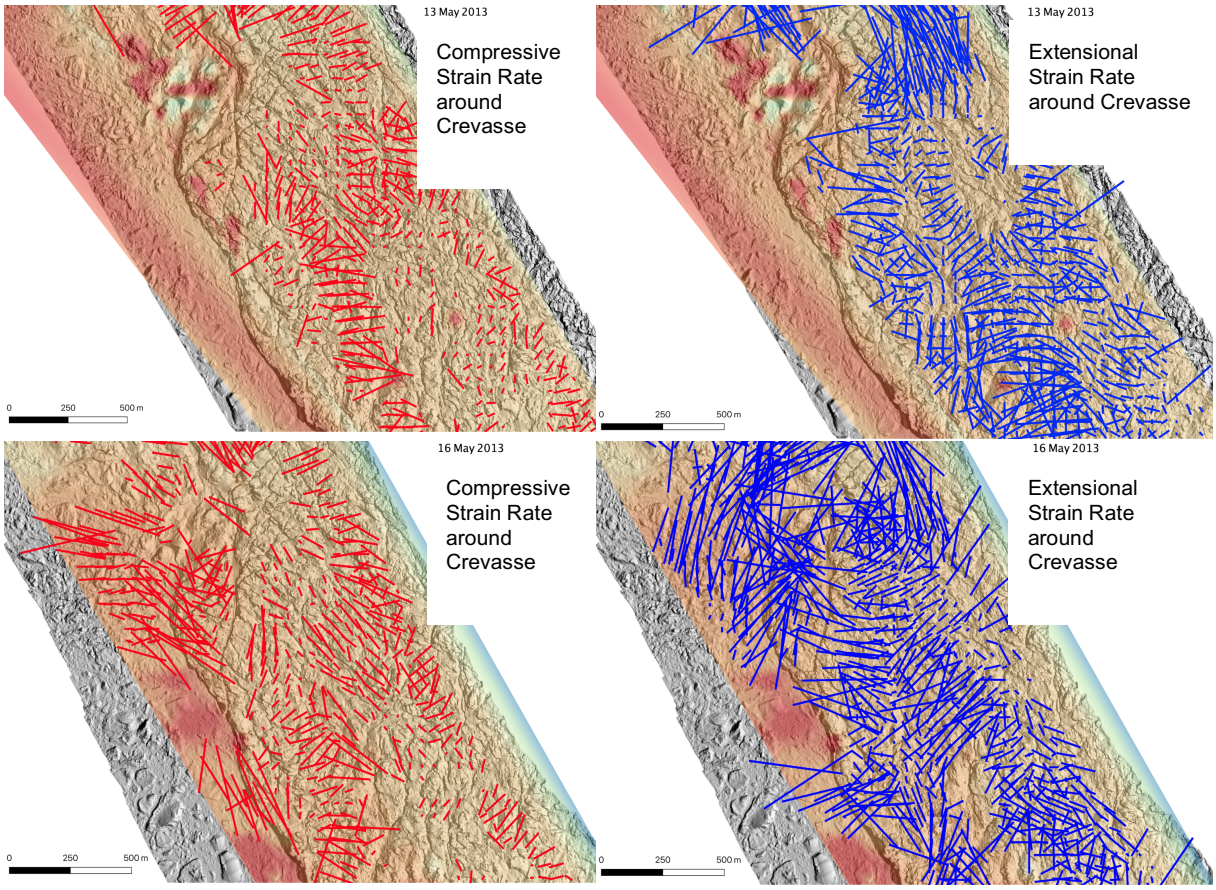

Figure 39: Strain rates for the terminus and mélange for the 10 May - 17 May 2014 calving event

Compressional (red) and extensive (blue) stress around the formation of the initial crevasse for the large calving event between 10 and 17 May. On the 13th the crevasse propagation is only about halfway through to the terminus with little compressive or extensive stress. On 16 May there were distinct extensive stress bands across the crevasse and a higher compressive stress directly in front of the detaching block. As the glacier moves forward and the block detaches, it is forced into the abutting mélange causing the compressive stress in the direction the block is being pushed off.

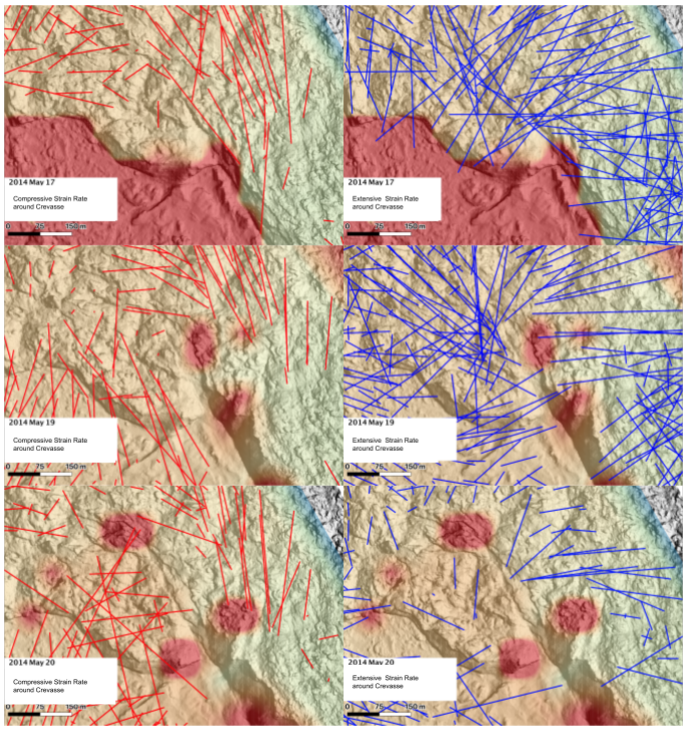

Figure 40: Strain rates for the terminus and mélange for the 17 May - 22 May 2014 calving event

Strain rate occurring around the 22 May calving event. The extensive stress is translated into the mélange as a compressive strain rate as the terminus advances; crushing the ice directly adjacent to it. There is a transition from primarily extensive stress to primarily compressive stress by 20 May. This shift is caused by the ice block detaching from the terminus. Once this happens the block is getting squeezed between the mélange and the advancing terminus.

The latter events occurred between 07 June - 16 June 2014 (**Fig. 41**) and and again between 18 June - 2 July 2014 (**Fig. 42**) respectively. These events were after the proglacial mélange had been evacuated from the fjord and were smaller in size than the initial event on 10 May. These events were harder to observe in the UAV imagery due to the acceleration occurring across the terminus during calving events. There were several other large calving events that occurred during this timeframe but due to the gaps in the photogrammetry across the terminus they weren't able to be observed in progression. Water intrusion was noted into the crevasse but only when it fractured the terminus of Store Glacier and was in direct contact with the fjord.

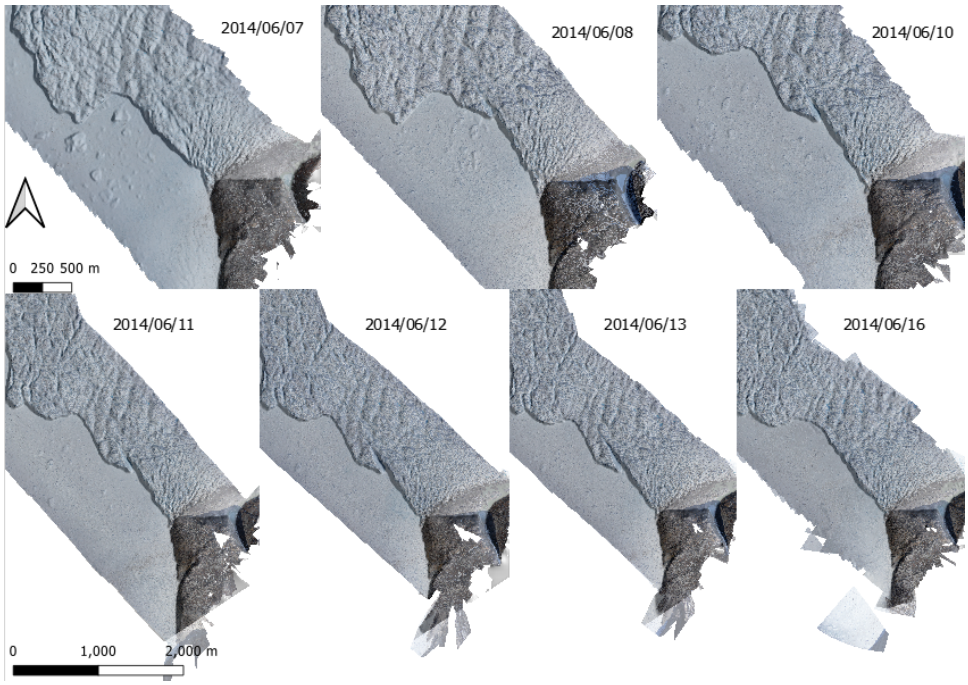

Figure 41: Crevasse propigation for the 4 June - 7 June 2014 calving event.

Crevasse propagation after the mélange breakup between the 4-7 June showing the 'zipper effect' of the crevasse slowly widening from the point of initiation. Unlike the previous examples, this calving event shows water inflow from the fjord as progression continues.

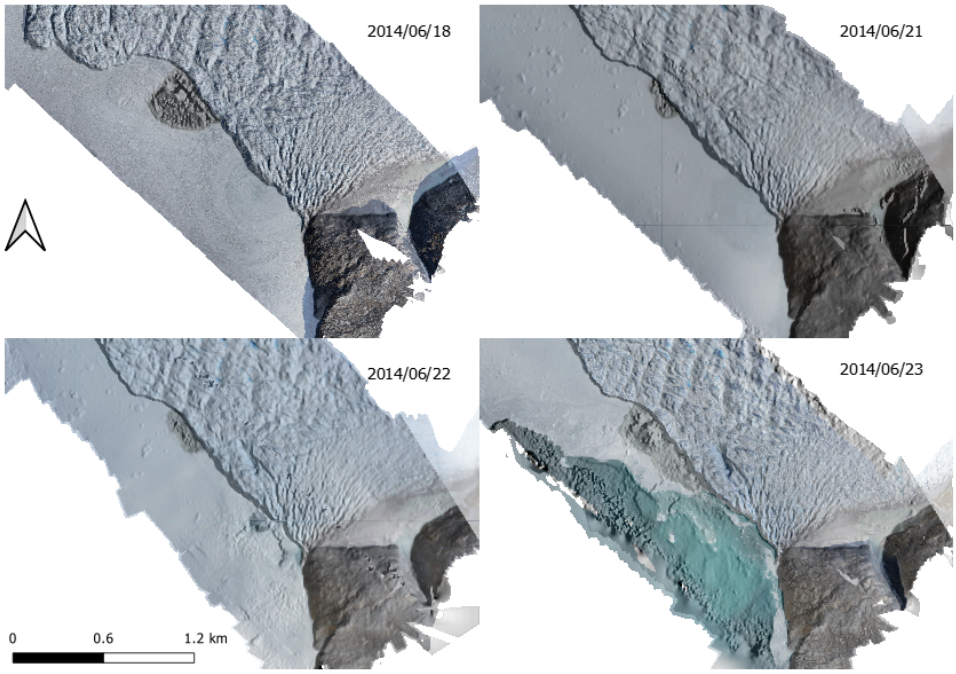

Figure 42: Crevasse propigation surrounding the 2 July 2014 calving event.

The initial formation of the calving event that occurred by 2 July 2014. The crevasse formation can be seen on the southern terminus of Store and slowly widens and sinks in the time prior to breaking off. This event follows the same characteristics of Event 3, however the crevasse moved from inside of the glacier to the terminus. It is possible to see multiple meltwater plumes (the brown grey discoloration along the terminus) as well as clear open water on 23 June. If zoomed in on this image a trail of ice debris is visible coming from the location of where the crevasse meets the fjord.

The third and fourth events occurred from the south side of the terminus and with the use of the orthophotos, visible water was observed flowing into the crevasse from the fjord in event 3. Event 4 appears as the crevasse starting from the interior of the glacier and moving outwards to the fjord (**Fig. 43**). Looking at the images taken from this timeframe, it appears as if there is a sliding plane allowing the upper elevation to slide off creating the over widened crevasse. These events appear as 'zipper events', meaning that as the crevasse size increases, the ice block starts to separate from the terminus at the initial point of crevasse propagation. These two events occur after the mélange has broken away resulting in the change in calving dynamics. Event four, while not the biggest, is the longest tracked crevasse propagation event seen within the dataset

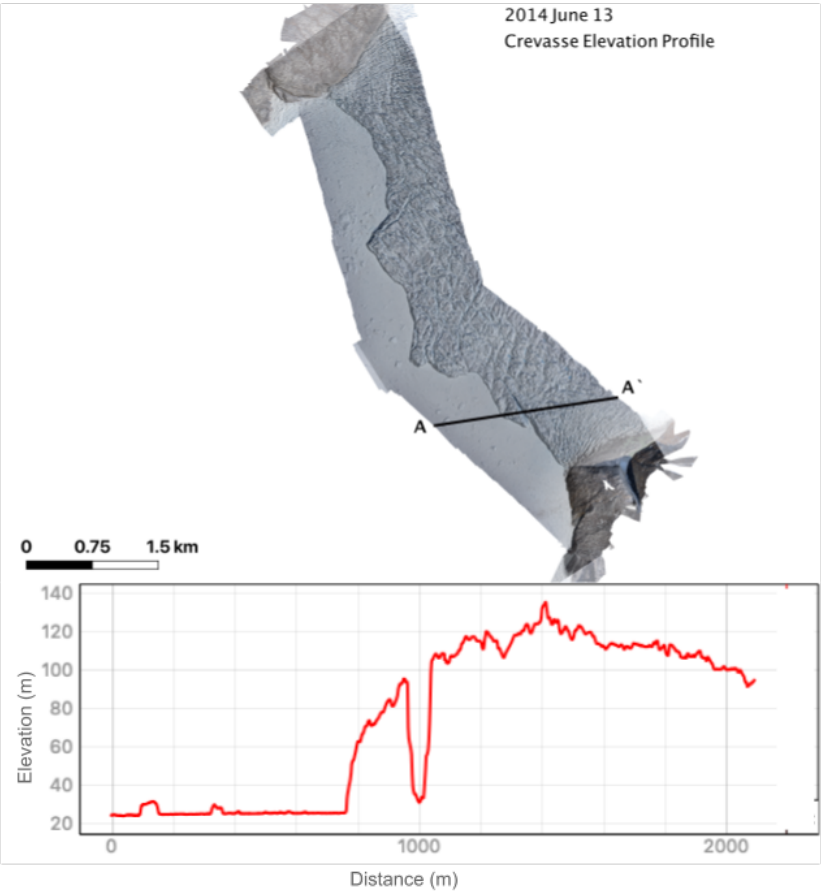

Figure 43: Elevation profile of the 2 July 2014 event crevasse formation.

Elevation profile across the southern portion of the terminus showing the ice block has fully separated from the upper portion of the glacial terminus. This progressive separation allows the influx of water from the fjord into the crevasse. It is determined to be from the fjord due to the elevation proximity instead of a meltwater lake.

Prior to the proglacial mélange evacuation it was possible to see nearly all calving events either through crack propagation or appearance of icebergs, even small events were able to be recognized and studied. While it is still possible to determine calving events from crevasse propagation, it becomes increasingly difficult with the current dataset due to the rate of data collection at one survey every 1.75 days once the mélange breaks apart. Some events, while having the defining features in crevassing, break off quickly and as such are not caught due to the duration of the event as well as the speed at which icebergs are able to move out of the fjord.

5.2 Regional Constraints on the Terminus of Store Glacier

The northern section of both the glacial and mélange experience lower average velocities than the rest of the terminus by 36.7% and 23.87% respectively caused by the forcing occurring along the bedrock. The bedrock margin turns toward the south, averaging the total alteration in glacial flow to 37.02˚, however more of the deformation occurs along the greater variation to the north. The 32˚ turn after the terminus position has less effect on the glacier during the summer months as the icebergs can freely move down the fjord; during the winter months it creates additional bottlenecks due to the ice mélange slowing glacial velocity. Once the majority of the proglacial mélange breaks up between 4 June and 7 June, embayments expand across the northern terminus. During the period of embayment expansion between 7 June and 12 June thick ice is still visible along the bedrock margin. This is supported by the regional velocity of the glacier in the northern section. The average velocity for the period of 10 May to 31 May 2014 before the mélange starts to lose strength across this section of glacier was 5.87 m/d. Once the mélange starts to lose strength after 1 June 2014 until 12 June 2014 the northern portion of the glacier velocity increases 78.86% to 27.6 m/d. After the breakup of the mélange the terminus velocity of the glacier becomes increasingly homogeneous. While the average velocity across the northern region of the glacial terminus is 6.8 m/d compared to the 16.7 m/d and 21.7 m/d rates of the central and southern regions before the mélange moves out, it increased to 27.6 m/d aligning more with the 28.8 m/d and 24.9 m/d velocities of the central and southern regions. As determined by the bathymetry and elevation modeling across the terminus, Store Glacier is grounded throughout the study period along with portions of the proglacial mélange. The most pronounced basal pinning occurs within the southern region of the glacial terminus. In each bathymetric profile the basal shallowing of the modeled fjord

corresponds to roughly the same position across the terminus determining the transect that D - D' followed. In all but the southern profile the fjord steeply deepens immediately after the pronounced shallowing. The narrowing of the fjord width by 2.2 km, coupled with the decrease in fjord depth by 210 m, ~37˚ turn provide enough restriction to the glacial flow, averaging a velocity of 21.6 m/d for the study period, stabilize the position of the terminus.

The change in bed topography alters calving characteristics across the glacial terminus. There are three distinct regions (**Fig. 44**) that correlate roughly to the location of basal topography change and create different size icebergs as well as exhibit variation in glacial velocity. The northern portion of the glacier averages a 55% lower velocity as compared to the terminus average while the mélange is in place. This portion of the glacier additionally never produced stable, large, grounded icebergs during the study period. Due to the bedrock forcing along the northern section as well as the fairly unrestrictive bathymetric topography it is unsurprising that the ice in this region tends to be more fractured and break off generally smaller icebergs. Pre-fracturing of the ice from impact with the bedrock margin could contribute to lack of large iceberg formation. None of the northern regional calving events are discernible within the strain rate profiles across the terminus of Store Glacier. The centerline sees a 42.1% velocity increase in the period during mélange breakup, with glacial velocity increasing from an average of 16.7 m/d to 28.9 m/d. The center region of the glacier is responsible for most of the large, grounded icebergs seen throughout the study timeframe. In addition large calving events across the central region of the glacier tend to correlate with increases in the average lateral compressive glacial strain rate. The large calving event occurring between 16 - 17 May 2014 saw a 42% increase in compressional lateral strain rate, however only a 1.8% in extensional longitudinal strain rate. By contrast the southern portion of the glacier exhibits longitudinal strain rate spikes coinciding with calving events. The event culminating in the 22 May calving event saw a 44.8% increase in extensional longitudinal strain rate and an average glacial acceleration of 10.3 m/d^2. The southern region is the portion of the glacier that is most constrained by the shallowing of the fjords' bathymetry and as such is continuously calving. The southern region doesn't create large protruding glacial tongues like the central region does prior to calving and remains fairly stable in location. The mélange has less of an effect on the glacial velocity in this region. In the period between 10 May and 31 May 2014 the average glacial velocity was 21.7 m/d, while in the succeeding period from 1 June to 13 June 2014 the glacial velocity only increased by 13.0% to 24.9 m/d.

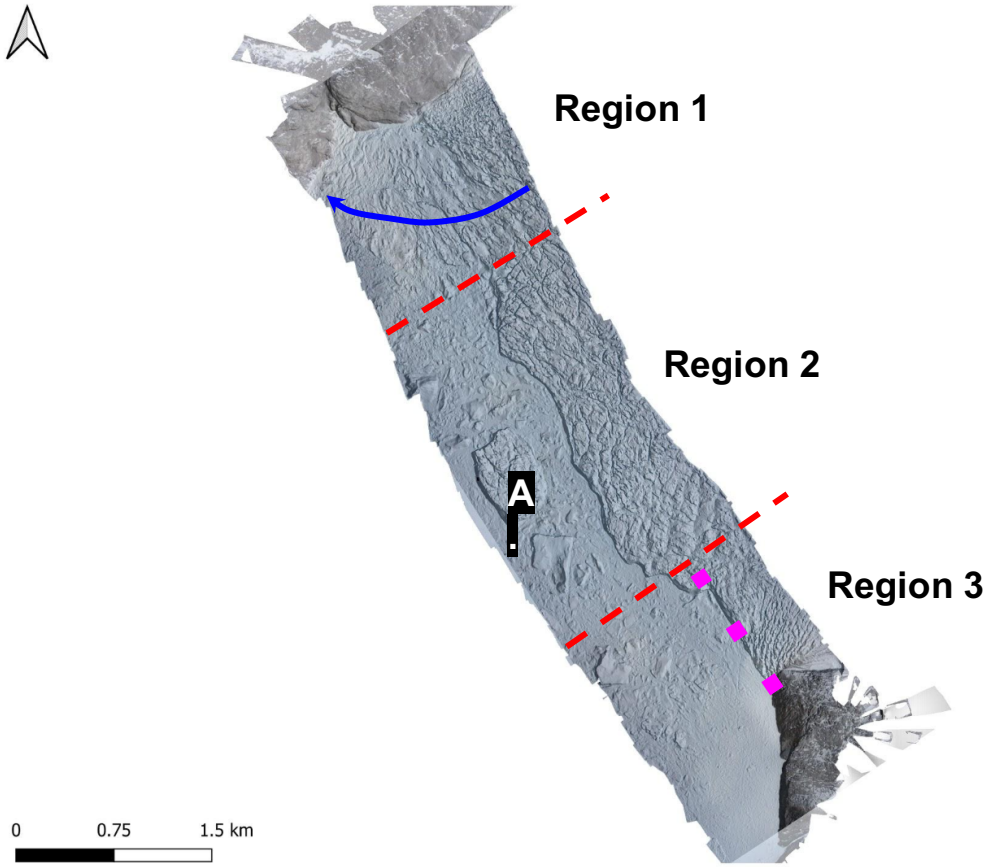

Figure 44: Regional sectioning of the temrinus of Store Glaicer

The three distinct calving regions across the terminus of Store glacier (17 May 2014). Region 1 is the Northern region and shows the ice being pinned by the curvature of the fjord wall. This presents as the large conglomeration of fractured ice curving towards the fjord (blue line). Region 2 is the central portion of the glacier that is free flowing. This is the area that produces large, grounded icebergs (**A.**) as seen in front of the terminus. Region 3 is the southern region that overrides the bathymetric shallowing of the fjord. This prefractures the ice so that it is continuously calving along a defined line (pink dots) perpendicular to the glacial terminus preventing extended terminus growth in this region.

Data from this study shows that the terminus of Store Glacier is largely controlled by the processes occurring at the ice-ocean interface as well as at the bed. The proglacial mélange drastically reduces the glacial velocity along the northern portion of the terminus to a rate four times lower than the period without the mélange, while halving the regional central velocity. Additionally the fjord topography allows the growth of a thick, fairly stable mélange in this region as shown by elevation and regional acceleration. The increasing magnitude of acceleration spikes of the glacier terminus in the period during which the mélange is evacuating the proglacial fjord confirms the modelled influence by Todd et al. 2018. The mélange exerts the greatest influence on seasonal terminus dynamics.

5.3 Bathymetric Constraints at the Terminus of Store Glacier

From bathymetric (Bedmachine) and elevation profile data it was determined that the terminus of Store Glacier is fully grounded throughout the duration of the study period. Furthermore, portions of the northern and southern mélange appear to be grounded. The central region of the mélange only grounds when containing icebergs of sufficient depth as to be grounded. The elevation of the proglacial mélange in front of the terminus lends to the majority being rafted. Throughout the presence of the proglacial mélange there are several large icebergs that are formed during calving events and are assumed to be grounded. Since full thickness of the icebergs was not able to be measured, volume calculations provide an estimate of size based on the shallower fjord depth for which the iceberg is situated. The elevation corresponding to that same point was used to determine height. Icebergs are assumed to be cuboid in shape under the water. In instances where the iceberg was floating, the minimum fjord depth was still used with the assumption that glacial volume would not exceed the calculated value. Determination that the icebergs didn't overturn was due to observations of the surface crevassing visible across the surface. Conversely icebergs that did overturn presented a much smoother ice face due to submarine melt. Once calved into the mélange the majority of independent iceberg movement occurs during periods of glacial advance or calving. There is visible lateral movement of IB-D perpendicular to flow in a southern direction after the large calving event along the glacial centerline that creates IB-A/A2/B. This is most likely due to the large amount of ice discharge and movement occurring during this calving event. After this IB-D returns to parallel movement with mélange velocity.

Of the larger icebergs that were measured IB-C is the only grounded iceberg that stays visible in the proglacial fjord until the breakup of the mélange between. This iceberg is also definable prior to its calving by crevasse propagation that occurs across the terminus by 20 May 2014. IB-C is one of only two large, grounded icebergs that are produced from the southern portion of the terminus during the study period while the mélange is in place. Most calving events from this area produce smaller ice blocks that quickly assimilate into the proglacial mélange. The northern portion of the terminus creates no large, grounded icebergs, with the mélange appearing as a mostly grounded conglomerate of ice. While there are portions of the discharge on the northern terminus that are floating, there are no discernable calving events that occur until the mélange moves out. Between 4 - 7 June 2014 an embayment was created on the

northern flank of the terminus and a large amount of ice was evacuated out. The embayment cut back until stabilizing on 13 June 2014.

While the Bedmachine_v3 dataset proves to be very useful in modeling the fjord bathymetry around Greenland there is question about its reliability around the terminus of glaciers and how realistic the bathymetric model is. For the portion of the fjord under the terminus of Store Glacier there are discrepancies that are visible using the Bedmachine_v3 0.5m resampled data as well as in the elevation profiles across the southern region of the glacier. While the velocity and strain rate data corroborate the theory that the terminus of Store Glacier is basaly pinned on a shallow region of the fjord, it is unlikely that the fjord depth increases to sea level in the region as seen in the C - C' profile. Additionally looking at the profile of fjord width, D - D', we see that it not only shallows extremely quick south of the glacial centerline, but that there is a rapid sequence of decreasing and increasing topography to depths in excess of 400 m.b.s.l over a horizontal distance less than 1000 m before returning to near surface elevations. It is highly unlikely that this portion of the modeled basal topography correctly represents the real fjord bathymetry. Error within the Bedmachine_v3 data arises as in many cases, no radar-derived ice thickness measurement is available within 50 km of glacier termini, despite being critical regions for ice sheet models. To map the bed beneath the ice, Bedmachine creation made use of the mass conservation approach (Morlighem et al. 2017). The accuracy of this mapping method degrades along flow away from radar lines (Morlighem et al. 2017), as the ice moves away from ice thickness constraints. In order to better and more accurately determine the basal topography in front of Store Glacier it is necessary to obtain near-terminus bathymetric data and radar profiles across the terminus. This is a difficult task though due to glacial terminus crevassing as well as the large ice discharge and calving events making data collection hazardous. Data collection from the terminus would benefit from modification of remotely operated collection methods like those described in (Kimball et al. 2014).

The creation of the floating ice mask layer further highlights the need for having near terminus bathymetric data to better constrain the mechanics of Store Glacier. Sampling of the Bedmachine_v3 data was completed at a 10 m resolution. While this is adequate for creating a

general bathymetric map for the entirety of Greenland, it limits how much data is captured on a micro level. Initial creation of the mask layer showed large bathymetric steps within the data that correlate to the grounding lines observed in the northern and southern regional proglacial mélange. These correlated to the edge of the pixel creating a large loss of data for features within the bathymetry ranging in size less than 10 m or if the feature terminated between the 'step' created by the pixel edge. Smoothing the Bedmachine_v3 to a 0.5 m resolution helped to eliminate the issue of the data 'step' but in doing so the data in between was interpolated by the computer programme. The 10 m resolution is an issue along the fjord margins, particularly in the southern region of the terminus. A whole portion of the proglacial mélange in this region is shown as grounded due to the depth data for this region being at or above sea level. It is probable, due to mélange thickness, that portions of the northern regional mélange would be grounded, data availability still creates regional uncertainties.

5.4 Seasonal Controls Acting on the Terminus of Store Glacier

The proglacial mélange remains in place across the terminus of Store Glacier from 10 May 2014 until the period between 4 - 7 June 2014, at which point the majority of the mélange is evacuated from the fjord. This is determined from orthoimagery, DEM elevation profiles, the lack of calving icebergs lingering in the proglacial fjord, and eventual loss of strain rate and velocity from the ImGraft processing. This period coincided with an extended period of warming, high katabatic winds coming off the glacier and an observed calving event. Due to the warming cycle and winds, the mélange would be unable to reform. In order for the ice reformation the air and ocean temperature would have to be below 0˚C for several days. An average wind direction of 185.5˚ means the wind is coming almost due south down off of the glacier contributing to the springtime breakup of the mélange.

The mélange typically moves out in the mid-spring due to warming temperature, warming water, or strong katabatic winds. These all work together to break down the bonds the mélange has with not only the terminus of the glacier but also the fast ice that is frozen to the fjord margin. Looking at the annual interpolated temperature data created from the DMI dataset we see that throughout the winter the air temperature stays sufficiently low to allow the growth of a thick proglacial mélange. The winter of 2014 was interspersed with several

uncharacteristic temperature spikes above 0˚C on 9 Jan (+0.56˚C), 29 Jan (+0.16˚C), and 28 February (+0.96˚C). The 28 February temperature increase was the greatest seen during 2014 as the temperature four days prior on 24 February was -23.02˚C. This was an increase of 23.98˚C occurring during the height of winter. Despite seasonal warming starting before the mélange moves out, there is a large prolonged temperature increase above +0˚C that occurs in conjunction with proglacial mélange breakup. Starting 31 May there is a +6.65˚C temperature increase before the temperature cools 3.39˚C on June 4 to +3.15˚C before rewarming 2.96˚C to +6.11˚C on June 5. The initial rapid heating of the proglacial mélange likely weakened the bonds that the ice had with the terminus of Store Glacier as well the fast ice attached to the bedrock. Exposed to heating and cooling cycles, ice will act as a crystalline solid and expand or contract in response. This quick cycle of heating and cooling during the 5 day period could further weaken the bonds of the ice, though melt, winds, and calving are the main driving forces. Corresponding orthoimages show the mélange in place after the initial warming prior to 4 June, however lateral and longitudinal strain rate both increased starting on 31 May 2014, signaling the initial breakup. Prior to 1 June 2014 the lateral strain rate of the mélange and glacial terminus were fairly well coupled. The period between 1 June and 4 June 2014 is also the timeframe that sees the greatest variation between regional acceleration.

Comparison of the observed calving events to temperature increases (**Fig. 45**) during the study timeframe show some correlation between temperature increases and the glacial calving. This comparison is however poorly constrained compared to that of glacial calving and increases in strain rate, acceleration or velocity. The increase in temperature has more effect on the proglacial mélange than it does on the calving dynamics of the glacier. However an increased winter warming trend could lead to earlier breakup of the mélange. As discussed from earlier studies, the mélange slows intrusion of warm water and leads to possible thickening of the glacier during the winter months. A loss of the seasonal mélange then could allow increased submarine melt rates of the terminus of Store Glacier throughout the winter months, possibly inducing glacial retreat. As shown by the glacial acceleration, a lack of proglacial mélange would create homogeneity between all three regions of the glacier allowing for an uninterrupted glacial calving regime.

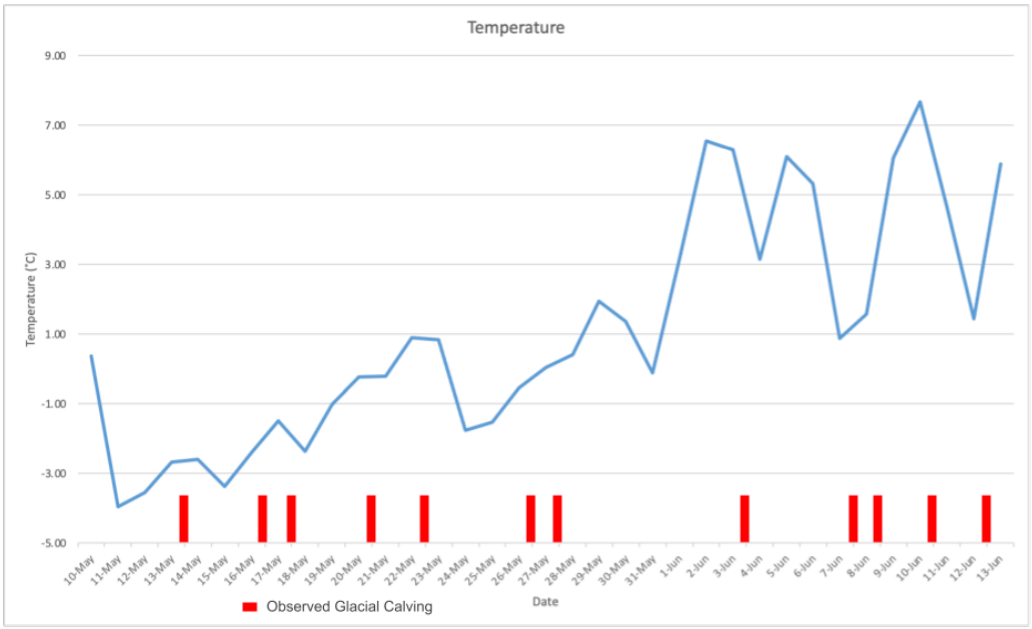

Figure 45: Study period temperature as compared to observed calving events.

Temperature for the study timeframe as compared to observed glacial calving events from the orthoimagery and GIS data. While there is some correlation between temperature increase and large-scale glacial calving it is poorly constrained.

There is a loose correlation between calving events and the longitudinal strain rate of the mélange (**Fig. 46**). A multi-day increase of 47.5% and 37.0%, starting on 10 May 2014, in both lateral and longitudinal strain rate respectively are seen prior to the calving event that occurs between 16 May and 17 May. The mélange decreased by 37.7% for lateral strain rate and 22.9% for longitudinal strain rate by 17 May 2014. For the prolonged calving event that is observed starting on 20 May and continuing through 27 May 2014 there is 25.7% increase in mélange longitudinal strain rate while only a 18.6% increase in lateral strain rate occurring on 23 May 2014. The longitudinal strain rate continues to stay at elevated levels through 26 May 2014 with an average strain rate of 1.46 u/a for the period. This then decreased by 47.9% on 27 May 2014. Conversely the lateral strain rate of the mélange decreased by 9.7% between 23 May 2014 and 27 May 2014. The calving events that occur during this time period both produce grounded icebergs into the mélange matrix. After 31 May 2014 the longitudinal strain rate of the mélange increased by 56.3%, peaking on 12 June at 2.09 u/a. Thus increase in strain rate coincides with the start of the prolonged warming trend on 31 May 2014 and signals the start of mélange breakup from the proglacial fjord. The longitudinal strain rate for this period increases as the ice is attenuated down the fjord. The lateral strain rate within the mélange for the same period experiences two distinct increases in strain rate on 1 June 2014

to -1.57 u/a and 4 June to -2.17 u/a coinciding with two additional calving events from the terminus of Store Glacier. This demonstrates that as the mélange weakens from warming it is less cohesive and more susceptible to the forces from glacial calving and advance. While there are increases in mélange strain around glacial calving events the mélange reacts more to changes in regional temperature. The average lateral strain rate across the glacial and mélange before the period of warming was -0.84 u/a and -0.94 u/a respectively signaling a close coupling between the glacial terminus and the seasonal proglacial mélange. The longitudinal strain rate for the glacier increased by 0.9% from the premélange break-up period to after the mélange moved out of the fjord while the mélange strain rate increased by 29.2%. The lateral strain rate across the glacier for this same period remained unchanged while the mélange rate increased by 33.3%. The mélange is the largest impact on seasonal calving dynamics within the dataset.

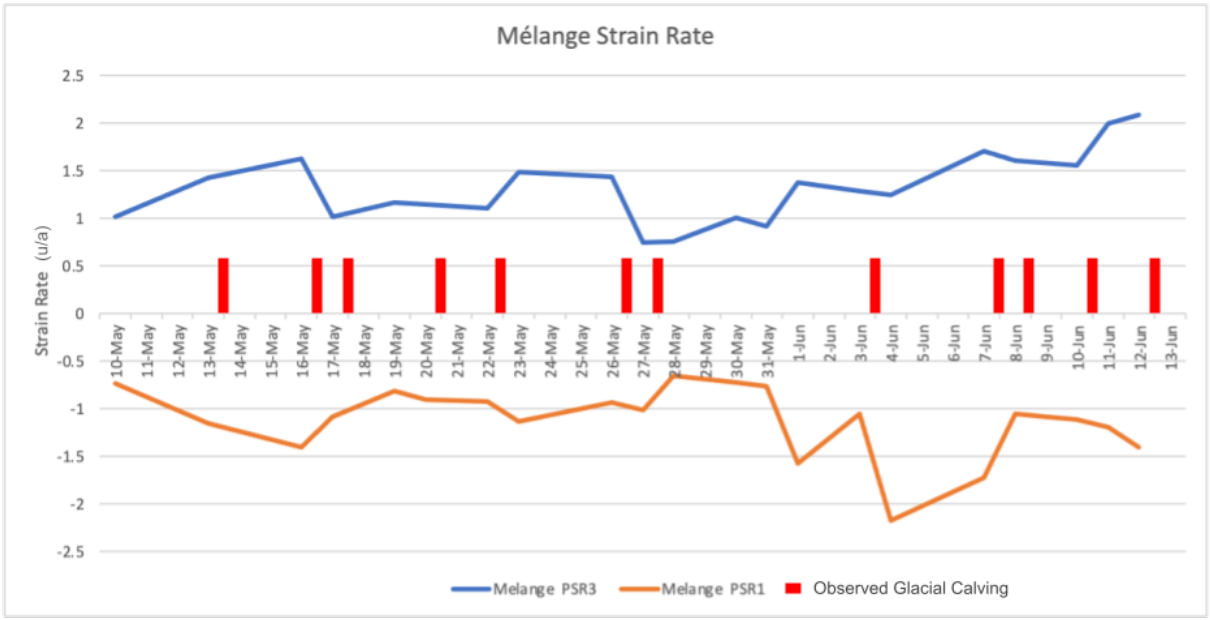

Figure 46: Mélange strain rates as compaired ot observed claving events.

The velocity during this period follows closely with the events seen within the strain rate and DEM observations. The average velocity for the mélange during the period from 10 May to 13 June 2014 was 25.1 m/d while that of the glacier was 21.6 m/d. There are several velocity spikes corresponding to 16 May, 22 May, 26 May, 3 June, 7 June, and 10 June. In these instances the glacier and mélange velocities are fairly similar until the event on 10 June when the mélange increases to 64.6 m/d and the terminus of Store Glacier reaches 50.8 m/d.

The acceleration, velocity and lateral strain rate across the glacial terminus compared to the same parameters from the immediate proglacial mélange show that the mélange is well coupled to the glacial terminus. The expanse and thickness of the mélange allow it to capture large calved icebergs providing localized grounding pylons to anchor floating parts of the mélange. There is a glacial velocity and strain rate increase that occurs during the timeframe in which the mélange loses strength and evacuates the fjord, however after the glacial strain rate and velocity both decrease with the strain rate trending towards normalized pre-breakout levels. The proglacial mélange is the largest seasonal control on the calving dynamics of Store Glacier, however it doesn't alter the flow drivers of the glacier. Glacial strain rate remains stable whether the mélange is present in the fjord or not.

5.5 Controlling Factors on the Frequency and Magnitude of Calving Events

Comparing the observed calving events across the terminus of Store Glacier between 10 May and 13 June 2014 to the daily average strain rates for the same period shows a correlation between the observed events and the increases in lateral compression (PSR1) and longitudinal extension (PSR3) within the strain rate graph (**Fig. 47**). The earliest calving event that was observed was between 10 May and 13 May 2014 along the southern region of the terminus. Looking at the compared timeframe for the strain rate there is a 51.3% decrease in lateral strain rate and longitudinal strain rate only increases by 11.6%. The partial collapse of the leading edge of the southern terminus on 16 May 2014 and the major central region calving seen on 17 May 2014 correlate to a 42% increase in lateral compression but only a 1.8% increase in longitudinal extension. After this calving event there were several rapid spikes in the longitudinal strain rate on 19 May, 22 May and 26 May 2014. While the increase on 19 May was only by 14.4%, the 22 May and 26 May values increased by 44.8% and 45.4% respectively. These three spikes as well as the 22.3% increase in lateral compression on 20 May all correspond to calving and terminus edge collapse in the southern region of the glacier. Using the orthoimagery, there is crevasse propagation after the initial ~14% strain rate increase on 19 May and in occurrence with the ~22% longitudinal increase on 20 May 2014. This crevasse propagation defines the shape of the iceberg that calves out on 22 May 2014. There is a small lateral collapse observed across the southern terminus that occurs in

conjunction with the crevasse propagation on the 20th. On 22 May 2014 the iceberg is observed to have calved along with another partial collapse of the regional southern terminus. At the same time the longitudinal strain rate increased by 44.8% while the lateral strain rate decreased by 22.1%. On 26 May 2014 there was a full collapse of the southern regional terminus observed within the dataset in occurrence with a 45.4% increase in longitudinal strain rate and a 10.7% increase in lateral strain rate. Lateral strain rate increased by 28.5% while longitudinal strain rate decreased by 37.6% on 27 May 2014 during a calving event that occurred within the central region of the glacier.

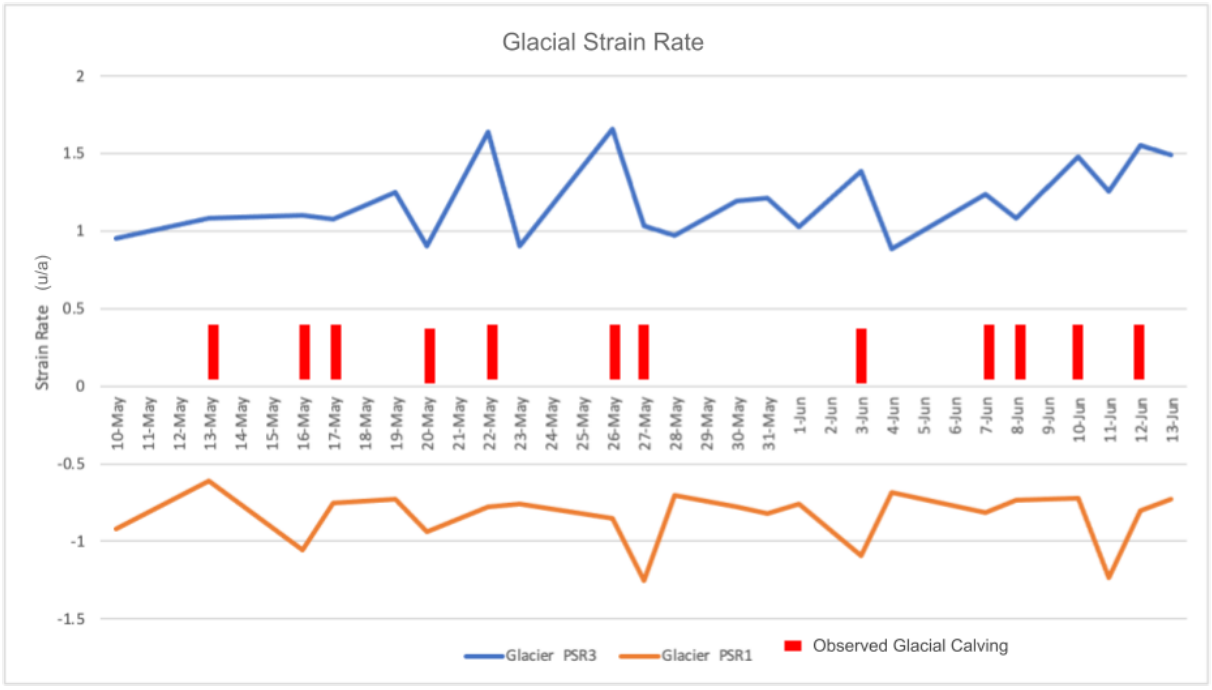

Figure 47: Glacial strain rate as comapired to observed calving events.

A graph showing the daily glacial strain rate through time as compared to observed calving events from the orthophotos and GIS data. Calving events that occur along the southern portion of the terminus correspond to increases in longitudinal (extensive) strain rate while increases in lateral (compressive) strain rate correlate more closely with glacial calving that occurs in the central region of the terminus. Calving within the northern region creates no noticeable increase within either lateral or longitudinal strain rate.

After 27 May 2014 the strain rates across the glacier returned closer to the period averages of 1.19 u/a for longitudinal and -0.84 u/a for lateral strain rate. This lasted for six days before both increased again by 25.7% for longitudinal strain rate and 30.4% for lateral strain rate. There are observed calving events that occur simultaneously in both the central and southern regions of the glacier. On 4 June both lateral and longitudinal strain rate decreased by 37.6% and 34.8% respectively. After 4 June however there is a steady increase in the longitudinal

strain rate and glacial velocity acceleration that corresponds to the calving induced after the proglacial mélange breaks out of the fjord. There is continued calving in the southern region of the terminus throughout the period of 7 - 8 June as well as 12 June 2014. Throughout the period between 8 June and 13 June there is continued crevasse propagation occurring across the southern terminus, however there is a gap in the dataset between 13 June and 16 June 2014 by which the previously defined block is no longer attached to the terminus. Even though the strength of the mélange is gone after 4 June 2014, there is no lateral compressional increase until 10 June 2014 after which it increases by 41.4% before decreasing to values observed prior to 10 June. While there is a large calving event that occurs between 8 June and 10 June 2014 across the central region of the glacier, the calving and the strain rate correlation is less constrained than in other events observed previously in the dataset.

In comparison of the calving events and the quantitative increases within the strain rate data, there is an apparent correlation between the type of strain rate and location of the glacial calving events. The longitudinal extensional strain rate (PSR3) is more reactive to the calving across the southern region of the terminus corresponding to the portion of the terminus that is impacted most by the basal fjord topography. Conversely lateral compressional strain rate increases correspond to the calving events observed across the central region of the terminus. Calving across the northern portion of the glacier appears to have no direct correlation with either the lateral or longitudinal strain rate.

The regional glacial velocity is in agreement with this assessment (**Fig. 48**) as the northern portion of the terminus only sees two velocity increases prior to mélange move out after 4 June 2014. The first occurs in the timeframe culminating in the calving event observed on 22 May 2014 and the second increase was observed prior to the 3 June 2014 calving event. There is an average acceleration 10 m/d^2 across the whole terminus and an increase by 77.7%, from 6.4 m/d to 28.7 m/d, for the northern portion of the terminus between 19 May and 22 May 2014. After this event the daily average velocity for the northern portion of the terminus decreases to less than 2 m/d. The second velocity increase along the northern region of the terminus occurs between 31 May and 1 June, peaking at 19.6 m/d which is up 88.6% from the 31 May average of 2.2 m/d and relates to a 51.2% increase in compressional strain rate across

the mélange for the same period. Looking at the velocity increases along the central region of the glacier as well as the southern region, there is more correlation not only between the two sections but also between strain rate variations and calving events across these regions of the terminus.

Prior to the mélange moving out of the fjord the major peaks within the central region of the glacier coincide with the large calving event occurring on 16 - 17 May and well as the event on 3 June with daily regional average velocity reaching 56.2 m/d and 53.8 m/d respectively. Immediately after both events the regional velocity slows by over 70%. Velocity across the southern region of the terminus corresponds to increases in longitudinal strain rate as well as the calving events that occur within the region. Prior to the mélange evacuation the southern region had a higher average velocity than the central region, though a lower peak velocity by comparison.

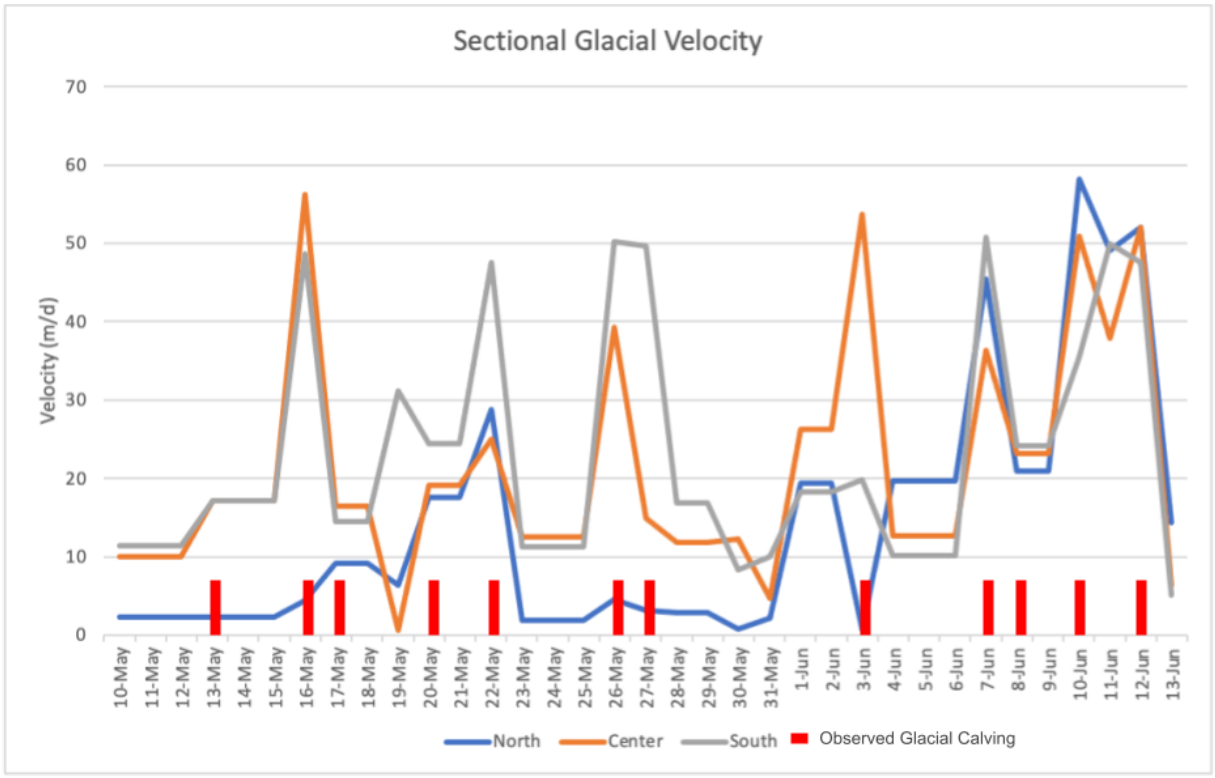

Figure 48: Regional glacial velocity as compaired to observed calving events.

A graph showing the regional daily glacial velocity through time as compared to observed calving events from the orthophotos and GIS data. Observed calving events correspond with the increases in southern and central region velocity increases. The northern region stays at a lower average velocity until the proglacial mélange starts to lose strength and breakup after the 3rd of June.

After 3 June 2014 all three regions experience acceleration until 12 June 2014, after which the terminus as a whole slows. There was an acceleration of -21.7 m/d^2 between 11 June and 13 June 2014.

Looking at the acceleration for the study period (**Fig. 49**) of the three regions of the glacier there is again evidence of coupling between the central and southern glacial regions until the evacuation of the mélange. In the period preceding each of the observed calving events there is a period of increased glacial acceleration followed by an immediate deceleration of the terminus coinciding with the calving events. Post glacial acceleration is the period of which the increased strain rates are observed within the dataset. Peak positive acceleration for the central region occurs immediately before the 16 May calving event reaching 19.6 m/d^2. This occurs in conjunction with the +15.7 m/d^2 acceleration of the southern terminus. The northern region of the glacier slows by -2.5 m/d^2 for the same period before accelerating +2.4 m/d^2 on 17 May 2014. The maximum positive acceleration for the southern portion of the terminus is +19.4 m/d^2 and occurs prior to the calving event that takes place on 26 May 2014. The central region of the terminus undergoes a +13.4 m/d^2 acceleration in the same time period prior to the calving on 27 May discussed previously. Similar to the event occurring on 16 May and 17 May 2014 the central and southern regions of the glacier quickly slowed, accelerating by -13.7 m/d^2 and -16.7 m/d^2. The northern portion of the terminus remains almost constant during the acceleration period of the central and southern region, accelerating by only -0.1 m/d^2 for the whole period.

The northern region of the glacial gradually accelerates over the period between 18 May and 21 May before undergoing a rapid negative acceleration immediately prior to the calving event that occurs on 22 May 2014. The northern region starts at 28.8 m/d before accelerating –13.4 m/d^2 to 1.9 m/d on 23 May 2014 after which it accelerates again to 4.5 m/d and enters a five day period of relatively little velocity change.

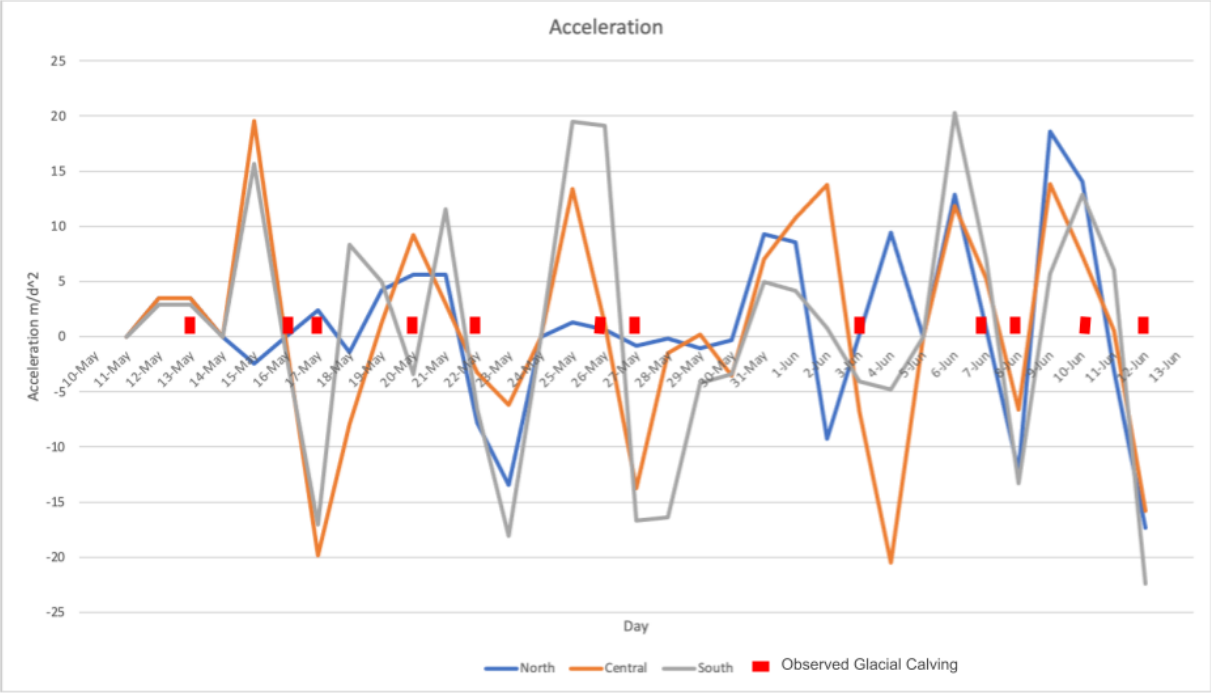

Figure 49: Galcial acceleration as compaired to observed calving events.

A graph showing the regional daily glacial acceleration through time as compared to observed calving events from the orthophotos and GIS data. Observed calving events tend to follow large increases, both positive and negative, in accelerations. Both the southern and central regions follow a rough cycle throughout the study timeframe with accelerations peaking roughly every 5 days. The northern portion of the terminus enters the cyclic nature of the terminus acceleration after the breakup of the proglacial mélange Evidence from this data shows that while the mélange doesn't affect the overall calving dynamics of the terminus, it does affect that of the northern region of the terminus.

Once the mélange starts losing strength around 1 June 2014 there is a shift in the acceleration dynamics of the glacier. The period between 1 June and 4 June 2014 see changes in regional acceleration that do not follow the coupling seen prior to this point. After 4 June 2014 however there is direct coupling between acceleration in all three regions in a much more cyclic fashion. The acceleration peaks surrounding the period between 5 June and 9 June 2014 align at the same point, while varying slightly in the rate of acceleration. Between 9 June and 13 June the positive acceleration peaks vary slightly, with the northern and central regions peaking at 18.6 m/d^2 and 13.6 m/d^2 respectively, prior to 10 June 2014 when the southern region accelerated by 12.9 m/d^2. After 12 June all three regions undergo rapid negative acceleration, the north by -17.4 m/d^2, the central region by -15.8 m/d^2, and the south by -22.4 m/d^2, to an average terminus velocity of 8.6 m/d.

Throughout the study timeframe the central and southern regions of Store Glacier's terminus remained fairly cyclical in both positive and negative acceleration with relatively little alteration from the time period while the mélange was in place to when it was evacuated from the proglacial fjord. Conversely the acceleration of the northern region of the terminus is heavily influenced by the presence of the proglacial mélange. For most of the period while the mélange was in place, the northern portion remained fairly stable with low region velocity except for the period around the 20 May - 22 May calving event. Once the mélange starts to lose strength around 1 June 2014 the acceleration of the northern portion starts to vary. South - central glacial acceleration and velocity coupled with strain rate increases correlate directly with observed calving events from the orthoimagery across the terminus for the given study period. Additionally the magnitude of the calving events vary across the three regions of the glacier and are primarily defined by the acceleration prior to calving as well as the strain rate across the terminus. The central region of the glacial produced the largest icebergs and changes to the terminus face within the study period and corresponded to increases in compression from the lateral strain rate of the glacier. Calving on the southern region of the terminus correlated directly with the increases in longitudinal strain rate of the glacier. While the central region of the glacier produced the largest calving events and the greatest changes to terminus shape, it is believed that the southern regional dynamics of the glacier have more impact on the overall stability of the terminus as evident by the direct correlation between southern glacial calving and longitudinal strain rate increases.

The average strain rates across the terminus of Store Glacier are stable throughout the study period. In comparing the calculated longitudinal and lateral strain rates before and after the evacuation of the mélange there is only a 0.01 u/a increase in the longitudinal strain from 1.15 u/a to 1.16 u/a. The lateral strain shows no alteration, remaining at -0.84 u/a. Showing no great trend in glacial strain rate variation during the loss of the mélange proves the terminus of Store Glacier is not only dominated by calving processes at the terminus, but specifically those at the bed of the glacier. This further confirms the modeling done by Todd et al. 2018 as well as that by Rignot et al. 2016 that calving processes, not submarine melt dominate the terminus.

5.6 Direction for Further Research

Refinement of this data series to include regional variations in glacier and mélange strain rates would allow better quantification of the driving forces behind the strain rates of the mélange as well as isolating those across the terminus of Store Glacier. Additionally being able to obtain fjord water temperature in conjunction with air temperature would help to better understand the period around the proglacial mélange losing strength and quantifying warm water influx to the terminus of Store Glacier in the winter months. Future studies should couple terminus data collection with upstream velocity and strain measurements to determine and quantify the attenuation of terminus forcing farther up the glacier, assuming they will be translated at least 16 km upstream. Coupling melt rate with strain data would help to better understand correlations between processes occurring at the glacial bed to the translated surface acceleration.

Increased data collection to accurately determine the bathymetry around and under Store Glacier is paramount to fully understanding the bed mechanisms. While the Bedmachine data provides plausible estimation of depth values near the terminus, there are glaring errors highlighted within the dataset that need to be corrected in order to fully understand the driving and resistive forces at the terminus. The 10 m resolution leads to gaps within the dataset causing modeled portions of the mélange and possibly terminus to be grounded when in actuality they might not. The lack of high resolution bathymetry data highlights the hazards with data collection around the terminus of a large marine terminating glacier. The prioritization of low budget remotely collected data is a key parameter in development of data collection techniques in order to allow scientists to remain a safe distance from the glacial terminus.

6 Conclusion

Data from this study shows that the terminus of Store Glacier is largely controlled by the processes occurring at the ice-ocean interface as well as at the bed. The proglacial mélange exerts the greatest influence on seasonal terminus dynamics, drastically reducing the glacial velocity along the northern portion of the terminus to 6.8 m/d, four times lower than the period without the mélange, while halving the regional central velocity. Presence of the mélange as well as the shallow slope of the proglacial fjord results in the extended entrapment of large calved icebergs as they are unable to efficiently evacuate the fjord. While the mélange is influenced by prolonged periods of temperature warming as well as regional forcings like calving and winds, the close correlation between lateral strain rates of the proglacial mélange and glacier terminus show that while in place, the melange is very well coupled to the terminus. The increasing magnitude of acceleration spikes of the glacier terminus in the period during mélange evacuation confirms the modelled influence by Todd et al. 2018, additionally the lack of proglacial mélange creates homogeneity between glacial acceleration across all three regions of the terminus.

The longitudinal and lateral strain across the terminus of Store Glacier remain stable through the study period. While there was a 0.9% increase in longitudinal strain during mélange breakup, glacial strain rate variation during the loss of the mélange proves the terminus of Store Glacier is not only dominated by calving processes at the terminus, but specifically those at the bed of the glacier. The narrowing of the fjord width by 2.2 km, coupled with basal pinning and ~37˚ turn provide enough restriction to the glacial flow, averaging a velocity of 21.6 m/d for the study period, to stabilize the position of the terminus. Moreover the changes in fjord topography and geometry effectively divide the terminus of Store Glacier into three distinct regions, each with different localized calving dynamics. While the central region of the glacier produced the largest calving events and the greatest changes to terminus shape, it is believed that the southern regional dynamics of the glacier have more impact on the overall stability of the terminus as evident by the direct correlation between southern glacial calving and longitudinal strain rate increases. Regional forcing within this part of the glacier appears to be the main control driving the frequency and magnitude of glacial calving events.

Using UAV imagery from the 2014 field season it was possible to predetermine the size of larger calving events by looking at the crevasse propagation across the terminus of Store Glacier. This was easiest in the earlier part of the season when the mélange was still buttressing the calving face. Even after the move out of ice between the 4th and 7th of June it was still possible to use crevasse propagation to determine calving events, though at a faster pace due to glacial acceleration surrounding calving events. Implications from this could allow for the prediction of glacial calving across the terminus of marine terminating glaciers up to a week before the actual event. Allowing predetermination of calving events will increase the accuracy of glacial modeling to better constrain the upstream dynamics driving determination of calving shape and size. This will additionally be able to help determine how marine terminating glaciers will react to changes from future climate scenarios.

While the regional velocity and terminus strain rate data corroborate the theory that the terminus of Store Glacier is basaly pinned on a shallow region of the fjord, the Bedmachine_v3 data doesn't accurately model the fjord bathymetry under Store Glacier. This is due to a lack of localized radar-derived measurements around the terminus. Collection of cross terminus radar profiles in addition to localized near terminus fjord bathymetric studies would greatly improve the accuracy of the given dataset. While high resolution datasets provide an excellent breadth of information, they are restricted by the resolution of the datasets that they are paired with. Further studies would be compelled to investigate the attenuation of terminus forcings further up on the ice stream.

Glaciers and ice sheets are committed to melting for decades to come and are irreversible on centennial time scales, Store Glacier will continue to play an important role in quantification of calving dynamics of marine terminating glaciers in order to better understand the full impact of the Greenland Ice Sheet on future sea level rise globally.

References

Ahn, Yushin, and Jason E. Box. 2010. “Glacier Velocities from Time-Lapse Photos: Technique Development and First Results from the Extreme Ice Survey (EIS) in Greenland.” *Journal of Glaciology*. https://doi.org/10.3189/002214310793146313.

Åkesson, Henning, Kerim H. Nisancioglu, and Faezeh M. Nick. 2018. “Impact of Fjord Geometry on Grounding Line Stability.” *Frontiers of Earth Science* 6 (June). https://doi.org/10.3389/feart.2018.00071.

Allan, Richard Philip. 2021. *Climate Change 2021: The Physical Science Basis : Working Group I Contribution to the Sixth Assessment Report of the Intergovernmental Panel on Climate Change.*

American Society of Civil Engineers. 1994. *Glossary of the Mapping Sciences*. ASCE Publications.

Amundson, Jason M., Christian Kienholz, Alexander O. Hager, Rebecca H. Jackson, Roman J. Motyka, Jonathan D. Nash, and David A. Sutherland. 2020. “Formation, Flow and Break-up of Ephemeral Ice Mélange at LeConte Glacier and Bay, Alaska.” *Journal of Glaciology* 66 (258): 577–90.

Amundson, J. M., M. Fahnestock, M. Truffer, J. Brown, M. P. Lüthi, and R. J. Motyka. 2010. “Ice Mélange Dynamics and Implications for Terminus Stability, Jakobshavn Isbræ, Greenland.” *Journal of Geophysical Research* 115 (F1). https://doi.org/10.1029/2009jf001405.

Barnier, B., L. Siefridt, L., P. Marchesiello, P. 1995. ‘Thermal forcing for a global ocean circulation model using a three-year climatology of ECMWF analyses’, *Journal of Marine Systems*, Volume 6, Issue 4, Pages 363-380, ISSN 0924-7963 https://doi.org/10.1016/0924-7963(94)00034-9.

Benn, Douglas I., and David J. A. Evans. 2010. *Glaciers & Glaciation*. Hodder Education.

Benn, Douglas I., Nicholas R. J. Hulton, and Ruth H. Mottram. 2007. “‘Calving Laws’, ‘sliding Laws’ and the Stability of Tidewater Glaciers.” *Annals of Glaciology* 46: 123–30.

Bigoni, Davide. 2012. *Nonlinear Solid Mechanics: Bifurcation Theory and Material Instability*. Cambridge University Press.

Box, Jason E., and David T. Decker. 2011. “Greenland Marine-Terminating Glacier Area Changes: 2000–2010.” *Annals of Glaciology* 52 (59): 91–98.

Burton, Justin C., Jason M. Amundson, Ryan Cassotto, Chin-Chang Kuo, and Michael Dennin. 2018. “Quantifying Flow and Stress in Ice Mélange, the World’s Largest Granular Material.” *Proceedings of the National Academy of Sciences of the United States of America* 115 (20): 5105–10.

Cappelen, John. 2020. *Weather Observations from Greenland 1958-2019: Observation Data with Description*.

Cassotto, Ryan, Mark Fahnestock, Jason M. Amundson, Martin Truffer, and Ian Joughin. 2015. “Seasonal and Interannual Variations in Ice Melange and Its Impact on Terminus Stability, Jakobshavn Isbræ, Greenland.” *Journal of Glaciology* 61 (225): 76–88.

Chauché, N., A. Hubbard, J-C Gascard, J. E. Box, R. Bates, M. Koppes, A. Sole, P. Christoffersen, and H. Patton. 2014. “Ice–ocean Interaction and Calving Front Morphology at Two West Greenland Tidewater Outlet Glaciers.” *The Cryosphere* 8 (4): 1457–68.

Clark, Peter U., Arthur S. Dyke, Jeremy D. Shakun, Anders E. Carlson, Jorie Clark, Barbara Wohlfarth, Jerry X. Mitrovica, Steven W. Hostetler, and A. Marshall McCabe. 2009. “The Last Glacial Maximum.” *Science* 325 (5941): 710–14.

Corripio, J. G. 2004. “Snow Surface Albedo Estimation Using Terrestrial Photography.” *International Journal of Remote Sensing* 25 (24): 5705–29.

DeConto, Robert M., David Pollard, Richard B. Alley, Isabella Velicogna, Edward Gasson, Natalya Gomez, Shaina Sadai, et al. 2021. “The Paris Climate Agreement and Future Sea-Level Rise from Antarctica.” *Nature* 593 (7857): 83–89.

Doyle, S. H., B. Hubbard, P. Christoffersen, T. J. Young, C. Hofstede, M. Bougamont, J. E. Box, and A. Hubbard. 2018. “Physical Conditions of Fast Glacier Flow: 1. Measurements From Boreholes Drilled to the Bed of Store Glacier, West Greenland.” *Journal of Geophysical Research: Earth Surface*. https://doi.org/10.1002/2017jf004529.

Dwyer, Gary S., and Mark A. Chandler. 2009. “Mid-Pliocene Sea Level and Continental Ice Volume Based on Coupled Benthic Mg/Ca Palaeotemperatures and Oxygen Isotopes.” *Philosophical Transactions. Series A, Mathematical, Physical, and Engineering Sciences* 367 (1886): 157–68.

Enderlin, Ellyn M., Ian M. Howat, Seongsu Jeong, Myoung-Jong Noh, Jan H. van Angelen, and Michiel R. van den Broeke. 2014. “An Improved Mass Budget for the Greenland Ice Sheet.” *Geophysical Research Letters* 41 (3): 866–72.

Fettweis, Xavier, Jason E. Box, Cécile Agosta, Charles Amory, Christoph Kittel, Charlotte Lang, Dirk van As, Horst Machguth, and Hubert Gallée. 2017. “Reconstructions of the 1900–2015 Greenland Ice Sheet Surface Mass Balance Using the Regional Climate MAR Model.” *The Cryosphere*. https://doi.org/10.5194/tc-11-1015-2017.

WCRP Global Sea Level Budget Group: Global sea-level budget 1993–present, Earth Syst. Sci. Data, 10, 1551–1590, https://doi.org/10.5194/essd-10-1551-2018, 2018.

Hanna, Edward, Sebastian H. Mernild, John Cappelen, and Konrad Steffen. 2012. “Recent Warming in Greenland in a Long-Term Instrumental (1881–2012) Climatic Context: I. Evaluation of Surface Air Temperature Records.” *Environmental Research Letters*. https://doi.org/10.1088/1748-9326/7/4/045404.

Härer, S., M. Bernhardt, J. G. Corripio, and K. Schulz. 2013. “PRACTISE – Photo Rectification And ClassificaTIon SoftwarE (V.1.0).” *Geoscientific Model Development* 6 (3): 837–48.

Heid, T., and A. Kääb. 2012. “Evaluation of Existing Image Matching Methods for Deriving Glacier Surface Displacements Globally from Optical Satellite Imagery.” *Remote Sensing of the Environment* 118 (March): 339–55.

Helm, V., A. Humbert, and H. Miller. 2014. “Elevation and Elevation Change of Greenland and Antarctica Derived from CryoSat-2.” *The Cryosphere*. https://doi.org/10.5194/tc-8-1539-2014.

Hofer, Stefan, Andrew J. Tedstone, Xavier Fettweis, and Jonathan L. Bamber. 2017. “Decreasing Cloud Cover Drives the Recent Mass Loss on the Greenland Ice Sheet.” *Science Advances* 3 (6): e1700584.

Holland, David M., Robert H. Thomas, Brad de Young, Mads H. Ribergaard, and Bjarne Lyberth. 2008. “Acceleration of Jakobshavn Isbræ Triggered by Warm Subsurface Ocean Waters.” *Nature Geoscience*. https://doi.org/10.1038/ngeo316.

Howat, Ian M., Jason E. Box, Yushin Ahn, Adam Herrington, and Ellyn M. McFadden. 2010. “Seasonal Variability in the Dynamics of Marine-Terminating Outlet Glaciers in Greenland.” *Journal of Glaciology*. https://doi.org/10.3189/002214310793146232.

Howat, Ian M., Ian Joughin, Mark Fahnestock, Benjamin E. Smith, and Ted A. Scambos. 2008. “Synchronous Retreat and Acceleration of Southeast Greenland Outlet Glaciers 2000–06: Ice Dynamics and Coupling to Climate.” *Journal of Glaciology*. https://doi.org/10.3189/002214308786570908.

IMBIE team. 2018. “Mass Balance of the Antarctic Ice Sheet from 1992 to 2017.” *Nature* 558 (7709): 219–22.

IMBIE Team. 2020. “Mass Balance of the Greenland Ice Sheet from 1992 to 2018.” *Nature* 579 (7798): 233–39.

Intergovernmental Panel on Climate Change, ed. 2014. “Sea Level Change.” In *Climate Change 2013 - The Physical Science Basis*, 1137–1216. Cambridge: Cambridge University Press.

IPCC, 2021: Climate Change 2021: The Physical Science Basis. Contribution of Working Group I to the Sixth Assessment Report of the Intergovernmental Panel on Climate Change [Masson-Delmotte, V., P. Zhai, A. Pirani, S.L. Connors, C. Péan, S. Berger, N. Caud, Y. Chen, L. Goldfarb, M.I. Gomis, M. Huang, K. Leitzell, E. Lonnoy, J.B.R. Matthews, T.K. Maycock, T. Waterfield, O. Yelekçi, R. Yu, and B. Zhou (eds.)]. Cambridge University Press. In Press.

Jenkins, Adrian. 2011. “Convection-Driven Melting near the Grounding Lines of Ice Shelves and Tidewater Glaciers.” *Journal of Physical Oceanography* 41 (12): 2279–94.

Joughin, Ian, Ian M. Howat, Mark Fahnestock, Ben Smith, William Krabill, Richard B. Alley, Harry Stern, and Martin Truffer. 2008. “Continued Evolution of Jakobshavn Isbrae Following Its Rapid Speedup.” *Journal of Geophysical Research* 113 (F4). https://doi.org/10.1029/2008jf001023.

Joughin, Ian, Ben E. Smith, Ian M. Howat, Ted Scambos, and Twila Moon. 2010. “Greenland Flow Variability from Ice-Sheet-Wide Velocity Mapping.” *Journal of Glaciology*. https://doi.org/10.3189/002214310792447734.

Kargel, J. S., A. P. Ahlstrøm, R. B. Alley, J. L. Bamber, T. J. Benham, J. E. Box, C. Chen, et al. 2012. “Brief Communication Greenland’s Shrinking Ice Cover: ‘Fast Times’ but Not That Fast.” *The Cryosphere* 6 (3): 533–37.

Khazendar, Ala, Ian G. Fenty, Dustin Carroll, Alex Gardner, Craig M. Lee, Ichiro Fukumori, Ou Wang, et al. 2019. “Interruption of Two Decades of Jakobshavn Isbrae Acceleration and Thinning as Regional Ocean Cools.” *Nature Geoscience*. https://doi.org/10.1038/s41561-019-0329-3.

Kimball, Peter, John Bailey, Sarah Das, Rocky Geyer, Trevor Harrison, Clay Kunz, Kevin Manganini, et al. 2014. “The WHOI Jetyak: An Autonomous Surface Vehicle for Oceanographic Research in Shallow or Dangerous Waters.” *2014 IEEE/OES Autonomous Underwater Vehicles (AUV)*.

https://doi.org/10.1109/auv.2014.7054430.

Mankoff, Kenneth D., Xavier Fettweis, Peter L. Langen, Martin Stendel, Kristian K. Kjledsen, Nanna B. Karlsson, Brice Noël, et al. 2021. “Greenland Ice Sheet Mass Balance from 1840 through next Week.” https://doi.org/10.5194/essd-2021-131.

Meier, M. F., and Austin Post. 1987. “Fast Tidewater Glaciers.” *Journal of Geophysical Research* 92 (B9): 9051.

Messerli, A., and A. Grinsted. 2015. “Image Georectification and Feature Tracking Toolbox: ImGRAFT.” *Geoscientific Instrumentation Methods and Data Systems* 4 (1): 23–34.

Moon, T., D. A. Sutherland, D. Carroll, D. Felikson, L. Kehrl, and F. Straneo. 2018. “Subsurface Iceberg Melt Key to Greenland Fjord Freshwater Budget.” *Nature Geoscience*. https://doi.org/10.1038/s41561-017-0018-z.

Moon, Twila, Ian Joughin, and Ben Smith. 2015. “Seasonal to Multiyear Variability of Glacier Surface Velocity, Terminus Position, and Sea Ice/ice Mélange in Northwest Greenland.” *Journal of Geophysical Research. Earth Surface* 120 (5): 818–33.

Morlighem, M., C. N. Williams, E. Rignot, L. An, J. E. Arndt, J. L. Bamber, G. Catania, et al. 2017. “BedMachine v3: Complete Bed Topography and Ocean Bathymetry Mapping of Greenland From Multibeam Echo Sounding Combined With Mass Conservation.” *Geophysical Research Letters* 44 (21): 11051–61.

Mouginot, Jérémie, Eric Rignot, Anders A. Bjørk, Michiel van den Broeke, Romain Millan, Mathieu Morlighem, Brice Noël, Bernd Scheuchl, and Michael Wood. 2019. “Forty-Six Years of Greenland Ice Sheet Mass Balance from 1972 to 2018.” *Proceedings of the National Academy of Sciences of the United States of America* 116 (19): 9239–44.

Nick, F. M., C. J. Van Der Veen, A. Vieli, and D. I. Benn. 2010. “A Physically Based Calving Model Applied to Marine Outlet Glaciers and Implications for the Glacier Dynamics.” *Journal of Glaciology* 56 (199): 781–94.

Pattyn, Frank, Catherine Ritz, Edward Hanna, Xylar Asay-Davis, Rob DeConto, Gaël Durand, Lionel Favier, et al. 2018. “The Greenland and Antarctic Ice Sheets under 1.5 °C Global Warming.” *Nature Climate Change* 8 (12): 1053–61.

Pfeffer, W. T., J. T. Harper, and S. O’Neel. 2008. “Kinematic Constraints on Glacier Contributions to 21st-Century Sea-Level Rise.” *Science* 321 (5894): 1340–43.

Plach, Andreas, Kerim H. Nisancioglu, Sébastien Le clec’h, Andreas Born, Petra M. Langebroek, Chuncheng Guo, Michael Imhof, and Thomas F. Stocker. 2018. “Eemian Greenland SMB Strongly Sensitive to Model Choice.” *Climate of the Past* 14 (10): 1463–85.

Pritchard, Hamish D., Robert J. Arthern, David G. Vaughan, and Laura A. Edwards. 2009. “Extensive Dynamic Thinning on the Margins of the Greenland and Antarctic Ice Sheets.” *Nature* 461 (7266): 971–75.

Rignot, E., Y. Xu, D. Menemenlis, J. Mouginot, B. Scheuchl, X. Li, M. Morlighem, et al. 2016. “Modeling of Ocean-Induced Ice Melt Rates of Five West Greenland Glaciers over the Past Two Decades.” *Geophysical Research Letters* 43 (12): 6374–82.

Robel, Alexander A. 2017. “Thinning Sea Ice Weakens Buttressing Force of Iceberg Mélange and Promotes Calving.” *Nature Communications* 8 (March): 14596.

Robinson, Marci M., Harry J. Dowsett, and Mark A. Chandler. 2008. “Pliocene Role in Assessing Future Climate Impacts.” *Eos, Transactions American Geophysical Union*. https://doi.org/10.1029/2008eo490001.

Ryan, J. C., A. L. Hubbard, J. E. Box, J. Todd, P. Christoffersen, J. R. Carr, T. O. Holt, and N. Snooke. 2015a. “UAV Photogrammetry and Structure from Motion to Assess Calving Dynamics at Store Glacier, a Large Outlet Draining the Greenland Ice Sheet.” *The Cryosphere*. https://doi.org/10.5194/tc-9-1-2015.

———. 2015b. “UAV Photogrammetry and Structure from Motion to Assess Calving Dynamics at Store Glacier, a Large Outlet Draining the Greenland Ice Sheet.” *The Cryosphere* 9 (1): 1–11.

Shepherd, Andrew, Erik R. Ivins, Geruo A, Valentina R. Barletta, Mike J. Bentley, Srinivas Bettadpur, Kate H. Briggs, et al. 2012. “A Reconciled Estimate of Ice-Sheet Mass Balance.” *Science* 338 (6111): 1183–89.

Solgaard, Anne M., Johan M. Bonow, Peter L. Langen, Peter Japsen, and Christine S. Hvidberg. 2013. “Mountain Building and the Initiation of the Greenland Ice Sheet.” *Palaeogeography, Palaeoclimatology, Palaeoecology*. https://doi.org/10.1016/j.palaeo.2013.09.019.

Straneo, Fiammetta, and Patrick Heimbach. 2013. “North Atlantic Warming and the Retreat of Greenland’s Outlet Glaciers.” *Nature*. https://doi.org/10.1038/nature12854.

Thiede, J., C. A. Jessen, P. Knutz, A. Kuijpers, and R. F. Spielhagen. 2010. “Millions of Years of Greenland Ice Sheet History Recorded in Ocean Sediments.” *Polarforschung* 80 (3): 141–59.

Todd, J., and P. Christoffersen. 2014. “Are Seasonal Calving Dynamics Forced by Buttressing from Ice Mélange or Undercutting by Melting? Outcomes from Full-Stokes Simulations of Store Glacier, West Greenland.” *The Cryosphere*. https://doi.org/10.5194/tc-8-2353-2014.

Todd, Joe, Poul Christoffersen, Thomas Zwinger, Peter Råback, Nolwenn Chauché, Doug Benn, Adrian Luckman, et al. 2018. “A Full-Stokes 3-D Calving Model Applied to a Large Greenlandic Glacier.” *Journal of Geophysical Research: Earth Surface*. https://doi.org/10.1002/2017jf004349.

Tollefson, Jeff. 2021. “IPCC Climate Report: Earth Is Warmer than It’s Been in 125,000 Years.” *Nature* 596 (7871): 171–72.

Truffer, Martin, and Roman J. Motyka. 2016. “Where Glaciers Meet Water: Subaqueous Melt and Its Relevance to Glaciers in Various Settings.” *Reviews of Geophysics* 54 (1): 220–39.

Walter, Jacob I., Jason E. Box, Slawek Tulaczyk, Emily E. Brodsky, Ian M. Howat, Yushin Ahn, and Abel Brown. 2012. “Oceanic Mechanical Forcing of a Marine-Terminating Greenland Glacier.” *Annals of Glaciology* 53 (60): 181–92.

Walters, Roy A., E. G. Josberger, and C. L. Driedger. 1988. “Columbia Bay, Alaska: An ‘upside Down’ Estuary.” *Estuarine, Coastal and Shelf Science*. https://doi.org/10.1016/0272-7714(88)90037-6.

Website, Nasa’s Global Climate. n.d. “Climate Change Adaptation and Mitigation.” Accessed December 15, 2021. https://climate.nasa.gov/solutions/adaptation-mitigation.

Weidick, Anker, Richard S. Williams, and Jane G. Ferrigno. 1995. *Greenland: Landsat Images are the Basis for a Discussion of the Glaciology, Geography and Climatology of Greenland, the Second Largest Areal and Volumetric Concentration of Present-day Glacier Ice. Landsat Images of Greenland*.

Xie, Surui, Timothy H. Dixon, David M. Holland, Denis Voytenko, and Irena Vaňková. 2019. “Rapid Iceberg Calving Following Removal of Tightly Packed pro-Glacial Mélange.” *Nature Communications* 10 (1): 3250.

Xu, Yun, Eric Rignot, Ian Fenty, Dimitris Menemenlis, and M. Mar Flexas. 2013. “Subaqueous Melting of Store Glacier, West Greenland from Three-Dimensional, High-Resolution Numerical Modeling and Ocean Observations.” *Geophysical Research Letters*. https://doi.org/10.1002/grl.50825.

Yau, Audrey M., Michael L. Bender, Thomas Blunier, and Jean Jouzel. 2016. “Setting a Chronology for the Basal Ice at Dye-3 and GRIP: Implications for the Long-Term Stability of the Greenland Ice Sheet.” *Earth and Planetary Science Letters*. https://doi.org/10.1016/j.epsl.2016.06.053.

Young, T. J., P. Christoffersen, S. H. Doyle, K. W. Nicholls, C. L. Stewart, B. Hubbard, A. Hubbard, et al. 2019. “Physical Conditions of Fast Glacier Flow: 3. Seasonally-Evolving Ice Deformation on Store Glacier, West Greenland.” *Journal of Geophysical Research. Earth Surface* 124 (1): 245–67.

Appendix

Glossary of Terms

Term	Definition	Source
ablation	Combined processes which remove snow or ice from the surface of a glacier, also used to express the quantity of these lost; melt.	National Snow and Ice Data Center Cryosphere Glossary
advance	When a glacier's terminus extends farther down the fjord, occurring when glacial flow is faster than terminus ablation.	National Snow and Ice Data Center Cryosphere Glossary
anthropogenic	Originating in human activity	Oxford Dictionary
basal movement	The act of the glacier sliding over the bed.	(Benn and Evans 2010)
basal pinning	A topographic constriction of the glacial bathymetry.	Earth Resources Observation and Science Center
bed	The surface over which a glacier moves.	(Benn and Evans 2010)
bergy bit	A large chunk of glacier ice floating in the sea.	National Snow and Ice Data Center Cryosphere Glossary
calving	Processes by which ice breaks off a glacier's terminus, usually in reference to tidewater glaciers.	National Snow and Ice Data Center Cryosphere Glossary
catchment area	The area of an ice sheet that is drained by a glacier.	(Benn and Evans 2010)
clast	A fragment.	Oxford Dictionary

crevasse	Open fissure on a glacier's surface	National Snow and Ice Data Center Cryosphere Glossary
deglacial period	Transition between full glaciation and warm interglacial period characterized by global warming and sea level rise.	(Benn and Evans 2010)
diurnal	Occurring daily.	Oxford Dictionary
embayment	A coastal recess that forms a bay.	Oxford Dictionary
englacial	Within the glacier.	National Snow and Ice Data Center Cryosphere Glossary
entrained	Chemistry - to carry along during a given process.	Oxford Dictionary
fjord	Glacial trough that fills with seawater.	National Snow and Ice Data Center Cryosphere Glossary
headland	A narrow piece of land (or ice) projecting from the coastline into the sea.	Oxford Dictionary
hydrographic	Relating to the measurement of physical characteristics of water.	National Oceanic and Atmospheric Administration
interstitial	The narrow spaces between rocks, ice clasts, or sediment.	National Snow and Ice Data Center Cryosphere Glossary
Jakobshavn Isbræ	A large outlet Glacier in Western Greenland	(Benn and Evans 2010)
Land biosphere	The portion of land where life occurs.	Copernicus Climate Change Service

mélange	A mixture of sea ice types without a clearly defined floe commonly the result of calving.	(Benn and Evans 2010)
meltwater plume	A buoyant column of meltwater typically from subglacial channels.	(Benn and Evans 2010)
Miocene	Geologic epoch occurring between 23 mya and 5.3 mya.	Encyclopedia Britannica
orographic precipitation	Precipitation occurring when moist air is lifted as it moves over a mountain range.	Encyclopedia Britannica
orthophoto	An aerial photograph that has been geometrically corrected.	(American Society of Civil Engineers 1994)
perturbation	Deviation in a system from its normal path.	Oxford Dictionary
Pliocene	Geologic epoch occurring between 5.3 mya and 2.6 mya	Encyclopedia Britannica
retreat	When a glacier's terminus doesn't extend as far down a fjord as it previously did; occurs when ablation surpasses accumulation.	National Snow and Ice Data Center Cryosphere Glossary
semidiurnal	Relating to a half day	Oxford Dictionary
shear bands	Narrow zone of shear strain from deformation.	(Bigoni 2012)
subaqueous melting	Glacial melting that occurs under the waterline usually of marine terminating glaciers.	(Benn and Evans 2010)
subglacial water flux	The movement of water	(Benn and Evans 2010)

	beneath a glacier.	
supraglacial lake	Lakes forming on the surface of the glacier.	National Snow and Ice Data Center Cryosphere Glossary
surface ablation	Surface Melt.	National Snow and Ice Data Center Cryosphere Glossary
tabular	Broad and flat topped.	Oxford Dictionary
temporal	As relating to time.	Oxford Dictionary
terminus	The lowest end of a glacier.	National Snow and Ice Data Center Cryosphere Glossary
thermal forcing	A period of rapid temperature fluctuation or temperature cycling.	(Barnier 1995)